Infra-red spectra of functionalized copper nanoparticles using ab initio molecular dynamics

Nitik Bhatia[1], Ondrej Krejci[1], Patrick Rinke[1]
[1]Department of Applied Physics, Aalto University, Espoo, Finland

Abstract: Vibrational spectroscopy facilitates in vivo analysis of chemical reactions. Characteristic peaks in the spectra serve as fingerprints for the identification of certain chemical groups or bonds (like C-X, O-X, M-X; M=metal, X=H, O, C) and thus deliver insight and understanding. At the same time, peak position and shapes can be affected by interactions of the probed species with its neighborhood. In this work we investigate such neighborhood effects for the vibrational spectra of several small molecules that are adsorbed on copper nanoclusters and are important in heterogenous catalysis. We compute the infra-red spectra with ab initio molecular dynamics (AIMD) [1], using the Fourier transform of the autocorrelation function of the molecular dipole moment obtained from AIMD. This method allows us to go beyond the harmonic approximation. The temperature of the AIMD simulations is controlled with a Nosé-Hoover chain thermostat [2] and density functional theory was used as an electronic structure method utilizing the Perdew–Burke–Ernzerhof (PBE) [3] exchange-correlation functional.

In this work, we are comparing the effects of temperature, cluster size, binding site and coverage on the simulated spectra (see Fig. 1 for an example of methanol bound to a small Cu_{13} nanocluster). We observe that the presence of the copper nanocluster shifts the peak positions in a non-uniform manner. The copper nanocluster furthermore broadens the vibrational peaks and enhances the contribution of certain vibrational modes. This work will help us to characterize vibrational spectra of catalytically relevant molecules and will, in the future, be part of an automatic approach to identify species using infra-red spectroscopy.

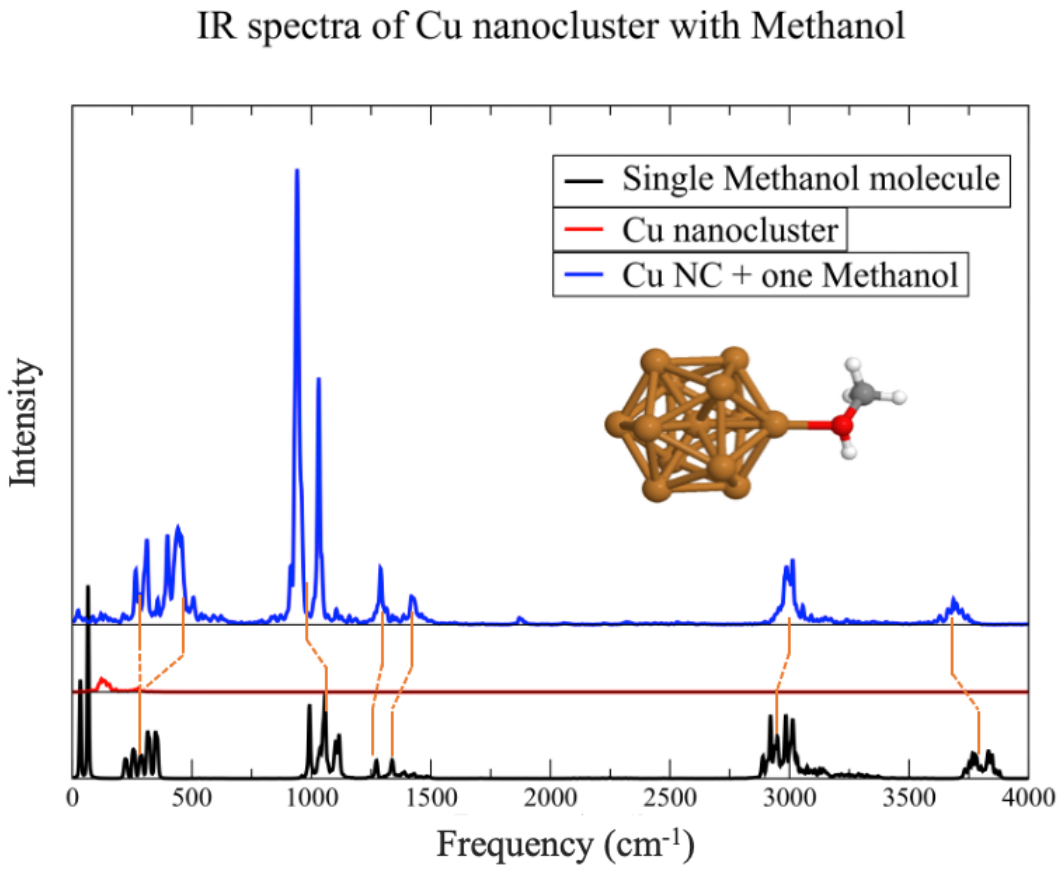

Figure 1 Computed infrared spectra of copper nanocluster (Cu_{13}) with adsorbed methanol on it using AIMD.

References

[1] M.-P Gaigeot, and, M. Sprik, J. Chem. Phys., Lett. **121**, 10111-10119 (2004).
[2] S. Nose, J. Chem. Phys. **81**, 511-519 (1984).
[3] J. P. Perdew, K. Burke and M. Ernzerhof, Phys. Rev. Lett., **77**, 3865–3868 (1996).

Corresponding author: nitik.bhatia@aalto.fi

DEVELOPMENT OF COMPUTATIONAL MAGNETIC RESONANCE FINGERPRINTING METHODS BASED ON NMR BLOCH FLOW EQUATIONS AND ARTIFICIAL NEURAL NETWORKS FOR DIFFERENTIATING INTRA-AXIAL BRAIN TUMORS.

Abstract

Magnetic resonance fingerprinting (MRF) enables fast and multiparametric Magnetic resonance imaging (MRI). Despite fast acquisition, the state-of-the-art reconstruction of MRF based on dictionary matching is slow and lacks scalability. To overcome these limitations, neural network (NN) approaches estimating MR parameters from fingerprints have been proposed. Here, exploring NN-based MRF reconstruction to jointly train the forward process from MR parameters to fingerprints and the backward process from fingerprints to MR parameters by leveraging Artificial neural networks (ANNs). As a proof-of-concept, various experiments were performed showing the benefit of learning the forward process, i.e., the Bloch simulations, for improved MR parameter estimation. The benefit especially accentuates when MR parameter estimation is difficult due to MR physical restrictions. Therefore, ANNs might be a feasible alternative to the current fully backward-based NNs for MRF reconstruction.

Aim and Objectives:

The aim of this study is to develop a computational magnetic resonance fingerprinting (MRF) methods based on nuclear magnetic resonance (NMR) Bloch flow equations and artificial neural networks (ANN) for differentiating intra- axial brain tumors.

The objectives of this study are:

i. to design a machine learning (ANN) for parameters estimation and trained with Bloch simulated data in other to avoid the need for huge database.

ii. to design ANN so as to allow parameters estimation of T1, T2 and T* relaxation times that is orders of magnitude faster than current database comparison.

iii. to determine model performance under MRF pattern matching.

iv. to determine quantitative differences between solid tumour regions of lower grade gliomas and metastases and peritumoral regions of glioblastomas and lower grade gliomas.

Optomechanical Readout of Donor Spins in Silicon

Henri Lyyra[*1], **Cliona Shakespeare**[1], **Antti Kanniainen**[1], **Jesse J. Slim**[2], **James P. Slack-Smith**[3], **Mykhailo Savytskyi**[3], **Amir Sammak**[4], **Giordano Scappucci**[5], **Jarryd J. Pla**[3], **Ewold Verhagen**[2], **Juha T. Muhonen**[1]

1. Department of Physics and Nanoscience Center, University of Jyväskylä, P.O. Box 35, FI-40014 University of Jyväskylä, Finland
2. Center for Nanophotonics, AMOLF, Science Park 104, 1098 XG Amsterdam, The Netherlands
3. School of Electrical Engineering and Telecommunications, UNSW Sydney, Sydney, NSW 2052, Australia
4. QuTech and Netherlands Organisation for Applied Scientific Research (TNO), Delft, The Netherlands
5. QuTech and Kavli Institute of Nanoscience, Delft University of Technology, PO Box 5046, 2600 GA Delft, The Netherlands

Donor spins in silicon are a promising implementation of qubits for scalable quantum computers. They have many beneficial features such as high gate fidelities and long coherence times [1]. Furthermore, the existing semiconductor infrastructure would allow starting mass production fast. However, there is no good way to couple individual spins to each other, and the current readout mechanism, namely the single electron transistor, requires millikelvin temperatures and bulky electric wiring for each qubit, complicating scalability.

Our goal is to use an optomechanical quantum bus which will allow optical readout of the donors, which themselves don't have optical transitions. The optomechanical system is a sliced silicon nanobeam in Fig. 1 [2]. The two beam halves oscillate freely, causing displacement and strain to the silicon. The donor spins couple to the nanobeam's motion via strain [3], causing changes in its resonance frequency which can be measured optically.

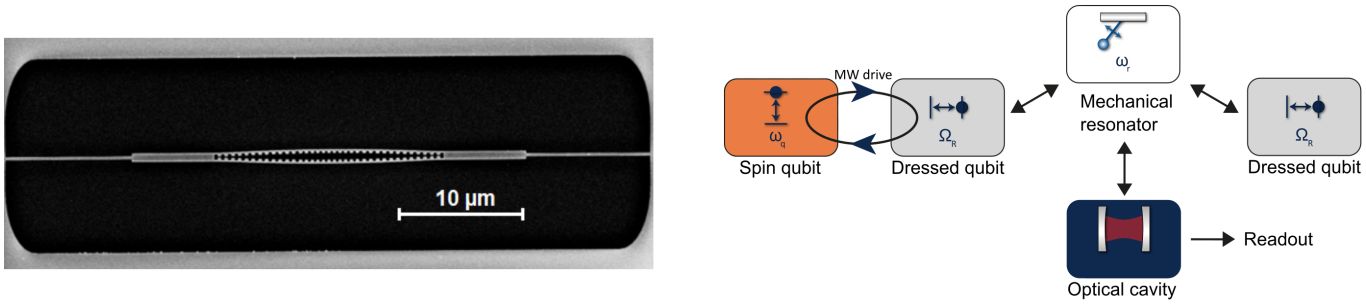

Fig. 1: Left: An SEM picture of the sliced silicon nanobeam. Right: The chain of interacting systems in our setup. When brought close to resonance with the mechanical frequency, the donor spins couple to the mechanical motion of the beam halves via strain. The mechanical motion couples to the electromagnetic field in the optical cavity, defined by the tooth pattern.

In addition to spin state readout, our setup could allow for coherent spin-mechanics state transfer when the nanobeam is cooled down close to its ground state. If multiple spin qubits are coupled to the same resonator, this can be exploited for controlled spin-spin coupling or even preparing the mechanical resonator into non-classical states to explore the fundamental boundaries between quantum and classical world.

In this presentation I will present numerical simulations and characterization of crucial elements of our setup.

References

[1] J. T. Muhonen & al., Nature Nanotechnology **9**, 986–991 (2014)
[2] R. Leijssen & al., Nat. Commun. **8**, 16024 (2017)
[3] J. Mansir & al., Phys. Rev. Lett. **120**, 167701 (2018)

*Corresponding author: henri.s.lyyra@jyu.fi

GaSb quantum dots emitting in the telecom S-band for quantum communication

Markus Peil[1,*], Abhiroop Chellu[1], Joonas Hilska[1], Lucie Leguay[2], Esperanza Luna[3], Andrei Schliwa[2], Mircea Guina[1] and Teemu Hakkarainen[1]

[1] Optoelectronics Research Centre, Tampere University, Korkeakoulunkatu 3, Tampere, FI-33720, Finland
[2] Institute for Solid State Physics, Technical University of Berlin, Hardenbergstrasse 36, Berlin, D-10623, Germany
[3] Paul-Drude-Institut für Festkörperelektronik Leibniz-Institut im Forschungsverbund Berlin e.V., Hausvogteiplatz 5-7, Berlin, D-10117, Germany

Semiconductor quantum dots (QDs) act as deterministic solid-state sources of single and entangled photons which can be used in long-distance coherent fiber optic links to enable a new generation of quantum key distribution - based communication networks [1]. In addition to quantum communication applications, semiconductor QDs pave the way for a scalable approach to integrating non-classical light sources with miniaturized quantum photonic or electronic components. A remarkably successful approach for the epitaxial growth of QDs used in quantum photonics is based on filling nanoholes created by local droplet etching (LDE) method. LDE-QDs based on the GaAs/AlGaAs material have pioneered the realization of non-classical light sources by providing state-of-the-art performance in terms of photon indistinguishability, purity, and entanglement fidelity [2-5]. However, the QDs in this material system are restricted to emission in the 680-800 nm wavelength range owing to their limited direct bandgap range, and thus are not suitable for long-haul transmission over optical fibers or integration with Si photonics.

In this work, we present our findings related to the development of novel GaSb QDs grown by filling LDE nanoholes on AlGaSb surfaces [6, 7]. Our key findings cover the details of the molecular beam epitaxy process of growing these GaSb QDs, their structural characteristics [Fig. 1(a)], and their photoluminescence (PL) properties [Fig. (b) and (c)]. The GaSb QDs exhibit extremely narrow-linewidth emission in the telecom S-band at around 1.5 µm with room for expansion towards 2 µm and beyond. Furthermore, recent studies on non-monolithic integration as well as direct epitaxial growth of GaSb light sources on silicon substrates provide promising paths for integrating our GaSb QDs with Si photonic devices [8, 9].

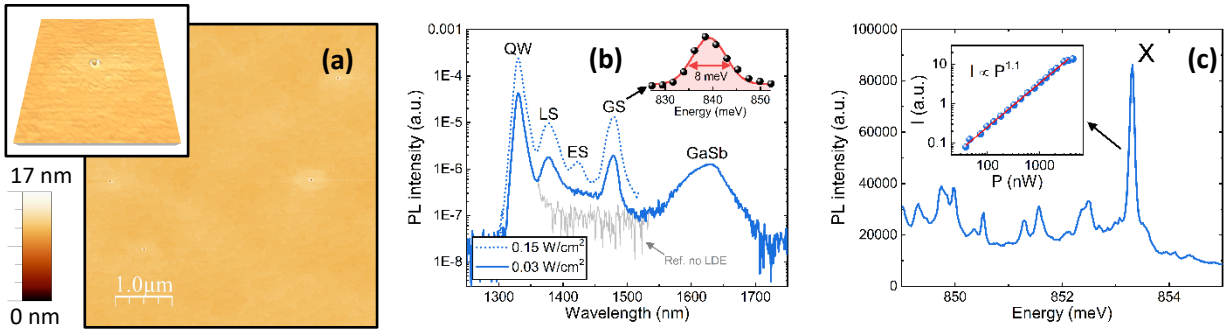

Figure 1. (a) AFM micrograph of the droplet-etched nanoholes on AlGaSb. (b) Homogeneous ensemble PL emission after filling the nanoholes by a thin GaSb QW layer and AlGaSb barrier in order to form GaSb QDs exhibiting narrow-linewidth ground state emission close to 1.5 µm. (c) Single-QD PL with narrow-linewidth excitonic emission with linear power dependency.

References

[1] M. Gurioli et al., Nature Materials **18,** 799 (2019).
[2] J. Liu et al., Nature Nanotechnology **14**, 586 (2019).
[3] D. Huber et al., Nature Communications **8**, 15506 (2017).
[4] E. Schöll et al., Nano Letters **19**, 2404 (2019).
[5] D. Huber et al., Physical Review Letters **121**, 033902 (2018).
[6] J. Hilska et al., Crystal Growth & Design **21**, 1917-1923 (2021).
[7] A. Chellu et al., APL Materials **9**, 051116 (2021).
[8] N. Zia et al., Optics Express **30**, 24995-25005 (2022).
[9] J. Rodriguez et al., Journal of Crystal Growth **439**, 33-39 (2016).

*Corresponding author: markus.peil@tuni.fi

Wide spectral band quantum-well design and gain-chip devices operating at 2 μm wavelength

Ifte Khairul Alam Bhuiyan*, Jukka Viheriäla, Mircea Guina
Optoelectronics Research Centre, Physics Unit, Tampere University, Korkeakoulunkatu 3, 33720, Tampere, Finland

Mid-Infrared light sources emitting at 2-3 μm are getting attention in industries for eye-safe Light Detection and Ranging (LIDAR) sensors, medical diagnostics, molecular spectroscopy, and trace-gas sensing due to molecular fingerprints in these spectral regimes [1]. Recently, high-power, broadband light sources operating at 2.0 μm become a choice for non-destructive imaging, and in-situ thickness monitoring due to the deep penetration of the wavelength [2-3]. Supercontinuum light sources can provide a widely tunable spectrum that can be used for Optical Coherence Tomography (OCT) scanning, however suffering from bulkiness, and high expense, which also requires a large tabletop fiber-optic setup [4]. Semiconductor chip-based miniaturized devices like high power Superluminescent diodes (SLDs) with limited bandwidth have been already reported that can address this problem [5]. However, in the mid-IR spectrum, very less studies have been made to improve the bandwidth of semiconductor light sources using asymmetric quantum wells (QWs). To this end, we have designed and fabricated a novel asymmetric quantum wells-based semiconductor gain structures emitting around 2.0 μm wavelength. These structures were used to study the photoluminescence of different QWs and to prepare laser diode chips for their performance analysis.

The active area of the devices consists of two compressively strained GaInSb/AlGaAsSb quantum wells having different thicknesses. We present analysis from laser diodes and photoluminescence samples to explore the characteristics of asymmetric QWs. The achieved result can also pave the way to produce ultra-broadband high-power single-mode gain chips to build low-cost, compact sensing and scanning systems.

Keywords: Semiconductors, Superluminescent Diodes, Quantum-wells, Imaging, Sensing

References

[1] I.E. Gordon, *et al*., J. Quant. Spectrosc. Radiat. Transf. **203**, 3-69 (2017).
[2] M. Read, *et al.,* Studies in Conservation, **67:3**, 168-175 (2022)
[3] C. S. Cheung, *et al.*, Opt. Lett., **39:22**, 6509-6512 (2014)
[4] J. Barrick, *et al.*, Opt. Lett. **41**, 5620-5623 (2016)
[5] N. Zia, *et al.*, Appl. Phys. Lett. **115**, 231106 (2019)

*Corresponding author: ifte.alambhuiyan@tuni.fi

ADVANCING PHOTONICS STUDENTS' EMPLOYABILITY SKILLS VIA COMPANY COLLABORATION

Kirsi Ikonen[*,1], **Risto Leinonen**[1], **Petri Karvinen**[1], **Markku Kuittinen**[1]
[1] Department of Physics and Mathematics, University of Eastern Finland, Joensuu

Trends such as advances in technology, globalization, changing population characteristics, and changes in natural environment are continuously reshaping the world of work. Especially in rapidly growing fields there is a need for being up-to-date of what is needed for companies to thrive in global competition. One of these growing fields is photonics [1], the technology of generating and harnessing light and other forms of radiant energy. Pressure has been rising for higher education to recognize the skill demands of the companies in order to promote students' post-graduate employment.

This photonics education development project aimed to improve students' employability skills in the international Master's Degree Programme in Photonics at the University of Eastern Finland, and to promote educational collaboration with technology companies. In this project, the laboratory education included in the programme was be reformed so that instead of conventional 'cookbook' type laboratory experiments students now get to develop solutions to authentic research assignments provided by photonics companies or other companies benefitting from photonics applications. While working around the authentic assignments, students get an insight on what it is like to Besides enhancing the mastery of subject matter, the new laboratory activities promote those employability skills that are pivotal in the perspective of modern workplaces, such as problem solving skills, analytical and critical thinking skills, and team working skills [2].

In developing the laboratory education, physics education research was utilized focusing especially on applying an instructional model called argument-driven inquiry (ADI). ADI is an approach to laboratory instruction that engages students in argumentative group discussions to make sense of natural phenomena or to solve a shared problem [3,4]. The ability to present and critically evaluate arguments can be considered an essential ability for knowledge workers and other specialists working in the fields of science and technology. At the same time, ADI gives students an opportunity to learn how to critically read, write, and speak in the context of science [3,4]. Hence, using the argument-driven inquiry as an instructional framework while engaging students with research assignments coming from businesses enables concurrent development of general employability skills without needing to bargain from the acquisition of the core academic skills.

As a result of this development project, the university photonics education meets the skill demands of the changing working life better than it has done in the past. Students reported average to high motivation owing to authentic research assignments and interaction with the representatives from the collaboration companies. Working in close proximity with the companies also made it easier for students' to contact them after the laboratory course and applying for summer jobs and discussing topics for master's theses. We suggest that further research would delve more into the possible methods to promote the employability skills in higher level science education and to intertwine educational collaboration with companies in the more conventional courses.

References

[1] Photonics industry in Finland. Survey results. Boost Brothers Oy, Helsinki, Finland. 2020. Available at: https://www.photonics.fi/wp-content/uploads/2020/05/Photonics-Industry-in-Finland-2020-Spring.pdf
[2] McGunagle D, Zizka L. Employability Skills for 21st-century STEM students: The employers' perspective. Higher Education, Skills and Work-Based Learning. 2020;10(3):591–606.
[3] Sampson V, Grooms J, Walker J. Argument-Driven Inquiry. The Science Teacher. 2009 11;76(8):42-47.
[4] Walker JP, Sampson V. Learning to argue and arguing to learn: Argument-driven inquiry as a way to help undergraduate chemistry students learn how to construct arguments and engage in argumentation during a laboratory course. Journal of Research in Science Teaching. 2013;50(5):561–96.

[*]Corresponding author: kirsi.ikonen@uef.fi

The Advanced Computing Hub at the Univeristy of Helsinki is a EUROfusion funded group dedicated to improving high performance computing codes for fusion research as well as developing AI based methods for the same purpose. The group has been effectively operational for about a year and a half. The highlights so far can be summarized as following: Development of a GPU-enabled quad-precision solver for the DREAM code that is designed for risk assessments of runaway electrons in fusion plasma; Optimization and parallelization of the MIGRAINE code for particle transport in plasma; 'Clean-up' of a 1980's designed Grad-Shafranov solver; Optimization of the TabGap potential implementation in LAMMPS for reactor wall material damage simulations; Application of Bayesian methods for parameter calibration and uncertainty quantification in fusion plasma prediction tools; Application of AI methods for data-driven predictions for theoretically and computationally challenging parts of the fusion plasmas and materials; Development of a disruptively new version of the EIRON code for neutran particle transport.

Do furans auto-oxidize? Flow reactor investigations with chemical ionization mass spectrometry detection

Sana Farhoudian,[1,*] Rabbia Asgher,[1,*] Shawon Barua,[1] Avinash Kumar, [1] Prasenjit Seal,[1] Siddharth Iyer,[1] Sakshi Jha,[1] Mojtaba Bezaatpour,[1] and Matti Rissanen[1,†]

[1]Aerosol Physics Laboratory, Tampere University, Tampere, 33720, Finland
[†]Department of Chemistry, University of Helsinki, Helsinki, 00014, Finland

Furan as one of the most common products of the thermal cracking of biomass is an important five-member heteroatom-containing VOC present in the atmosphere existing in sufficient quantities to affect atmospheric oxidant levels and secondary pollutant formation. Being an aromatic hydrocarbon, furan is very reactive according to its electrophilic substitution reactions. In the troposphere, atmospheric furan is expected to be mainly oxidized by OH during the daytime and NO_3 at night. Furan and its alkyl derivatives (furans) and their chemical transformations are generally oversimplified in gas-phase chemical mechanisms used for air quality predictions and atmospheric modeling studies. They are typically lumped as reactive aromatics, which largely underpredicts their oxidation rates. So, it is important to assess the SOA formation potential of furan and its role in SOA production since its emission contributes to the formation of ultrafine particles [1,2,3].

- The experimental work involves chemical ionization and detection of highly oxygenated molecules (HOM) using
  - Chemical ionization orbitrap mass spectrometer (CIMS)
  - Multischeme chemical ionization inlet (MION) (Fig.1) [4]
  - Variable reaction time-scale flow reactor setup
- Bromide (Br^-) ionization was used for product detection.
- OH radicals were produced by the reaction of trimethylolethane (TME) with O_3.

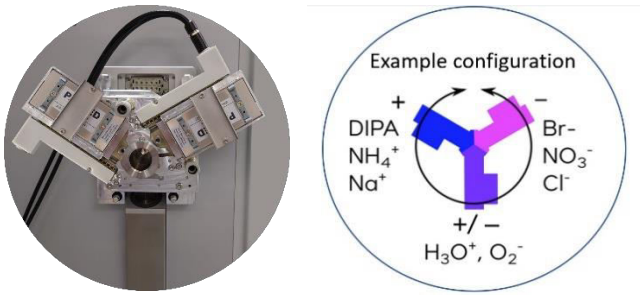

Figure 1. Multi scheme ionization inlet (MION)

- Primary analysis of 2-methylfuran and 2,5-dimethlfuran oxidation spectrum show formation of HOM using 5 s, 7.5 s and 10 s residence time setup respectively.
- The background oxidation was analyzed without turning on the VOC flow. The peaks grew after 2,5-dimethylfuran flow was turned on and dropped when 2,5-dimethylfuran flow was disconnected.
- The production of OH was also terminated to ensure that formation of HOM is because of oxidation of 2-methylfuran.
- We plan to analyze other furans as well as more hydrocarbon systems and give constraints (in terms of different substitutions, residence time, temperature, and pressure) for their potential HOM formation.

References

[1] X. Jiang, N. T. Tsona, L. Jia, S. Liu, Y. Xu, & L. Du, Atmospheric Chemistry and Physics Discussions, 1-27 (2018).
[2] J. Jiang, W. P. L. Carter, D. R. Cocker, K. C. Barsanti, ACS Earth Space Chem., 1254–1268 (2020)
[3] C. A. Whelan, J. Eble, Z. S. Mir, M. A. Blitz, P. W. Seakins, M. Olzmann, D. Stone, J. Phys. Chem. A, 7416–7426 (2020)
[4] M. P. Rissanen, J. Mikkilä, S. Iyer, J. Hakala, Atmos. Meas. Tech., 6635–6646, (2019)

*Corresponding authors: sana.farhoudian@tuni.fi & rabbia.asgher@

Electron-to-proton ratios in solar energetic particle events

Ghulam Ume Farwa[*,1], **Rami Vainio**[1], **Nina Dresing**[1], **Christian Palmroos**[1], **Seve Nyberg**[1]
[1] Department of Physics and Astronomy, 20014 University of Turku, Finland

Solar energetic particle (SEP) events are major outbursts of energetic charged particle radiation from the Sun. These events are related to solar flares and fast coronal mass ejections (CMEs). Flares are presumed to accelerate particles in magnetic reconnection processes, whereas fast (speeds > 1000 km s^{-1}) CMEs drive shock waves through the corona that are known to be able to accelerate particles. Electron acceleration has traditionally been ascribed to reconnection in flares whereas proton acceleration is believed to be efficient in CME-driven shocks. Recent observational evidence [1], however, suggests that shocks may be important in electron acceleration as well. Almost all major eruptions are related to both flares and CMEs so the association of the accelerated particles to these eruptive phenomena is often subject to debate.

We have analysed a set of 31 SEP events using data from recently launched heliospheric spacecraft, i.e., ESA's *Solar Orbiter* and *BepiColombo* and NASA's *Parker Solar Probe*. In addition, we use data from near-Earth spacecraft (*SOHO* and *Wind*) as well as from the *STEREO A* spacecraft in orbit around the Sun somewhat away from the Earth's. We determined the peak intensities of ~25 MeV protons and ~100 keV and ~1 MeV electrons in these events and performed correlation studies of the intensities against each other with different values of the angular distance of the observer from the eruption centre. The distance is measured as the heliolongitudinal separation of the footpoint of the interplanetary magnetic field line connecting the observer to the Sun and the site of the X-ray flare related to the event. We separated the events to well connected (separation ≤ 30°) and poorly connected events (separation > 30°) and correlated the electron and proton observations. Poorly-connected events show a single population of events with weakly correlated proton and electron peak intensities, consistent with the idea that these particles are all accelerated by the CME-driven shock wave. Well-connected events, on the other hand, show two event populations. One, where proton intensities are low and weakly anti-correlated with electron intensities, and another with higher proton peak intensities, but with weakly correlated electron and proton peak intensities.

A possible interpretation of these results is that well-connected events have a contribution from the flare accelerated events, which is absent from the poorly connected events. Poorly connected events would thus be accelerated by shocks. Shock accelerated events would also constitute the proton-rich population of the well-connected events.

We will present the correlations as well as analyse other key parameters like the intensity rise times (from back ground to peak) in our event sample.

References

[1] Dresing, N. Kouloumvakos, A., Vainio, R., Rouillard, A., Astrophys. J. Lett., 925, L21.

[*]Corresponding author: ghulam.u.farwa@utu.fi

Laboratory-based X-ray phase-contrast and dark-field imaging

Henrik Mäkinen[*1], **Heikki Suhonen** [1], **Simo Huotari** [1]
1. Department of Physics, University of Helsinki, Finland

X-ray phase-contrast and dark-field imaging are novel imaging methods that are very attractive, especially, for soft-tissue analysis [1]. Phase-contrast imaging (PCI) utilizes the phase shift or refraction taking place when X-rays interact with a sample. Dark-field imaging (DFI), in turn, measures differences in (small-angle) scattering power inside the sample. Compared to conventional attenuation-based imaging, PCI provides higher contrast between materials of similar density [2], while DFI gives information from structures even below the spatial resolution capabilities of the setup (micrometer or sub-micrometer scale) [3]. X-ray phase-contrast and dark-field imaging were recently made available to laboratories using conventional X-ray tubes by advancements in grating interferometry [3], [4]. In recent years, the method has advanced towards clinical applications (such as mammography [5] and chest X-ray imaging [6]), but stability and dose issues [7], [8], mainly, have held it back from reaching routine use.

We have built a three-grating Talbot-Lau interferometer at the University of Helsinki X-ray laboratory offering a test bed for new developments, and for interesting scientific studies. It provides phase shift, attenuation/transmission and dark-field images in 2D and 3D, all in one measurement. We will present the current state of our setup, and show results from our work concerning the optimization of the device, as well as imaging of several phantoms and biological samples. These results show that our setup can be used in a relatively unstable laboratory setting with the help of software and hardware optimizations, and can provide much higher contrast with soft-matter samples. Additionally, the transmission, phase-contrast and dark-field images all provide complementary information, each having benefits depending on the sample.

Fig. 1: Lateral slices from reconstructed tomography data sets of a piece of pork (a and b) and a sausage (bratwurst) filled with cheese and bacon (c and d). Both samples were placed in a cylindrical plastic tube filled with ethanol. The pork sample was additionally submerged in a water container (to reduce beam-hardening and phase-wrapping artefacts). A clear improvement in contrast is seen in the phase-contrast image (b) compared to the transmission image (a). In the case of the sausage sample, the dark-field image provides the most useful complementary information: While some areas in the transmission image (c) have nearly the same gray values, the contrast between the same areas in the scattering-based dark-field image (d) is much more pronounced.

References

[1] L. Birnbacher, E.-M. Braig, D. Pfeiffer, F. Pfeiffer, J. Herzen, Eur. J. Nucl. Med. Mol. Imaging **48** 4171-4188 (2021)
[2] A. Momose, T. Takeda, Y. Itai, K. Hirano, Nature Medicine **2** 473-475 (1996)
[3] F. Pfeiffer, M. Bech, O. Bunk et al., Nature Materials **7** 134-137 (2008)
[4] F. Pfeiffer, T. Weitkamp, O. Bunk et al., Nature Physics **2** 258-261 (2006)
[5] L. Heck, J. Herzen, Physica Medica **79** 69-79 (2020)
[6] K. Willer, A. Fingerle, W. Noichl et al., The Lancet Digital Health **3(11)** e733-e744 (2021)
[7] M. Seifert, S. Kaeppler, C. Hauke et al., Phys. Med. Biol. **61** 6441-6464 (2016)
[8] A. Tapfer, M. Bech, A. Velroyen et al., Proc. Natl. Acad. Sci. U. S. A. **109(39)** 15691-15696 (2012)

[*]Corresponding author: henrik.makinen@helsinki.fi

My Abstract for Physics Days 2023

M. Ghaemi[*,1], **A. Lopez-Cazalilla**[1], **K. Sarakinos**[1,2], **G. J. Rosaz**[3], **S. Calatroni**[3], **F. Djurabekova**[1]

[1] Helsinki Institute of Physics and Department of Physics, P.O. Box 43, FI-00014 University of Helsinki, Finland

[2] KTH Royal Institute of Technology, Department of Physics, Roslagstullsbacken 21, 114 21 Stockholm, Sweden

[3] CERN, European Organization for Nuclear Research, 1211 Geneva, Switzerland

In the field of particle accelerators, the coating of Niobium over Copper has been considerably pronounced due to some desirable advantages, such as stable superconducting properties of Nb, affordable costs and high electrical conductivity of Cu. Accordingly, Nb-coated Cu can be a suitable candidate for superconducting radio frequency (SRF) cavities [1]. Two techniques have been widely performed to synthesize the Nb films over Cu, i.e., direct current magnetron sputtering (DCMS) and high power impulse magnetron sputtering (HiPIMS). The quality and surface morphologies of the deposited films are different in DCMS and HiPIMS because of the different working conditions. DCMS brings a higher degree of porosity and surface roughness to the films as well as the film grows in columnar structure [2]. On the other hand, in HiPIMS, the thin films are denser, smoother, and void-free thin films [3]. Here, through modeling the conditions of each deposition method, i.e., DCMS and HiPIMS, we employed molecular dynamics simulations to investigate the deposition of Nb over Cu. By comparing the experimental results with our computational simulations on several features (e.g., surface roughness), it was found that our results have high accuracy in mimicking the Nb-deposited films. Additionally, we focused on the temperature of the sample and the deposition energy to explore the differences between the two simulated methods at the atomic level. According to the results, in the HiPIMS technique, the combination of dynamic thermal annealing and ballistic effects can explain the formation of the most compact Nb film grown on the Cu substrate.

References

[1] D. K. Finnemore, T. F. Stromberg, C. A. Swenson, Phys. Rev. **149**, 231–243 (1966).

[2] G. Rosaz, A. Bartkowska, C. PA Carlos, T. Richard, M. Taborelli, Surface and Coatings Technology **436**, 128306 (2022).

[3] R. Shu, H. Du, G. Sadowski, M. M. Dorri, J. Rosen, M. A. Sortica, D. Primetzhofer, D. Lundin, A. L. Febvrier, P. Eklund, Surface and Coatings Technology **426**, 127743 (2021).

[*]Corresponding author: milad.ghaemikermani@helsinki.fi

Effects of emission sources on the particle number size distribution measured in the residential area

Sami D. Harni[1], Sanna Saarikoski[1], Joel Kuula[1], Aku Helin[1], Minna Aurela[1], Jarkko V. Niemi[2], Anu Kousa[2], Topi Rönkkö[3], Hilkka Timonen[1]

[1] Atmospheric Composition Research, Finnish Meteorological Institute, Erik Palménin aukio, 00560 Helsinki
[2] Helsinki Region Environmental Services Authority (HSY), Helsinki, Finland
[3] Aerosol Physics Laboratory, Tampere University, Tampere, 33100 Finland

Particle size distribution in ambient air has significant impacts on both climate and human health. For example, light scattering and particle's ability to act as cloud condensation nuclei are strongly affected by particle size [1] and the location of deposited particle in the respiratory system is determined by particle size [2]. Particle size distributions from different emission sources vary significantly. Therefore, the information on the particle size distributions from different sources is essential when assessing their health and climate impacts.

In this study atmospheric aerosol size distributions were studied during the events with a different dominant particle source [3] Measurement was made in northern Helsinki at a detached housing area. Instrument used in the measurements was a Scanning Mobility Particle Sizer (SMPS). The studied particle sources are traffic (TRA), wood combustion (WB), biogenic aerosol (BIO) and long-range transport (LRT). The event types were identified based on the existing knowledge of the sources in the area, time of the events, particle chemistry and gaseous chemistry.

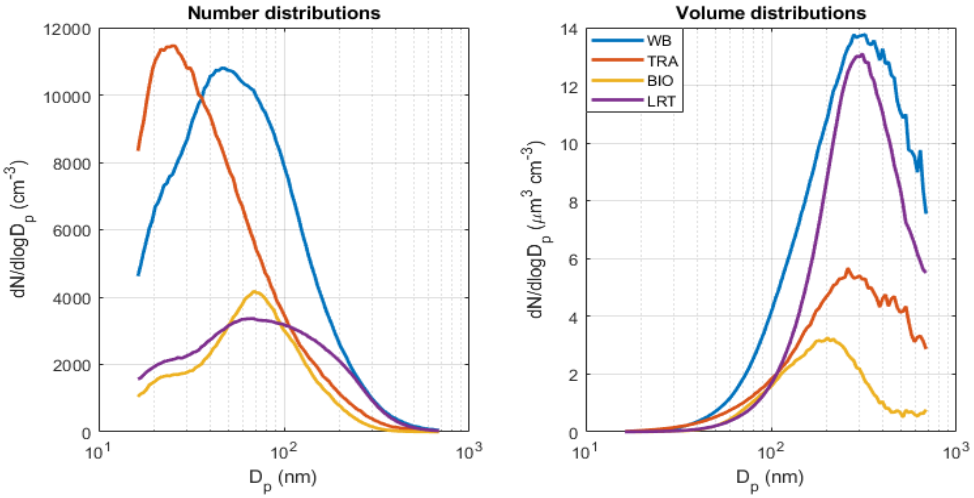

Figure 1. Average particle number and volume size distributions during wood burning (WB), traffic (TRA), biogenic (BIO), and long-range transport (LRT) events.

The particle number size distributions were found to be significantly different from the different sources with TRA producing the smallest particles with mode of 25 nm, followed by WB with mode of 46 nm, BIO and LRT with modes of 69 nm (Fig. 1). Notably, the size distributions also had very different shapes in addition to different modes. Number-wise the strongest events in the area were TRA and WB events, but when considering particle volume, the most significant events were WB and LRT events. As a conclusion the WB produces particles in a wide size range and has significant contributions in both number and volume distributions. Whereas TRA is a significant contributor to number concentration but the effect on volume is limited and LRT contributes significantly to volume but not to the number concentrations. BIO events have minor contribution in both number and volume.

Acknowledgements

Black Carbon Footprint project funded by Business Finland (Grant 528/31/2019) and participating companies, and Grant agreement No 101036245 (RI-URBANS), Urban Air Quality 2.0 project funded by Technology Industries of Finland Centennial Foundation and by the Academy of Finland via the project Black and Brown Carbon in the Atmosphere and the Cryosphere (BBrCAC) (decision nr. 341271) and Academy of Finland Flagship funding (grant no. 337552, 337551).

References

[1] U. Dusek, G.P. Frank, L. Hildebrandt, J. Curtius, J. Schneider, S. Walter, D. Chand, F. Drewnick, S. Hings, D. Jung, S. Borrmann, M.O. Andreae, Size matters more than chemistry for cloud-nucleating ability of aerosol particles, Science. **312,** 5778 (2006)
[2] J. Heyder, Deposition of inhaled particles in the human respiratory tract and consequences for regional targeting in respiratory drug delivery, Proc. Am. Thorac. Soc. **1**, 4 (2004)
[3] S. Harni, S. Saarikoski, J. Kuula, A. Helin, M. Aurela, J.V. Niemi, A. Kousa, T. Rönkkö, H. Timonen, Effects of emission sources on the particle number size distribution of ambient air in the residential area, Amos. Environ., **293**, 119419 (2023)

*†Corresponding author: sami.harni@fmi.fi

Exploring the mixed-metal chalcohalides $A_2BCh_2X_3$ compound space for photovoltaic applications

Pascal Henkel[*1], **Jingrui Li** [2], **Patrick Rinke** [1]

1. Department of Applied Physics, Aalto University, P.O.Box 11100, FI-00076 AALTO, Finland

2. Electronic Materials Research Laboratory, Key Laboratory of the Ministry of Education and International Center for Dielectric Research, School of Electronic Science and Engineering & International Joint Laboratory for Micro/Nano Manufacturing and Measurement Technology, Xi'an Jiaotong University, Xi'an 710049, China

Photovoltaic technologies are crucial for the transition from conventional to green and renewable energy production. New material systems are continuously being explored to increase power conversion efficiencies, reduce cost, and improve device longevities. Hybrid organic-inorganic perovskites emerged a decade ago as promising materials. While the efficiencies of perovskite solar cells rival those of silicon-based devices, commercial adoption has been hampered by stability and toxicity problems. In this study, we explore the perovskite-inspired quaternary mixed-metal chalcohalides $A_2BCh_2X_3$ material system, where the A-site is occupied by ns^2 lone pair cations (group IV), the B-site by group V elements, the Ch-site by chalcogens and the X-site by halogens. $A_2BCh_2X_3$ materials have the potential to overcome the aforementioned problems [1], [2], [3], and still deliver high conversion efficiencies [4]. The experimental band gap of the lead-free $Sn_2SbS_2I_3$ material, for example, is $\sim 1.5\,$eV and a conversion efficiency of 4% has already been reported [3], [5].

We apply density functional theory to the $A_2BCh_2X_3$ system to find materials with band in the range of 1.5 to 2.0 eV. For the B-site we consider antimony (Sb), bismuth (Bi), and indium (In), for the Ch-position sulfur (S), selenium (Se), and tellurium (Te), and for the X-position chlorine (Cl), bromine (Br), and iodine (I). For the A-site, we are primarily interested in tin (Sn), but include lead (Pb) for comparison. For each of the 54 $A_2BCh_2X_3$ compounds, we computed the structural and energetic stability (e.g., formation energy) within three space groups - *Cmcm*, $Cmc2_1$ and $P2_1/c$, see Fig. 1 - and calculated the fundamental band gaps. The formation energies vary in the range of -360 to -797, -365 to -855, and -412 to $-825\,$meV Atom^{-1}, and the band gaps in the range of 0 to 2.519, 0.186 to 2.316, and 0.021 to 2.913 eV for *Cmcm*, $Cmc2_1$, and $P2_1/c$, respectively. Screening the tin-based compounds for stability and suitable band gap, we identify $Sn_2InS_2Br_3$, $Sn_2SbS_2I_3$, and $Sn_2SbSe_2Cl_3$ as promising materials, which will be further studied experimental and theoretically to test their performance in photovoltaic devices.

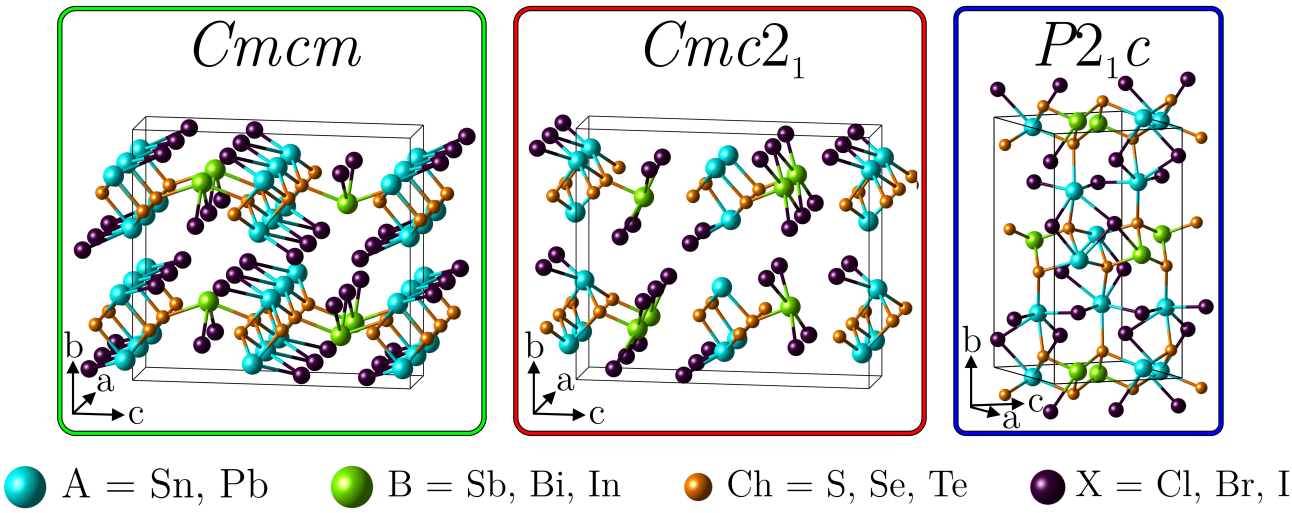

Fig. 1: Three space groups [*Cmcm* (left), $Cmc2_1$ (center) and $P2_1/c$ (right)] in which the $A_2BCh_2X_3$ system can be found.

References

[1] J. Olivier-Fourcade, J. C. Jumas, M. Maurin, E. Philippot, Z. Anorg. Allg. Chem. **468**, 91-98 (1980). [2] A. Ibanez, J.-C. Jumas, J. Olivier-Fourcade, E. Philippot, J. Solid State Chem. **55**, 83-91 (1984). [3] V. I. Starosta, J. Kroutil, L. Beneš, Cryst. Res. Technol. **25**, 1439-1442 (1990). [4] S. R. Kavanagh, C. N. Savory, D. O. Scanlon, A. Walsh, Mater. Horiz. **8**, 2709 (2021). [5] R. Nie, K. S. Lee, M. Hu, M. J. Paik, S. I. Seok, Matter **3**, 1701-1713 (2020).

[*]Corresponding author: pascal.henkel@aalto.fi

Atomistic modeling of a superconductor-transition-metal dichalcogenide-superconductor Josephson junction

Jouko Nieminen[*1,2], **Sayandip Dhara** [3], **Wei-Chi Chiu** [2], **Eduardo R. Mucciolo** [3], **Arun Bansil** [2]

1. Computational Physics Laboratory, Tampere University, FIN-33014, Tampere, Finland
2. Department of Physics, Northeastern University, Boston, Massachusetts, USA
3. Department of Physics, University of Central Florida, Orlando, Florida, USA

Using an atomistic tight-binding model, we study the characteristics of a Josephson junction formed by monolayers of MoS_2 sandwiched between Pb superconducting electrodes. We derive and apply a Green's function-based formulation to compute the Josephson current in this system, as well as the local density of states in the junction. Our computations of diagonal and off-diagonal components of the local density of states reveal the presence of triplet superconducting correlations in the MoS_2 monolayers and a spin-polarized subgap (Andreev bound) states. Our formulation can be extended to study other systems where atomistic details and large scales are needed to obtain accurate modeling of Josephson junction physics.

Our studies reveal that the contributions to the spin polarization coming from different regions of the Brillouin zone differ substantially, with the dominant one coming from states near the K and K' symmetry points where spin splitting of the valence band of MoS_2 is the strongest. Our analysis goes further and identifies a clear manifestation of the important interplay between lattice symmetry and spin-orbit coupling in establishing the intensity of this spin polarization, with monolayer systems (where mirror symmetry is present) showing stronger polarization and a richer structure of in-gap states than bilayer systems (where inversion symmetry occurs). The same effect appears in the amount of induced triplet superconductivity on MoS_2, which is markedly stronger for monolayer systems. Put together, these results point to the possibility of manipulating the spin polarization in dichalcogenide Josephson junctions by employing junction geometries that enhance the contributions from certain regions in k-space.

The methodology developed in this paper could be applied to study supercurrents and resonant bound states in other Josephson-junction-based systems where atomistic, large-scale modeling is required for an accurate description of the physics involved.

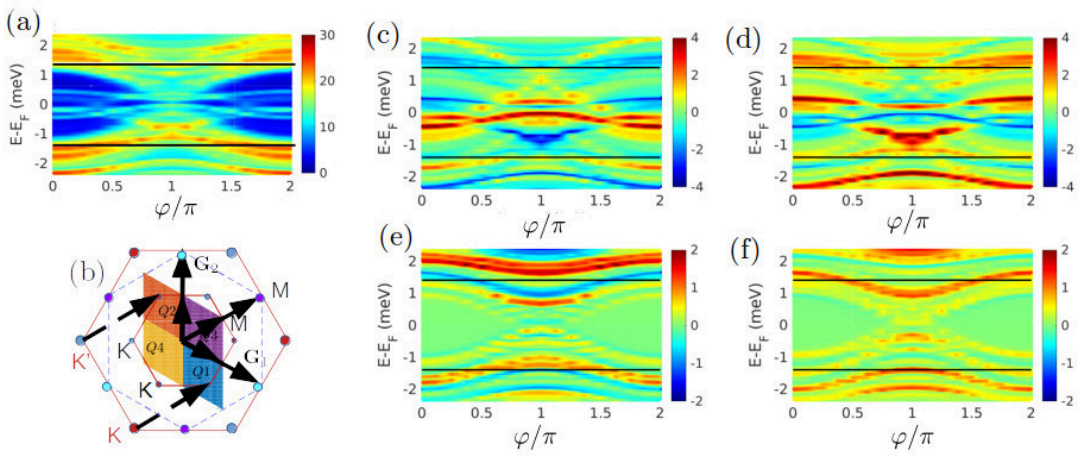

Fig. 1: (a) Local density of states (LDOS) showing Andreev bound states (ABSs) for a single monolayer Pb-MoS_2-Pb Josephson junction as a function of the phase difference. (b) The primitive cell of reciprocal space where quadrants are indicated for spin resolved calculations. The spin polarization of the LDOS calculated ABSs over a quadrant of the primitive cell: (c) quadrant Q1 (blue), (d) quadrant Q2 (red), (e) quadrant Q3 (magenta), and (f) quadrant Q4 (yellow).

[*]Corresponding author: jouko.nieminen@tuni.fi

Generalized lattice-sum approach for predicting optical responses of hybrid metasurface–waveguide systems

Jussi Kelavuori[*1], **Ali Panahpour**[1], **Mikko J. Huttunen**[1]
1. Photonics Laboratory, Tampere University, Korkeakoulunkatu 3, Tampere, Finland

Surface lattice resonances (SLRs) are hybrid collective resonances of localized plasmon resonances in nanoparticles (NPs) and diffractive modes of periodic lattices. They have been shown to dramatically decrease losses compared to pure plasmonic resonances, giving rise to stronger local fields and thus improving the applicability of NP arrays in applications such as nonlinear optics and lasing [1,2]. Efforts have also been made to develop approaches to actively tune the properties of SLRs [3]. The decrease of losses in SLRs is attributed to the lowering of radiative losses associated with NPs [4] because the collective mode restricts the radiation to specific solid angles. The main techniques to reduce the radiative losses associated with NP lattices and SLRs have been to utilize small NPs and to increase the lattice spacing. Unfortunately, both design strategies also decrease the visibility of SLRs, necessitating to compromise between the quality factor (Q-factor) and the visibility of the resonance peak [5].

Here, we propose an approach that can potentially overcome the above limitations enabling to design and realize SLRs that simultaneously exhibit ultrahigh Q-factors ($>10^4$) and high peak visibilities. We utilize dipolar electric Green's function of the first kind in a rectangular waveguide to calculate dyadic empty-lattice approximation of an arbitrary unit cell. Lattice-sum approach (LSA) is then utilized to estimate the linear properties of the system. The results show that collective resonances in plasmonic–waveguide systems appear near wavelengths that satisfy

$$\lambda = n_{\text{eff}} \times p/N \tag{1}$$

where n_{eff} is the effective refractive index of the waveguide mode, p is the periodicity of the unit cell in the direction of propagation and N is a non-negative integer. Interestingly, the resonances can be enhanced or suppressed completely in the dipolar approximation by carefully considering NP positions and driving fields. This effect can potentially allow mode-selective coupling of light into the waveguides. The effect is demonstrated in Fig. 1, where the NP positions at the center of the waveguide forbid coupling of light into certain waveguide modes (such as TE_{11}, TE_{13}, etc.). We also observe efficient zero-order coupling between NPs near the cutoff frequencies of waveguide modes. This behavior is associated with epsilon-near-zero properties of the waveguide near these frequencies, resulting in all of the NPs oscillating in the same phase. These results and their effect on the overall Q-factors of the collective resonances will be presented at the conference.

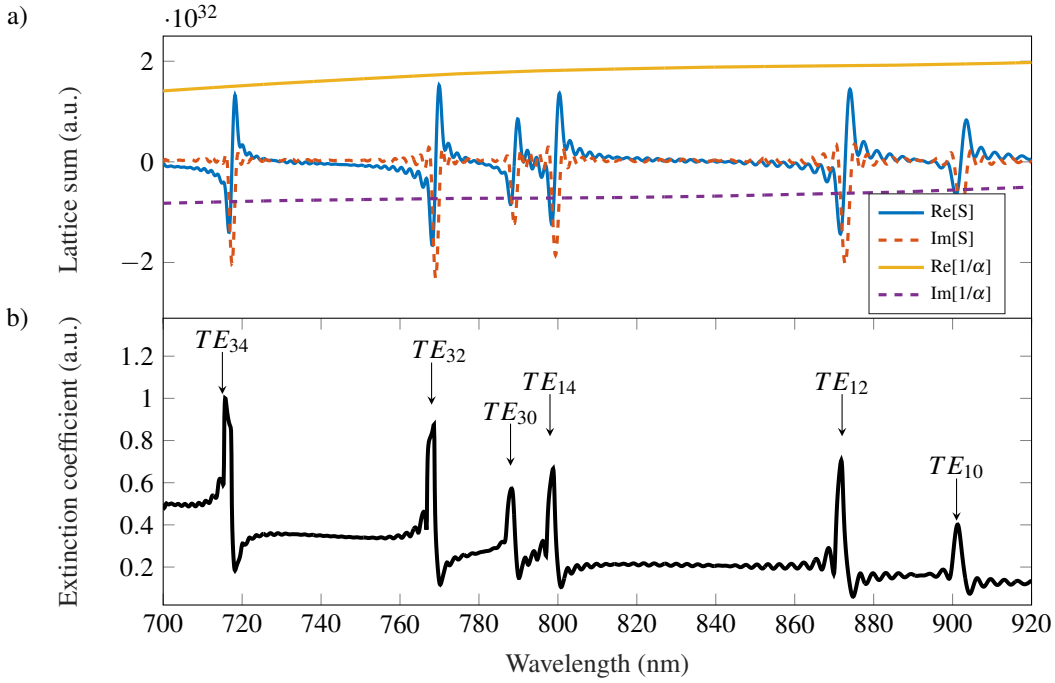

Fig. 1: LSA results for a 1D array spherical aluminium NPs inside a perfectly conducting rectangular waveguide. a) Real and imaginary parts of and NP polarizability α, and lattice-sum term S. b) Extinction coefficients for the NPs in the structure. Different peaks account for different modes inside the waveguide following eq. 1.

References

[1] R. Guo, M. Nečada, T. K. Hakala, A. I. Väkeväinen, and P. Törmä, Phys. Rev. Lett. **122** 013901 (2019)
[2] T. Stolt, A. Vesala, H. Rekola, P. Karvinen, T. K. Hakala, M. J. Huttunen, Opt. Express **30**, 3620-3631 (2022)
[3] J. Kelavuori, V. Vanyukov, T. Stolt, P. Karvinen, H. Rekola, T. K. Hakala, M. J. Huttunen Nano Lett. **22** (10), 3879-3883 (2022)
[4] S. Tsoi, F. J. Bezares, A. Giles, J. P. Long, O. J. Glembocki, J. D. Caldwell, and J. Owrutsky , Appl. Phys. Lett. **108**, 111101 (2016)
[5] M.S. Bin-Alam, O. Reshef, Y. Mamchur, M. Z. Alam, G. Carlow, J. Upham, B. T. Sullivan, J. Ménard, M. J. Huttunen, R. W. Boyd, K. Dolgaleva Nat. Commun. **12**, 974 (2021).

[*]Corresponding author: jussi.kelavuori@tuni.fi

Analysis of Solid-State Nuclear Track Detectors With Optical Scanning System

Matti Kalliokoski[*1]
1. Helsinki Institute of Physics, P.O.Box 64 (Gustaf Hällströmin katu 2), 00014 University of Helsinki, Finland

MoEDAL-MAPP -experiment searches for avatars of new physics with the Large Hadron Collider (LHC) [1],[2]. Its main detectors are Nuclear Track Detectors (NTD) and Magnetic Monopole Traps. The NTDs are stacks of plastic foils which are etched after being exposed to radiation. This will reveal the tracks of the charged particles which traversed the material since the damaged areas etch faster than the surroundings. The tracks appear as conical pits which have specific diameter and depth based on the amount of ionization. The shapes of the pits will also depend on the angle of impact and intensity of the radiation environment.

During Run 2 of the LHC, over 30 square meters of CR-39 foils were exposed in the Interaction Point 8 (IP8) at the MoEDAL experiment. Due to large overall area and hard radiation environment, the identification and analysis of tracks is complicated and require machine vision methods. We utilized the optical scanning system [3] of the Detector Laboratory of Helsinki Institute of Physics (HIP) to detect and identify the etch pits of the foils. We developed the system by introducing different illumination wavelength options and by processing the scanned foils to reduce the background scattering effects.

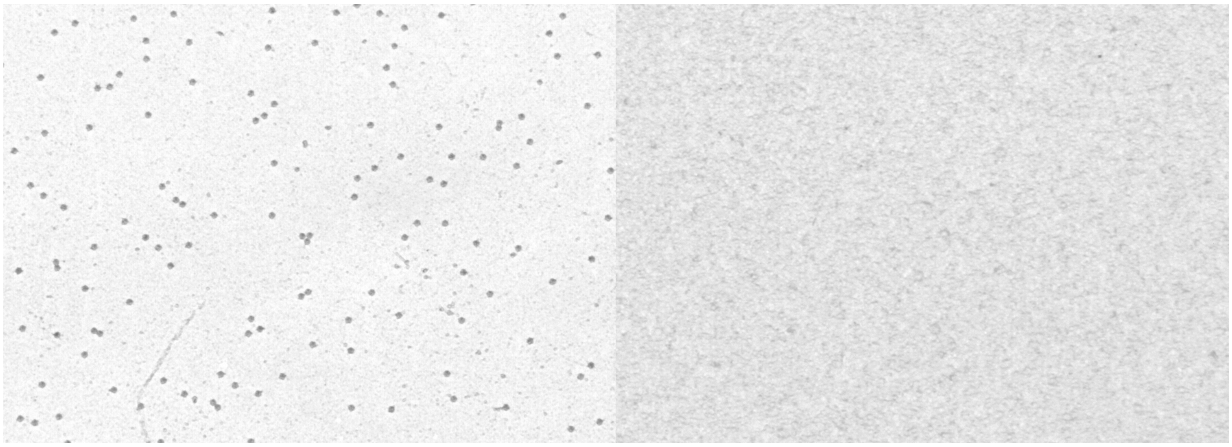

Fig. 1: Images of Si-ion tracks on CR-39 foils taken with the optical scanning system. The left image was taken from a foil which was exposed only to the Si-beam and the right one from a foil which was in addition exposed to the radiation background in the IP8.

After the scans we analysed the foils with various feature extraction and machine learning techniques. With the tools we can produce hit-maps with the information about the pit dimensions. The pit information was then compared with profilometer and white light interferometer measurements to calibrate the results.

Finally we used this information to reproduce the primary interaction with Geant4 based simulation tools. From the simulation results we are able to study the underlying processes that generated the tracks in the foils.

In this contribution we will present the optical scanning system and introduce various updates to improve the foil analysis. We will also present the machine learning tools which are required to identify and measure tracks from the scans. We will also use the measurement results to simulate the primary interactions at the IP8 to identify the underlying physics models.

References

[1] MoEDAL Collaboration, B. Acharya et al., Nature **602** p. 63 (2022)
[2] MoEDAL Collaboration, B. Acharya et al., Phys. Rev. Lett. **126** 071801 (2021)
[3] M. Kalliokoski et al., Nucl. Instr. Meth. A **664** p. 223-230 (2012)

[*]Corresponding author: matti.kalliokoski@helsinki.fi

Towards an optical interface for donor spin qubits in silicon

Antti Kanniainen, Teemu Loippo and Juha T. Muhonen
Department of Physics and Nanoscience Center, University of Jyväskylä, Jyväskylä, Finland
Contact: antti.j.kanniainen@jyu.fi

Keywords: bound exciton, spin readout, quantum computing, photonics

Spin qubits in silicon are a promising candidate for processing quantum information. Silicon based quantum computing benefits from all the large-scale infrastructure and fabrication methods already developed for classical computing. Furthermore, shallow donor electron and nuclear spins in silicon have been reported to have very long coherence times [1,2]. However, donor spin qubits in silicon are, to some degree, constrained by the lack of an optical interface. One proposed way of reading out the spin state is to use donor bound exciton transition. Donor bound exciton transition enables a hybrid electro-optical readout, where transition is excited optically and detected electrically [3]. Scaling this method down to single spins will require microfabricated structures and exploiting silicon photonics platforms. The latter will require moving to silicon-on-insulator (SOI) substrates where electrical exciton transition readout has not been demonstrated yet.

Due to thermal contraction, at low temperatures the metal electrodes required for localised spin readout will unavoidably cause sharp strain profiles around them. Previous research [4] has demonstrated that strain can alter donor spin states and their decoherence characteristics, however, the impact of strain on hole and exciton states has not been thoroughly explored. Integrating readout with SOI technology and considering the combined effects of strain and SOI substrate is an unresolved challenge. Here we investigate the influence of strain on exciton transitions with the goal of combining readout and SOI technology for interfacing with silicon photonics.

In this work [5], we present the outcomes of our recent measurements of donor bound exciton transitions in bulk silicon substrates equipped with microfabricated electrodes. Our findings reveal numerous transitions with an interesting dependence on magnetic fields, which can primarily be explained through strain effects. We delve into the modeling of these strain effects and assess the mixing of states caused by strain. Finally, we consider exciton signal in an SOI structure.

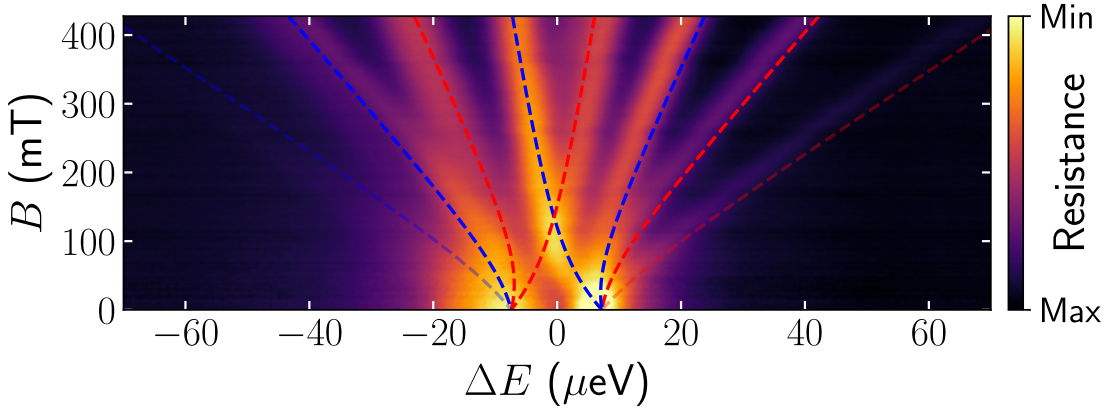

Figure 1: Measured transition energies as a function of the magnetic field overlaid with the calculated transition energies.

1. M. Steger, et al., "Quantum information storage for over 180 s using donor spins in a ^{28}Si "semiconductor vacuum" ", Science 336, 1280, (2012)
2. J. T. Muhonen, et al.,"Storing quantum information for 30 seconds in a nanoelectronic device", Nature Nanotechnology 9, 986, (2014)
3. C. C. Lo, et al, "Hybrid optical–electrical detection of donor electron spins with bound excitons in silicon " Nature Materials 14, (2015)
4. J. J. Pla, et al., "Strain-induced spin-resonance shifts in silicon device", Phys. Rev. Applied 9, 044014 (2018)
5. T. Loippo et al., "Strain effects in phosphorus bound exciton transitions in silicon", Phys. Rev. Materials 7, 016202 (2023)

Theoretical Analysis of Loss-driven Topological Transitions in Lasing

Grazia Salerno[*1], **Rebecca Heilmann**[1], **Kristian Arjas**[†1], **Kerttu Aronen**[1], **Jani-Petri Martikainen**[1], **Päivi Törmä**[1]

1. Department of Applied Physics, Aalto University School of Science

Bound-states in continuum (BIC:s) are non-radiative solutions to the wave-equation. They are characterized by their high quality factors and come with an associated topological charge q. In real 2D systems, such as plasmonic lattices, BIC:s can be coupled to the environment via ohmic losses or the edge of the lattice. In our recent publication we were able to observe transition in lasing states of different topological charges [1]. These changes were achieved in a triangular lattice of hexamers where the inter-particle distance in a single hexamer t was varied. Four different lasing states were found, three of which were BIC:s of charges $-2, -1$ and 1.

To understand the transitions between these states the eigenstates of the system are identified from the C_6 rotational symmetry of the group. For comparison with the experiments, their polarization patterns and topological charges are identified with the coupled dipole approximation. To find the energies and losses of these modes, the T-Matrix method is used. Tracking the quality-factors Q of the eigenmodes as a function of the structure parameter t we show that the mode with the highest Q corresponds to the experimentally observed mode. Our findings demonstrate a way of manipulating and selecting the polarization properties of the laser allowing for greater control in design of potential devices.

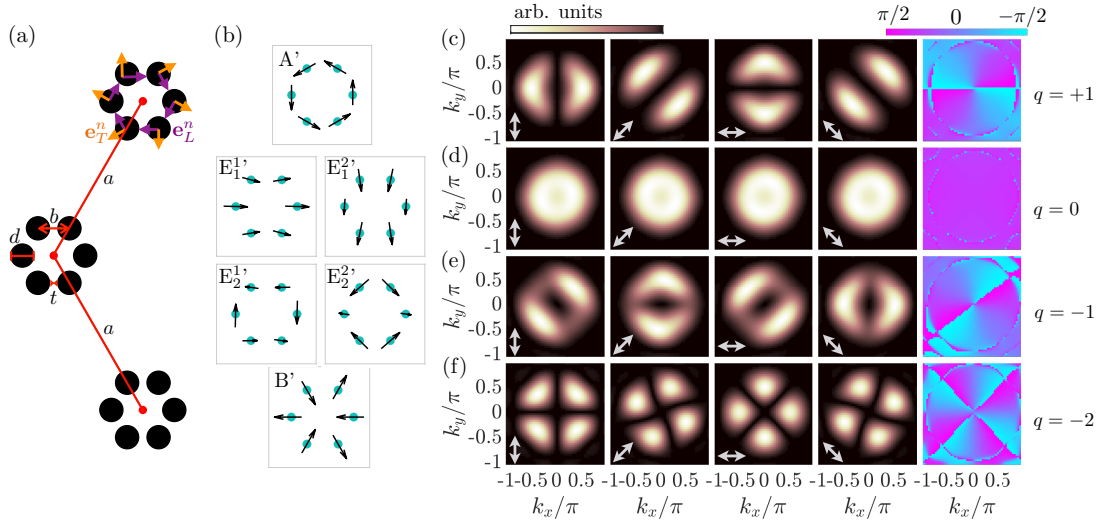

Fig. 1: a) The structure under study. (b) The six eigenmodes of a single hexamer. (c) The polarization patterns with filters, polarization windings and the topological charges of the eigenmodes.

References

[1] G. Salerno, R. Heilmann, K. Arjas, K. Aronen, J.P. Martikainen, P.Törmä, Loss-driven topological transitions in lasing, Phys. Rev. Lett. **129(17)** 173901 (2022)

[*]Corresponding author: grazia.salerno@aalto.fi
[†]Corresponding author: kristian.arjas@aalto.fi

A Quasi-Two-Dimensional Analogy to Axisymmetric Three-Dimensional Liquid Drops

Tytti Kärki[†,1], **Into Pääkkönen**[1], **Jaakko V. I. Timonen**[*,1]
[1]Department of Applied Physics, Aalto University, P.O. Box 15100, 02150 Espoo, Finland

Sessile drops are ubiquitous and important in both technological applications and everyday life. Drop sizes range from nano- to millimeters and their static three-dimensional (3D) shapes are determined by interfacial, gravitational and contact line forces[1], further modified by viscous forces when the drops are moving, as have been shown by extensive studies[2]. Here, we show that there exists an interesting analogy between the aforementioned 3D sessile drops and what can be called Quasi-Two-Dimensional (Q2D) Pseudo-Sessile Drops (Fig. 1).

We create such Q2D drops by confining various liquids between vertical parallel solid surfaces, resulting in very low aspect ratio capillary bridges that adopt projected shapes closely resembling those of true 3D sessile drops. Capillary force holds drops inside and apparent perfect 180° contact angle is formed since there is only air below the drop (analogous to e.g. 3D Leidenfrost and fizzy drops[3,4]). We modify the classic theory for 3D drop shapes to Q2D geometry and reach a good agreement with experiments when Park-Homsy correction[5,6] is taken into account. The effective capillary length in the Q2D geometry can be continuously modified by controlling the tangential component of the gravity by tilting the drop, which is not possible in 3D systems.

Analogous to the tilt experiments often performed with 3D drops, Q2D pseudo-sessile drops can be also tilted to probe the lateral force required to unpin and move the drop. In contrast to 3D, in Q2D the terminal velocity is nearly instantaneously reached and is orders of magnitude smaller due to large viscous dissipation in the confinement. Our results suggest that viscous dissipation dominates for most liquids, but some liquids such as water exhibit anomalously small terminal velocities, suggesting presence of additional contact line forces. The presented 3D-Q2D analogy suggests that many experiments and phenomena observed with 3D sessile drops can be investigated in the Q2D geometry. This is foreseen to be advantageous because of immensely better optical access to internal structures and flows within the drops and because of new physics arising from the reduced dimensionality.

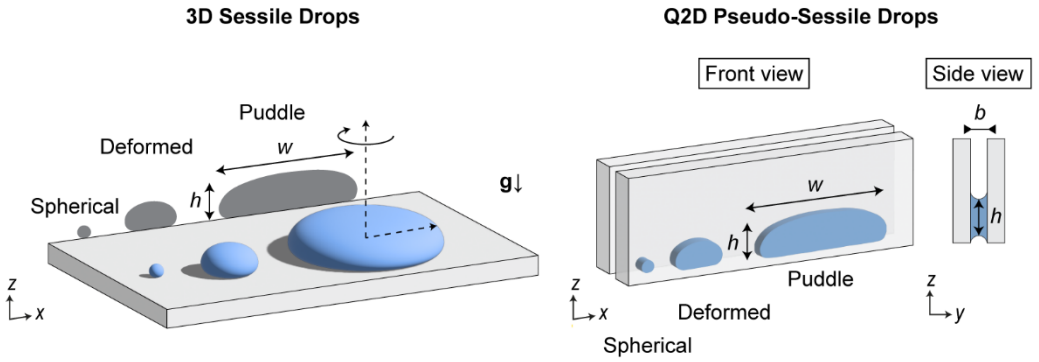

Figure 1. Quasi-Two-Dimensional (Q2D) pseudo-sessile drops are analogous to axisymmetric Three-Dimensional (3D) liquid drops with large contact angles. The shape of Q2D pseudo-sessile drops resembles closely the projected shape of 3D drops: small spherical, deformed drops and large puddles. Despite the confinement, which is determined by the distance between parallel vertical plates (*b*), Q2D pseudo-sessile drop height (*h*) and width (*w*) are determined by capillary length as in 3D drops.

References

1. Gennes, P.-G. de, Brochard-Wyart, F. & Quéré, D. *Capillarity and wetting phenomena: drops, bubbles, pearls, waves*. (Springer, 2010).
2. Mouterde, T., Raux, P. S., Clanet, C. & Quéré, D. Superhydrophobic frictions. *Proc. Natl. Acad. Sci. U.S.A.* **116**, 8220–8223 (2019).
3. Quéré, D. Leidenfrost dynamics. *Annu. Rev. Fluid Mech.* **45**, 197–215 (2013).
4. Panchanathan, D. *et al.* Levitation of fizzy drops. *Sci. Adv.* **7**, eabf0888 (2021).
5. Park, C.-W. & Homsy, G. M. Two-phase displacement in Hele Shaw cells: Theory. *J. Fluid Mech.* **139**, 291–308 (1984).
6. Reyssat, E. Drops and bubbles in wedges. *J. Fluid Mech.* **748**, 641–662 (2014).

[*]Corresponding author: jaakko.timonen@aalto.fi
[†]Corresponding author: tytti.karki@aalto.fi

Who wants to be a physicist? Incoming student attitudes at the University of Helsinki

Inkeri Kontro[*1,2]
1. Physics Unit, Tampere University, P.O. Box 692, FI-33014 Tampere
2. Department of Physics, University of Helsinki, POB 64, FI-00014 University of Helsinki

Physics instruction at universities aims to teach both physics content and scientific thinking, but also attitudes and beliefs about science. The Colorado Learning Attitudes about Science Survey (CLASS) is a survey for examining students expert-like attitudes towards physics [1]. Generally, physics majors have higher CLASS scores than minor students, and male students have, on average, higher scores than female students. Usually, the students have more expert-like beliefs in the beginning of the studies, and the beliefs decline during instruction [2]. The CLASS, when administered to Finnish university students, measures student attitudes towards physics in three factors: Personal Application and Relation to Real World (PARRW), Effort and Sensemaking (ESM), and Problem Solving Self-Efficacy (PSSE) [3]. Self-efficacy means beliefs about one's capabilities in a given situation, which in this context is in solving physics problems.

At the University of Helsinki, students were administered the CLASS survey from 2012 to 2021. The survey was administered at the beginning of the studies and again in the beginning of the second semester. The resulting data set yielded $N = 951$ unique answers from the beginning of studies and $N = 482$ paired answers where the same student answered the survey on consecutive autumn and spring semesters.

Table 1: CLASS scores by gender, % favorable.
Significant differences pre-test to post-test are marked with *,**,*** (significant at $p < 0.05$, $p < 0.01$ and $p < 0.001$, respectively).

Factor	All	Men	Women
N	482	293	181
Overall pre	70 (14)	72 (13)	66 (15)
Overall post	69 (15)	71 (14)	65 (16)
PARRW pre	76 (23)	74 (24)	78 (22)
PARRW post	76 (23)	75 (23)	77 (24)
ESM pre	86 (19)	87 (18)	85 (21)
ESM post	83^{**} (20)	83^{*} (19)	82 (22)
PSSE pre	64 (29)	70 (26)	53 (29)
PSSE post	58^{***} (31)	64^{**} (30)	49^{*} (30)

The students who study physics at University of Helsinki have comparably high expert-like attitudes. Students who major in Physical Sciences have higher average scores than students of other disciplines. As is common in other countries, there is a gender gap (see Table 0). The gender gap is most pronounced in the factor PSSE. This reflects the typical finding that female students have lower self-efficacy beliefs than male students.

However, the gender gap in ESM is negligible. Curiously, there is a small but robust reversed gender gap in PARRW, meaning women consistently have more expert-like attitudes in statements probing the relationship between physics and their everyday experience. This reversed gender-gap is only a few percentage points, but it robustly appears in the data collected in autumn, in spring and across the different study tracks. Reverse gender gaps have not been reported for CLASS previously.

To summarize, the incoming physics students at the University of Helsinki have fairly expert-like beliefs about physics. The negative changes from first to second term in studies are small but statistically significant in factors relating to sense-making and self-efficacy. Gender gaps are smaller than reported from other countries.

References

[1] W.K. Adams, K.K. Perkins, N.S. Podolefsky, M. Dubson, N.D. Finkelstein, C.E. Wieman, Phys. Rev. ST . Phys. Edu . Res **2** 010101 (2006)
[2] A. Madsen, S.B. McKagan, E.C. Sayre, Phys. Rev. ST . Phys. Edu . Res **11** 010511 (2015)
[3] I. Kontro, D. Buschhüter, Phys. Rev. Phys. Edu . Res **16** 020104 (2020)

[*]Corresponding author: inkeri.kontro@tuni.fi

Superconducting Spintronics and Nonequilibrium Effects

Kurt Meier*, **P. Virtanen, T.T. Heikkilä**
Nanoscience Center and Department of Physics, University of Jyväskylä

The nonlinear σ-model gives rise to linear-response quantities as well as information about the electron system via the non-equilibrium distribution function. The latter can then be used to assess non-linearities, far-from-equilibrium noise, and other features [1]. Recently, the nonlinear σ-model with strong spin-orbit interaction was derived [2]. This theory leads to the Usadel equation, from which one can derive the kinetic equation for the electron distribution function in different types of conductors.

Employing Kuprianov-Lukichev boundary conditions and the kinetic equation on hybrid structures like a normal conductor coupled to two reservoirs, we determine the charge current and the induced spin Hall current perpendicular to it [3]. The spin battery effect by ferromagnetic resonance is studied using an analogous approach. We plan to study this effect in consideration with strong spin-orbit interaction, along with other effects such as the spin-Nernst effect. The theory approach works also for superconductors, thus allowing us to treat spin Hall effects in the superconducting state, ϕ_0-effect, and the Josephson diode effect, just to name a few.

In the poster I will explain the overall structure of the non-linear σ-model and discuss how to use it for observable phenomena.

References

[1] A. Kamenev, and A. Levchenko, *Adv. Phys.* **58**,197–319 (2009).
[2] P. Virtanen, F. S. Bergeret, and I. V. Tokatly, *Phys. Rev. B* **104** (2021).
[3] F. S. Bergeret, A. Verso, and A. F. Volkov, *Phys. Rev. B* **86** (2012).

*e-mail: kurt.k.meier@jyu.fi

VOLUNTARY RADIATION MEASUREMENT TEAM TO ENHANCE THE RADIATION MEASUREMENT PREPAREDNESS IN FINLAND

Maarit Muikku[*,1], Petri Smolander[1] and Jukka Sovijärvi[1]
Presented by Ari Leppänen[†,2]
[1] STUK – Radiation and Nuclear Safety Authority, Jokiniemenkuja 1, 01370 Vantaa, Finland
[2] STUK – Radiation and Nuclear Safety Authority, Lähteentie 2, 96400 Rovaniemi, Finland

A large scale nuclear or radiological emergency like a severe accident at a nuclear power plant, use of a nuclear weapon or a radiological dispersion device could threat the functioning of the whole society. Radiation and Nuclear Safety Authority (STUK) has together with The National Defense Training Association of Finland (MPK) and National Emergency Supply Agency (NESA) launched a co-operation program to enhance the national radiation measurement preparedness by recruiting, training and equipping a voluntary radiation measurement team. The team is equipped with diverse and modern measurement tools and it improves Finland's radiation measurement capacity in situations that require plenty of information on radiation in order to ensure safety and to support official decision making. The focus lays primarily on the measurement of potentially contaminated people. In later phase the measurement of the surroundings and infrastructure will become important.

The voluntary radiation measurement team consists of about 40 persons divided into three measurement groups and one supporting group. The team is capable to independently carry out its duties, for example, to determine the radiation situation, to check the contamination of people and vehicles as well as to support other organizations with radiation measurements.

By the end of year 2022 about 100 volunteers have been trained. The background of the volunteers is diverse. However, there are different kinds of tasks available for the volunteers, from a member of monitoring patrol to more challenging tasks like trainer or the operative leader in the volunteer organization. Further training of the team will continue.

Figure 1. Training on dose rate measurements. (Photo: STUK)

[*]Corresponding author: maarit.muikku@stuk.fi
[†]Corresponding author: ari.leppanen@stuk.fi

Highly tunable induced topological superconductivity in twisted bilayer graphene

Maryam Khosravian[1], **Elena Bascones**[2], **and Jose L. Lado**[1]

1. Department of Applied Physics, Aalto University, 02150 Espoo, Finland

2. Instituto de Ciencia de Materiales de Madrid (ICMM), Consejo Superior de Investigaciones Científicas (CSIC), Sor Juana Inés de la Cruz 3, 28049 Madrid, Spain

Moiré van der Waals heterostructures [1],[2], including graphene multilayers [3],[4] have risen as a highly tunable material for realizing unconventional superconductivity. Interestingly, twisted graphene multilayers provide a playground for engineering tunable electronic dispersion, even in cases when interactions do not dominate electronic properties. Here [5] we demonstrate how a topological superconducting state can be induced in a 1.5-degree twisted graphene bilayer proximitized to an s-wave superconductor and a ferromagnet. The topological character is enabled by the Moiré pattern and the Chern number can be tuned through gate-controlled electronic filling, strain, and Ising spin-orbit coupling. We show that Ising spin-orbit coupling allows switching the Chern number of the topological state, and we address the tunability of the state via strain in the system. Our results put forward a protocol to engineer highly tunable topological superconducting states by exploiting proximity effects in twisted graphene bilayers

References

[1] Kezilebieke, S., Huda, M.N., Vaňo, V. et al. Topological superconductivity in a van der Waals heterostructure. *Nature* **588**, 424-426 (2020).

[2] S hawulienu Kezilebieke, Viliam Vaňo, Md N. Huda, Markus Aapro, Somesh C. Ganguli, Peter Liljeroth, and Jose L. Lado, *Nano Letters* **22**, 328-333 (2022).

[3] Cao, Y., Fatemi, V., Fang, S. et al. Unconventional superconductivity in magic-angle graphene superlattices. *Nature* **556**, 43–50 (2018).

[4] Cao, Y., Park, J.M., Watanabe, K. et al. Pauli-limit violation and re-entrant superconductivity in moiré graphene. *Nature* **595**, 526–531 (2021).

[5] Maryam Khosravian, Elena Bascones, and J. L. Lado, in preparation (2023).

My Abstract for Physics Days 2023

Mayank Kumar[*,1,3], Mayank Kumar[†,1,3], K. Murawski[1], B. Kuzma,[2] E.K.J. Kilpua,[3] L. Kadowaki[1]

1 Institute of Physics, Maria Curie-Skłodowska University, Pl. M. Curie-Skłodowskiej 1, 20-031 Lublin, Poland
[2] Centre for Mathematical Plasma Astrophysics / Department of Mathematics, KU Leuven, Celestijnenlaan 200B, 3001 Leuven, Belgium
[3] Department of Physics, University of Helsinki, Helsinki, Finland

Tittle: Impulsively generated two-fluid waves in the solar chromosphere: heating and generation of plasma outflows

Abstract

Context. The source of thermal energy release in the solar chromosphere and the origin of the solar wind remains unsolved problems.

Aims. The plasma in the chromosphere radiates more heat energy than the corona. To heat it up, an additional source of heating is required. This study attempts to reveal the mechanism responsible for chromosphere heating and plasma outflows which higher up may result in the generation of the solar wind. The ion-neutral collisions can play a significant role in the heating of the partially ionized plasma. The main aim of this paper is to investigate the impulsively generated two-fluid waves in a 2.5-dimensional (2.5D) model of the chromosphere that is permeated by the vertical magnetic field with a focus to examine the heating and its related generation of plasma outflows. Fine attention is paid to wave damping due to ion-neutral collisions.

Methods. Two-fluid equations are solved by the **JO**int **AN**alytical **N**umerical **A**pproach (JOANNA) code. Here electrons + ions and neutrals are treated as separate fluids which are coupled via ion-neutral collisions. The latter acts as a dissipation mechanism for energy carried by two-fluid waves and may ultimately lead to the frictional heating of the partially ionized plasma. The two-fluid waves, which are launched from the bottom of the chromosphere, are excited by a localized pulse in the horizontal components of ion and neutral velocities.

Results. The impulsively generated two-fluid waves propagate through the chromosphere, with their amplitude increasing due to pressure scale-height. In the middle and top chromosphere, a substantial amount of energy carried by large amplitude two-fluid waves is dissipated in ion-neutral collisions, resulting in temperature increase, and plasma outflows are generated.

Conclusions. In conclusion, large amplitude two-fluid waves may be responsible for heating the chromosphere, which higher up may contribute to the origin of the solar wind, and a net vertical ion flow is directed outward, leading to plasma outflows in the low solar corona.

Key words. Sun: Chromosphere - Sun: Activity - Sun: Transition region - Methods: Numerical

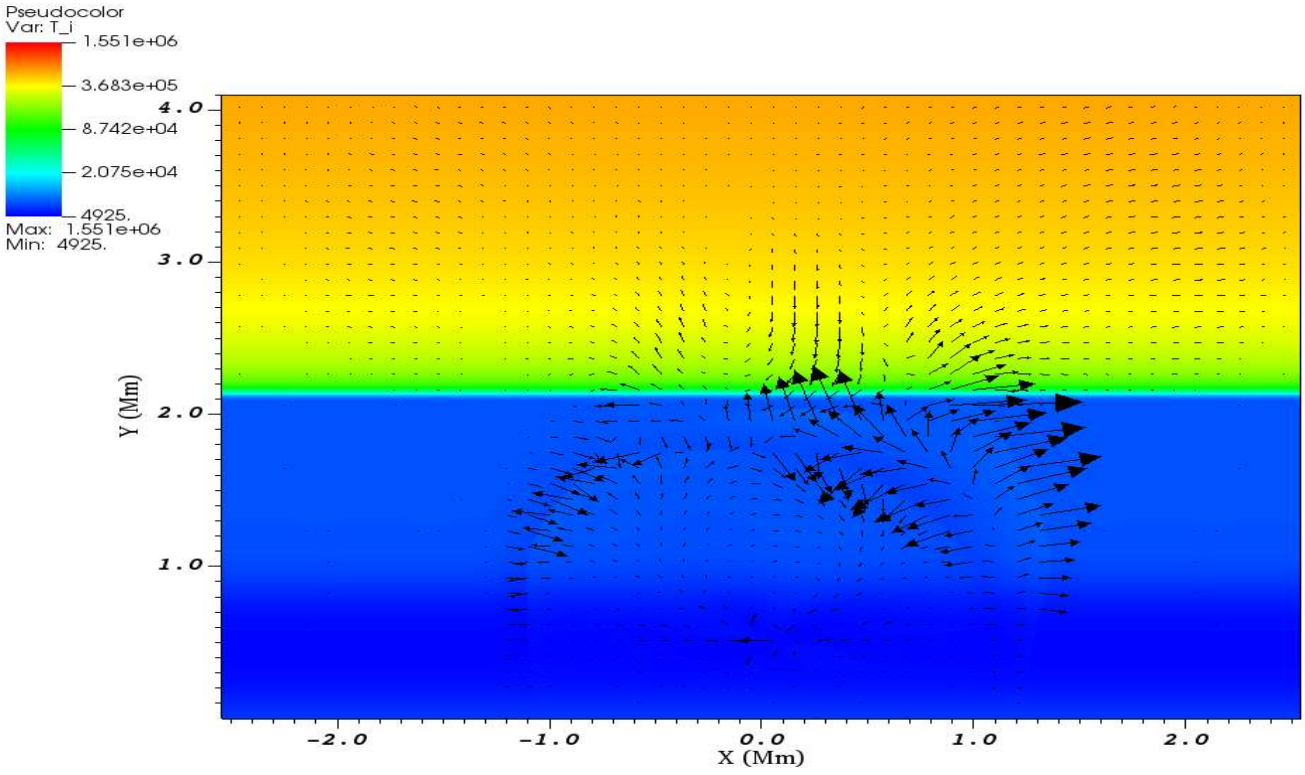

Fig. 1: Sprofiles of ion temperature (color map), expressed in Kelvins, and ion velocity (arrows) at t = 150s for Bz = 0 Gs.

[*]Corresponding author: mayankgis786@gmail.com
[†]Corresponding author: mayankgis786@gmail.com

Towards the Synthesis of Semiconducting Single-Walled Carbon Nanotubes by Floating-Catalyst Chemical Vapor Deposition

Er-Xiong Ding[*,1], Peng Liu[†,1], Abu Taher Khan[1], Qiang Zhang[1], Nan Wei[1], Hua Jiang[1], Esko I. Kauppinen[1]

[1] Department of Applied Physics, Aalto University School of Science, Puumiehenkuja 2, 00076, Aalto, Espoo, Finland

High-purity semiconducting single-walled carbon nanotubes (s-SWCNTs) are of paramount significance for the fabrication of high-performance electronics. Here, we present continuous production of high-purity, long, and isolated s-SWCNTs by gas-phase synthesis, retaining the pristine morphologies of as-synthesized nanotubes. The purity of as-produced s-SWCNTs with a mean length of 15.2 μm can reach 98% as determined by the optical absorption spectrum. The overpressure in the reactor and methanol were found to be the principal causes of the enrichment of s-SWCNTs. The mechanism of gas-phase synthesis of s-SWCNTs was also explored with in-situ infrared spectrometer and aerosol electrometer, indicating that the s-SWCNTs are more negatively charged, and oxygen-contained species play critical roles in s-SWCNT synthesis. Through the demonstration of field-effect transistors, the s-SWCNTs exhibit a high mean charge carrier mobility of 485.3 $cm^2 V^{-1} s^{-1}$ which is 2.4 times higher than that of the transistors fabricated with high-quality solution-processed SWCNTs. Our study represents an important step towards the scalable production of clean, long, and isolated s-SWCNTs with high purity and narrow bandgap distribution.[1]

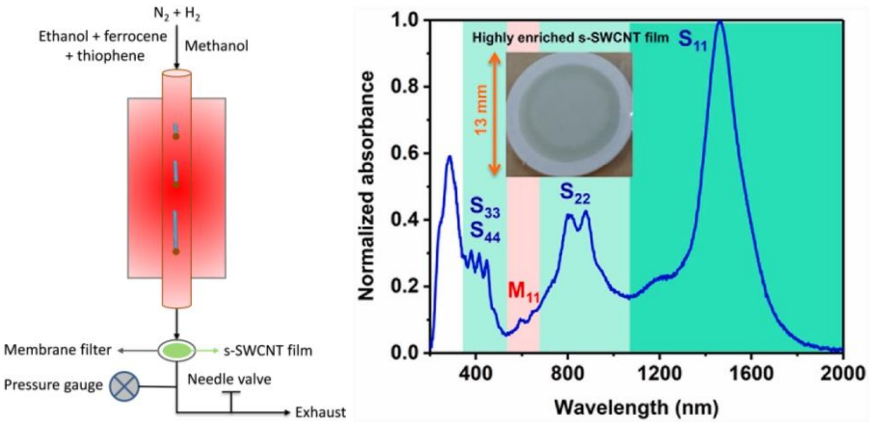

Figure 1. (a)The schematics of the floating catalyst chemical vapor deposition reactor for the synthesis of s-SWCNTs. (b) Highly enriched s-SWCNT film[1]

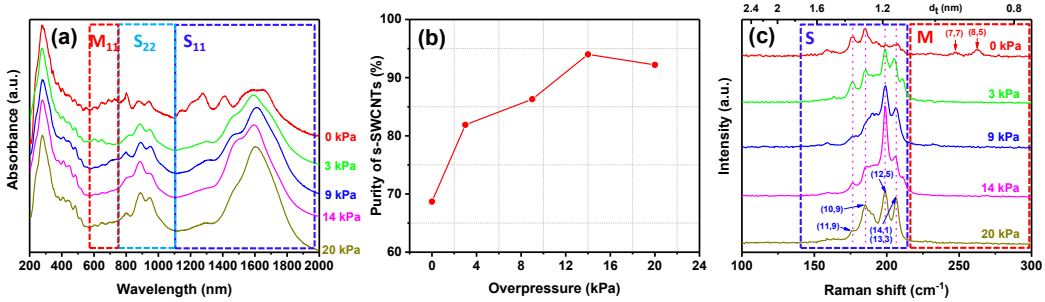

Figure 2. Optical characterizations of the effect of barometric pressure inside the quartz tube on the purity of s-SWCNTs.

The barometric pressure was found to be able to modulate the purity of as-synthesized s-SWCNTs. We hypothesize that this arises because overpressure promotes the growth of s-SWCNTs with specific chiral indices by lowering their nucleation barriers and accelerating the formation of corresponding carbon caps,[2] or by producing catalyst particles with more even morphology and/or structure distribution.[3,4] Theoretical calculations have predicted that large-chiral angle SWCNTs need lower activation energies for cap formation compared to those with smaller chiral angles.[5,6] It has also been reported that higher pressure inside the reaction system favours the growth of SWCNTs with specific chiral indices, narrowing either the chirality distribution[2] or the diameter distribution.[7] In our work, a few low absorption peaks can be found in the S_{11} region of the spectrum labelled with 0 kPa. Whereas other spectra present a sharp and dominant peak in the S_{11} region while the neighbouring absorption peaks are suppressed, revealing the enrichment of s-SWCNTs with certain chiral indices and narrow chirality distributions.

References

[1] E.-X. Ding, P. Liu, A. T. Khan, Q. Zhang, N. Wei, H. Jiang, E. I. Kauppinen, Carbon, **195**, 92, (2022)
[2] B. Wang, L. Wei, L. Yao, L. J. Li, Y. Yang, Y. Chen, J. Phys. Chem. C **111**, 14612, (2007).
[3] F. Zhang, P.-X. Hou, C. Liu, B.-W. Wang, H. Jiang, M.-L. Chen, D.-M. Sun, J.-C. Li, H.-T. Cong, E. I. Kauppinen, H.-M. Cheng, Nat. Commun. **7**, 11160, (2016).
[4] F. Yang, X. Wang, J. Si, X. Zhao, K. Qi, C. Jin, Z. Z. Zhang, M. Li, D. Zhang, J. Yang, Z. Z. Zhang, Z. Xu, L.-M. M. Peng, X. Bai, Y. Li, ACS Nano **11**, 186, (2017).
[5] S. Reich, L. Li, J. Robertson, Chem. Phys. Lett. **421**, 469, (2006).
[6] V. I. Artyukhov, E. S. Penev, B. I. Yakobson, Nat. Commun. **5**, 4892, (2014).
[7] Y. CHEN, J. Catal. **226,** 351, (2004).

[*]Corresponding author: erxiong.ding@aalto.fi
[†]Corresponding author: peng.1.liu@aalto.fi

Photoluminescence of 1T-TaS_2 at different phases

Zixuan Ning*[,1], Yi Zhang[1], Zhipei Sun[1]
[1] Department of Electronics and Nanoengineering, Aalto University, Espoo 02150, Finland

1T-phase metallic tantalum disulfide TaS_2 is one of the most frequently investigated two-dimensional (2D) materials due to its exotic states introduced by the collective electronic phases [1]. The phase of 1T-TaS_2 is characterized by charge density wave (CDW) that is coupled with periodic lattice distortion, which turns out to be commensurate with the crystal lattice and shows a metal-to-insulator phase transition without significant Fermi surface nesting [2]. Although the phase transition has been studied by various methods (e.g., Raman spectroscopy), a detailed study on photoluminescence (PL) of metallic 1T-TaS_2 is still lacking. Here we study the temperature-dependent PL of few-layer mechanically exfoliated 1T-TaS_2 deposited on a SiO_2/Si-substrate.

Figure 1(a) shows a schematic of the experimental setup for Raman and PL spectroscopies, the excitation wave is a CW laser with a wavelength of 532 nm. The inset in Fig. 1(a) is the optical image of a few-layer 1T-TaS_2 without the wrap of hexagonal boron nitride (hBN). The power used for Raman and PL measurement is 0.741 mW 4.78 mW, respectively. The temperature during the investigation is precisely controlled in the range of 83K to 283K with a step of 20 K. Figure 1(b) shows the temperature-dependent Raman spectra from few-layer TaS_2 encapsulated with a top hBN as the protection layer, which is fabricated in the isolated condition. It is obvious that one peak disappears when the temperature increases from 83 K to 143 K, which is associated with phase transition due to lattice distortion [3, 4]. Note that the main peak at 71 cm^{-1} shows a small red shift. Figure 1(c) shows the temperature-dependent PL of 1T-phase metallic TaS_2. As the temperature increases from 83 K to 263 K, the PL intensity decreases first and then increases. However, when the temperature goes up to 283 K, the PL intensity goes down a lot.

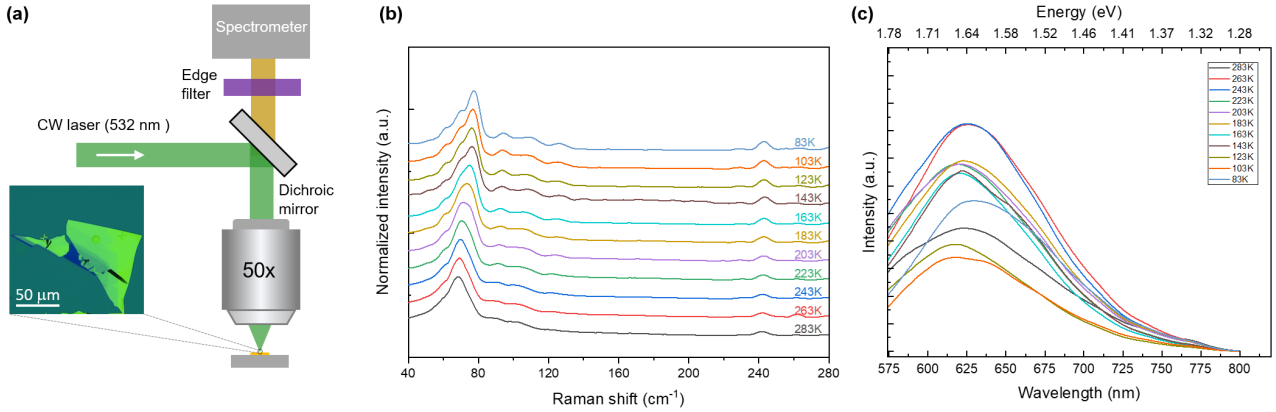

Figure 1. Temperature-dependent Photoluminescence (PL) and Raman spectra of few-layer 1T-TaS_2. (a) Schematic Experiment setup for the PL and Raman measurement, the inset is the optical image of 1T-TaS_2 without the hBN encapsulation. (b) Temperature-dependent Raman spectra of the 1T-TaS_2. (c) Temperature-dependent PL spectra of the 1T-TaS_2.

In conclusion, we studied the temperature-dependent PL and Raman characteristics of 1T-phase metallic TaS_2. To minimize the influence of defects and impurities on the PL measurements, we fabricated the sample with a protective hBN layer in isolated conditions. From the Raman spectra, it is justified to attribute the PL signal below 143 K to the 2H-phase TaS_2, which has been reported due to the photon excited electron radiation [5]. The explanation for the PL signal above 143 K needs further investigation, where the 1T-phase TaS_2 is a metal. The exploration shown here may cause interest in the study of phonon energy, exciton recombination, and electron-phonon interaction in different 2D-CDWs [6, 7].

References

[1] Zhu, C. et al. "Light-tunable 1T-TaS_2 charge-density-wave oscillators", ACS Nano **12**, 11203–11210 (2018).
[2] Ying, J. et al. "Unusual pressure-induced periodic lattice distortion in $SnSe_2$", Phys. Rev. Lett. **121**, 27003 (2018).
[3] Lacinska, E. M. et al. "Raman Optical Activity of 1T-TaS_2", Nano Lett. **22**, 2835–2842 (2022).
[4] Zhao, R. et al. "Tuning phase transitions in 1T-TaS_2 via the substrate", Nano Lett. **17**, 3471–3477 (2017).
[5] Mahajan, M. et al. "Light emission from the layered metal 2H-$TaSe_2$ and its potential applications", Commun. Phys. **2**, 88 (2019)
[6] Shi, J. et al. "Two-dimensional metallic tantalum disulfide as a hydrogen evolution catalyst", Nat. Commun. **8**, 1–9 (2017)
[7] Zhang, Y. et al. "Coherent modulation of the electron temperature and electron–phonon couplings in a 2D material", Proc. Natl. Acad. Sci. **117**, 8788–8793 (2020).

*Presenting and corresponding author: zixuan.ning@aalto.fi

Sensitivity of rt-TDDFT electronic stopping calculations in semiconductor crystals with plane-wave pseudopotentials.

Rafael Núñez[*1], **Andrea Sand** [1]
1. Department of Applied Physics - Aalto University

The development of a model that includes electronic energy losses in a molecular dynamics formalism for carrying out large scale radiation damage simulations is an active research area [1]. To provide meaningful insights, in particular for the high-energy electronic stopping regime, we investigate the significance of simulations of electronic energy losses in silicon and germanium using the *ab-initio* rt-TDDFT technique with plane-wave pseudopotentials [2].

We characterize the effect of increasing the number of explicit electrons on both projectile and target atoms and determine the regions where a higher number of electrons is needed in terms of the projectile path, its kinetic energy, and its impact parameter with target atoms. We want to provide a complete picture of how to obtain high fidelity predictions of instantaneous electronic energy losses in semiconductor crystals, without the expense of explicitly considering all the electrons in the system.

References

[1] Thomas Jarrin, Antoine Jay, Anne Hemeryck, and Nicolas Richard. Parametric study of the two-temperature model for molecular dynamics simulations of collisions cascades in si and ge. Nuclear Instruments and Methods in Physics Research Section B: Beam Interactions with Materials and Atoms, 485:1–9, 2020
[2] Alfredo A. Correa. Calculating electronic stopping power in materials from first principles. Computational Materials Science, 150:291–303, 2018.

[*]Corresponding author: rafael.nunez@aalto.fi

Modeling Wave Evolution in Heliospheric Plasma

Seve Nyberg[*1], **Rami Vainio** [1], **Alexandr Afanasiev** [1]
1. Department of Physics and Astronomy, University of Turku, Vesilinnantie 5, 20014 Turku

Under Wentzel–Kramers–Brillouin (WKB) approximation, a magnetohydrodynamic (MHD) wave propagates in a static background plasma conserving its frequency and refracting under the laws of geometric optics. Alfvén waves have the property that their group velocity is directed along the magnetic field and the refraction of the wave vector is towards the lower values of the Alfvén speed. MHD wave spectra in magnetized plasmas determine the transport parameters of energetic charged particles [Schlickeiser 1989], which are an important element of solar eruptions like solar flares and coronal mass ejections. Thus, modeling wave evolution is important in self-consistent particle acceleration modeling.

The model presented solves the spectral energy density of waves efficiently using a diffusionless semi-Lagrangian scheme. The model can be used to solve for different kinds of wave evolution scenarios, including, e.g., wave-wave interactions and spatially and temporally variable magnetic fields and plasma parameters.

As an example, we present a model for wave evolution in a coronal loop. Coronal loops are closed magnetic field structures in the solar atmosphere, filled with dense plasma. They vary greatly in lengths ranging from tens to tens of thousands of kilometers, or even further. Loops are important in many regions of the corona, including the active regions where the solar active phenomena, such as flares, are hosted. In the case of a closed field line, both ends of the field line can inject waves into the system. This leads us to a situation where counter-propagating waves are present. Thus, wave-wave interactions between counter-propagating waves become a topic of investigation to find out how the spectral energy density of the waves is evolving beyond the WKB approximation.

To the lowest order, i.e., under the weak turbulence approximation, wave-wave interactions can be treated as three-wave interactions, where two waves either coalesce to produce a single wave or a single wave decays to produce two waves. We consider the effects of three-wave interactions on Alfvén wave spectra on a closed magnetic field line. The spectra are then used to evaluate the transport parameters of energetic particles in a coronal loop. The wave-wave interaction model and results were discussed in detail in Nyberg & Vainio [2022].

Additionally, we'll shortly discuss applications in models of particle acceleration in coronal shocks to solve for global particle transport parameters.

References

[1] Schlickeiser, R. 1989: Astrophysical Journal, 336, 243
[2] Nyberg, S. & Vainio, R. 2022: Physics, 4, 394-408.

[*]Corresponding author: shonyb@utu.fi

Optical emission spectroscopy of nanoparticle flame for active optical fiber fabrication

Joonas Ojala[*1], **Juha Toivonen**[1], **Juha Harra**[2], **Jyrki M. Mäkelä** [1]
1. Tampere University, Physics unit, P.O. Box 692, FI-33014 Tampere University, Finland
2. nLight, Sorronrinne 9, 08500 Lohja, Finland

Spray-based flame synthesis methods are cost-effective and scalable methods of generating nanoparticles, mostly oxides, for both industrial and research purposes. The method is based on spraying a liquid precursor into the flame, where it then enters the gas phase and later condenses into particles. The highly turbulent flame itself is sustained with separate hydrogen and oxygen gas feeds. It is possible to fine-tune the end-product by varying the process parameters empirically, but the specifics depend upon the associated process pathways that are largely unknown. [1]

In this work, we study optical fiber fabrication using a flame-based synthesis method called direct nanoparticle deposition (DND) [2]. Spatially varying optical emission spectroscopy (OES) measurements are conducted on the flame with varying compositions to gain insight into the associated flame dynamics, aerosol processes and the evolution of the chemical composition. The flame consists of multiple different components, such as chemical precursors and product particles, in various phases. The spectrum, shown in Figure 1 on the right, shows the line peaks corresponding to the chemicals in the gas phase, as well as the black body radiation arising from the formed particles. Spectra are captured at different positions, which allows one to determine the evolution of the aforementioned features. In addition to this, a high speed camera with different filters is used to gain information about the spatial distribution of the flame at specific wavelength regions. This is seen in Figure 1 on the left. Size and material dependent calculations are used to model the optical properties of the nanoparticle to study the broadband radiation and to gain information about the particles.

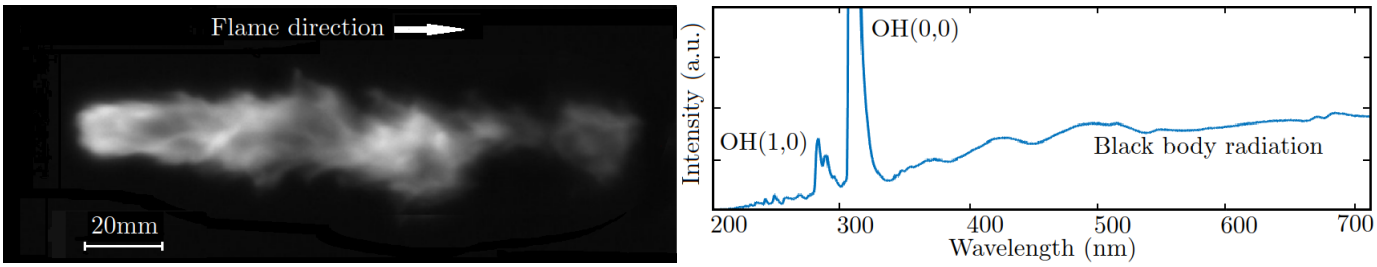

Figure 1: Left: Image of the flame without a filter with 50μs shutter speed. Right: Emission spectrum measured at a distance of 95 mm from the start of the flame. Black body radiation due to silica nanoparticles is visible, as well as the (0,0) and (1,0) vibration bands of the OH-molecule.

Although flame-based synthesis methods have been in use for a long time, research focusing on the process pathways of spray-based flame synthesis methods is still ongoing [3]. In 2022, Lalanne, et al. [4] reported on the particle formation of iron oxide particles. Silica was chosen as a baseline for this study, as it is an important material in technological applications, such as fiber optics. A very limited amount of studies have been conducted towards silica-based flame via OES or the optical properties of silica at high temperatures in general. This study allows for a better understanding of the flame details and aids in the development of in-situ monitoring for flame-based industrial purposes.

References

[1] Rajala M., Janka K., Kykkänen P., An industrial method for nanoparticle synthesis with a wide range of compositions, Reviews on Advanced Materials Science, 5 (2003) 493–497.
[2] Tammela S., Söderlund M, Koponen J., Philippov V., Stenius, P., The potential of direct nanoparticle deposition for the next generation of optical fibers, in: Digonnet M.J., Jiang S. (Eds.), Proceedings of SPIE 6116, Optical Components and Materials III, Society of Photo-Optical Instrumentation Engineers, San Jose, 2006, 61160G.
[3] Florian Meierhofer and Udo Fritsching Energy & Fuels 2021 35 (7), 5495-5537 DOI:10.1021/acs.energyfuels.0c04054
[4] Lalanne MR, Wollny P, Nanjaiah M, Menser J, Schulz C, Wiggers H, et al. Early particle formation and evolution in iron-doped flames. Combust Flame 2022:244.

[*]Corresponding author: joonas.ojala@tuni.fi

Non-Hermitian topological modes from local loss engineering in photonic arrays

Elizabeth Pereira[1], Jose L. Lado[1] and Andrea Blanco-Redondo[2]

[1]Department of Applied Physics, Aalto University, 02150 Espoo, Finland
[2]Nokia Bell Labs, 600 Mountain Ave., New Providence, New Jersey, NJ, 07974, United States of America

Non-Hermitian systems have risen as a powerful strategy to engineer new forms of topological excitations [1]. A variety of non-Hermitian models displaying topological modes rely on non-reciprocity, the change in probability of left-right propagation. However, non-reciprocity has remained challenging to implement in photonic devices. In stark contrast, modulated photonic losses provide an alternative way of implementing non-Hermiticity, representing a realistic approach to non-Hermitian photonics. Here [2] we present a family of photonic models relying on the real-space modulation of photonic losses giving rise to non-Hermitian topological excitations. We demonstrate that the non-Hermitian topological modes survive spatial fluctuations in the loss and couplings of the system, and we elucidate the topological invariant protecting these excitations. Our results provide a realistic strategy to create topological modes in photonic systems from real-space loss engineering.

[1] Emil J. Bergholtz, Jan Carl Budich, and Flore K. Kunst, Rev. Mod. Phys. 93, 015005 (2021)
[2] Elizabeth Pereira, Jose L. Lado and Andrea Blanco-Redondo, in preparation (2023)

Vacancy diffusion in equi-atomic WMoTaVNb refractory high entropy alloy

Eryang Lu[*,1], Kenichiro Mizohata[1], Anna Liski[1], Ilja Makkonen[1], Ko-Kai Tseng[2], Che-Wei Tsai[2,3], Jien-Wei Yeh[2,3] and Filip Tuomisto[1,2]

[1] Department of Physics, University of Helsinki, P.O. Box 43, 00014 Helsinki, Finland
[2] Department of Materials Science and Engineering, National Tsing Hua University, Hsinchu 30013, Taiwan
[3] High Entropy Materials Center, National Tsing Hua University, Hsinchu 30013, Taiwan

High entropy alloy, or multi-principal element alloy, have gained particularly strong research interest in recent decades [1-2]. In this work, we have applied in-situ positron annihilation lifetime measurements [3] to characterize particle irradiation-induced mono-vacancy defects in equi-atomic WMoTaVNb refractory high entropy alloy at cryogenic temperatures. Isochronal annealing started from 40 K up to 850 K were carried out in order to understanding the evolution and recovery characteristics of mono-vacancies in the samples. We find the mono-vacancy migration is activated with the annealing temperature over 600 K. A widely recovery stage of irradiation-induced damage has been obtained with the annealing temperature 600 – 750 K, which suggests a wide distribution of vacancy migration barriers in the random alloy. On the other hand, vacancy clustering has been observed by increasing the annealing temperature owing to the lattice distortion and chemical complexity, which suppression the long-range diffusion of vacancy defects.

References

[1] J.W. Yeh, S.K. Chen, S.J. Lin, J.Y. Gan, T.S. Chin, T.T. Shun, C.H. Tsau and S.Y. Chang, Adv. Eng. Mater. **6**, 299 (2004).
[2] D. B. Miracle and O. N. Senkov, Acta Mater. **122**, 448 (2017).
[3] F. Tuomisto and I. Makkonen, Reviews of Modern Physics, **85,** 1583 (2013)

[*]Corresponding author: first.author@email.com
[†]Corresponding author: presenting.author@email.com

Capillary interaction driven ordering of multiwalled carbon nanotubes at the air-water interface

E. Hyyryläinen, J. Merikoski, M. Ahlskog[†]
Department of Physics and Nanoscience Center, University of Jyvaskyla, FI-40014, Finland

The anisotropy of small particles has very apparent consequences for how capillary forces affect their ordering at fluid interfaces [1]. Particles that are called "small" in this context, usually mean such that buoyancy forces are negligible, less than 10 mm. Carbon nanomaterials, fullerenes, nanotubes, and graphene, have in this particular field had a rather modest role, compared with their impact elsewhere. However, especially the micron scale carbon nanotubes, that are either single wall nanotubes (SWNT) or multiwall nanotubes (MWNT), should be of interest, not least due to the superior aspect ratio and stiffness. Intrinsically, they are starkly hydrophobic.

We have investigated experimentally the ordering of multiwalled carbon nanotubes (MWNT) induced by capillary forces at the air-water interface [2]. The arc-discharge synthesized MWNTs had typical dimensions with diameters of around 10 nm and lengths at around 1 μm, and were of high quality, but were mixed with graphitic impurity particles in the 10 – 100 nm size range [3]. The experiments were conducted with a special technique that distributed the hydrophobic MWNT material on a spreading water droplet [4]. We observed chain-like structures of end-to-end ordered MWNTs with the graphitic impurity particles attached to the tubes and attachment of chain ends to the contact line. We analyze this ordering as a result of the capillary interaction between the tubes and that resulting from the curvature of the droplet surface. The drying process displayed similarities with the well-known coffee ring effect. The MWNT chain structures survived the drying of the droplet and could be inspected with SEM, as shown in Fig. 1.

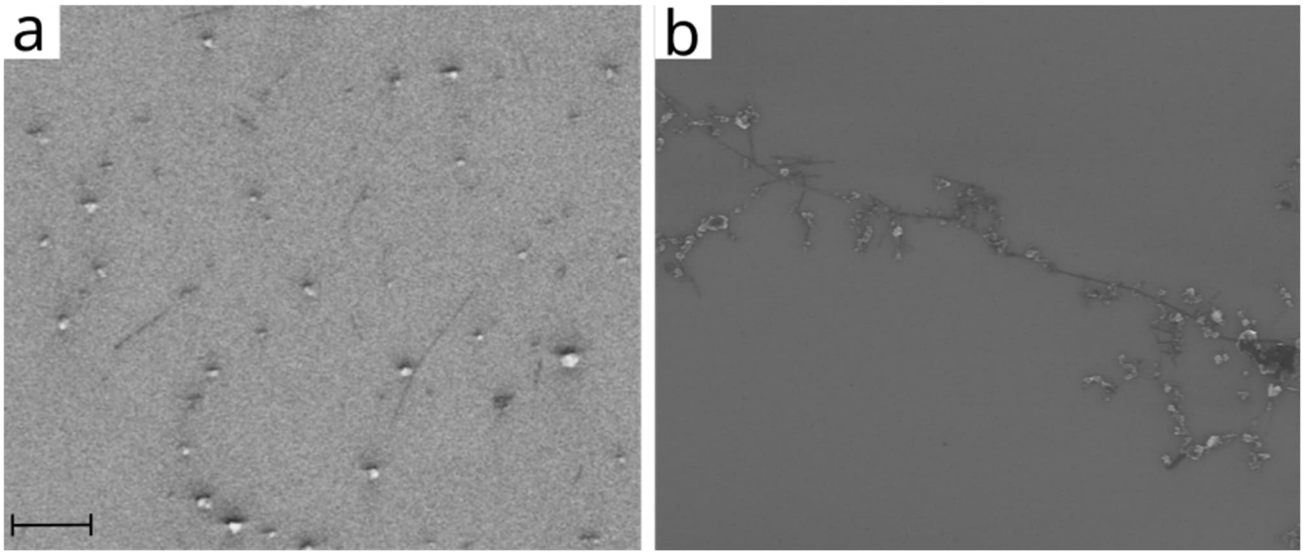

Figure 1. SEM images of the MWNT material before (a) and after (b) the experiment. (a) Typical deposition of the spin-coated MWNT material on a Si chip. Besides MWNTs, there is plenty of graphitic amorphous carbon particles (ACP). (b) Part of an MWNT chain after redeposition from the water droplet used in the experiment. Scale bar 1 μm.

References

[1] I.B. Liu, N. Sharifi-Mood, K.J. Stebe, Ann. Rev. of Cond. Matt. Physics, **9**, 283 (2018)
[2] E. Hyyryläinen, J. Merikoski, M. Ahlskog, unpublished.
[3] M. Ahlskog, M.J. Hokkanen, D. Levshov, K. Svensson, A. Volodin, C. van Haesendonck, J. Vac. Sci. Technol. B **38**, 042804 (2020)
[4] M.J. Hokkanen, S. Lautala, E. Flahaut, M. Ahlskog, Colloids and Surfaces A, **533**, 109 (2017)

[†]Corresponding author: ahlskog@jyu.fi

Molecular dynamics studies on swift heavy ion-induced nitrogen-vacancy center formation in diamond

Chloé Nozais, Aleksi Leino†, Flyura Djurabekova
Department of Physics, University of Helsinki, P.O. Box 43, FI-00014, Finland

Nitrogen vacancy centers (NV-) in diamond are promising candidates for qubits due to the stability and longevity of their quantum states. The states can also be entangled in multiple ways for building quantum networks. These defects can be produced in nitrogen-doped diamonds using ion beam techniques, but the formation mechanism is not yet well understood. Typically, the samples are first irradiated with keV ions and must be subsequently annealed to form the centers [1]. Recently, it was observed that when the irradiation is performed at GeV energy instead, NV- centers form in the beam direction along a well-defined chain without annealing [2]. This observation makes high energy ions potentially useful for manufacturing the defects and provides insights into their formation mechanism. We have studied both energy regimes using molecular dynamics simulations. Preliminary results suggest that the difference can be explained in terms of the vacancy formation and diffusion behaviours at the different energy regimes.

References

[1] F. Jelezko and J. Wrachtrup, Phys. Status Solidi A **203**, 3207–3225 (2006)

[2] R. E. Lake, A. Persaud, C. Christian, E. S. Barnard, E. M. Chan, A. A. Bettiol, M. Tomut, C. Trautmann, and T. Schenkel, Appl. Phys. Lett. **118**, 084002 (2021)

†Corresponding author: aleksi.leino@helsinki.fi

Effects of Surface Wettability and Humidity on Nano and Micro-scale Electrical Breakdown of Air

Ali Afzalifar[*,1], Gentrit Zenuni[1], Robin H. A. Ras[1,2]

[1] Department of Applied Physics, Aalto University School of Science, Puumiehenkuja 2, 02150 Espoo, P.O. Box 15100, Aalto FI-00076, Finland

[2] Department of Bioproducts and Biosystems, Aalto University School of Chemical Engineering, P.O. Box 16000, Aalto FI-00076, Finland

Unlike larger scales, the Paschen's law fails to predict the electrical breakdown when the gap between electrodes is smaller than ~5µm [1,2]. Over the past three decades, there has been a growing interest in research on electrical breakdown at micro-scales or even smaller scales, i.e. when the distance between the electrodes is smaller than 10 µm. The interest is fuelled by two different communities with opposite aims. From the standpoint of the microelectromechanical systems (MEMS) community, the electrical breakdown is an undesirable phenomenon which has to be avoided. The reason is that due to ever-decreasing size of MEMS systems (dealing with micro- and nanoscale dimensions), many new electrical equipment is prone to damage by electrical breakdown and micro-discharge between biased parts at microscale distances. In contrast, in the plasma research community, the aim is to generate and facilitate breakdown and thus enhance plasmas at microscales. Moreover, micro-discharge is extensively used in many fields as diverse as chemical analysis, biomedical processes, and surface patterning for nanomaterials. Therefore, regardless of the aim, understanding and providing a means of control over the breakdown process at microscales are of great significance in numerous applications.

We have performed experimental work to assess the effect of surface wettability of electrodes in presence of humidity on the process of electrical breakdown at different distances between the electrodes (0.1, 0.2, 0.3, 0,4, 0.5, 1.0, 2.0, 3.0, 4.0 and 5.0 µm). In our work, in line with the results available in literature, it is observed that the Paschen's law cannot be applied for these range of distances between the electrodes. We have shown that humidity considerably decreases the voltage required for the breakdown process for micro and nano-scale gaps. Moreover, for the first time, we have shown that by changing the hydrophobicity of the elected surface, it is possible to control (decrease/increase) the voltage required for the breakdown of air.

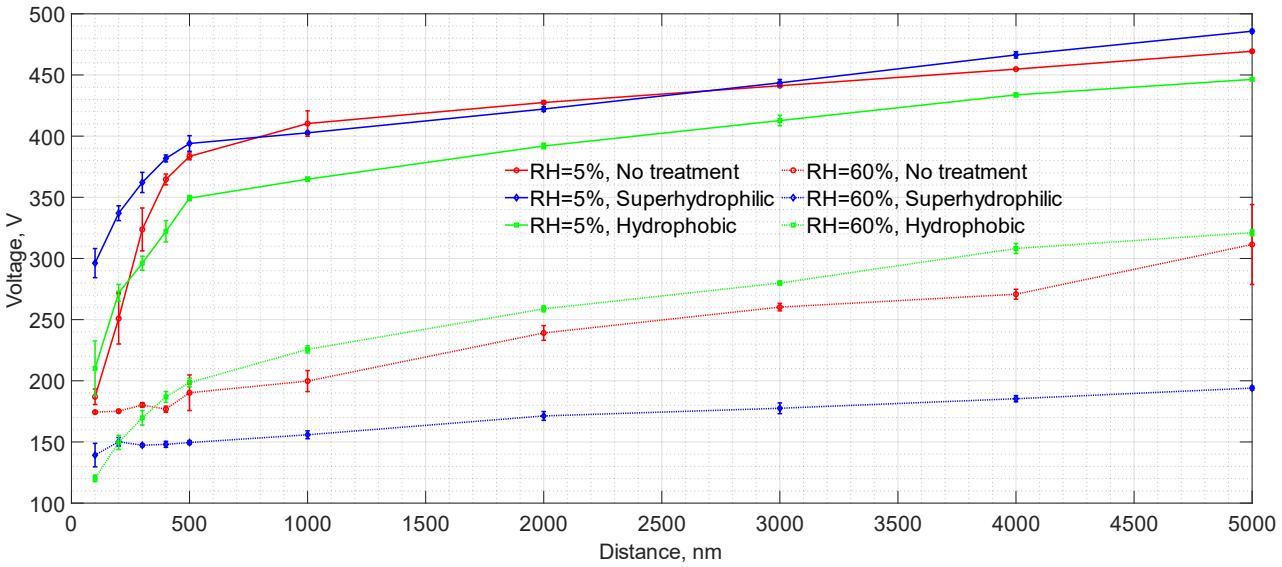

Table 1. The voltage required for electrical breakdown at different distances between electrodes and electrode surface treatment in terms of wettability, RH stands for the relative humidity.

References

[1] 3] J.-M. Torres and R. S. Dhariwal, Nanotechnology **10**,102-107, (1999).
[2] R.-T. Lee, H.-H. Chung, and Y.-C. Chiou, IEE Proc. Sci. Meas. Technol., **148**, (2001).

*Corresponding author: ali.afzalifar@aalto.fi

My Abstract for Physics Days 2023

Henri Savolainen[*,1], **Matilda Backholm**[1], **Olli Ikkala**[1], **Hang Zhang**[1†]
1 Department of Applied Physics, Aalto University, P.O. Box 15100, FI 02150 Espoo, Finland

Tuned, reversible, interfacial adhesion is crucial for hydrogel-related device development. Despite the remarkable progress in controlling the interfacial adhesion in water-containing materials, strong and quick adhesion combined with easy removal still poses a challenge. In this work, we demonstrate resilient crosslinked hydrogels with light-triggered strong self-adhesion and time-dependent debonding. A swollen hydrogel containing gold nanoparticles achieves quick phase transition-induced interfacial adhesion, where the irradiation precisely controls local polymer entanglement and interactions. The adhesion strength is time-dependent and decreases with time, decreasing to 0% in 24 hours. With a dehydration-based polymer entanglement mechanism, the dominant role of water in controlling adhesion is further revealed in measurements. The proposed mechanism, manifesting in facile, efficient, and light-programmable hydrogel adhesion, can be applied to various fields like soft robotics, biomedical, and flexible electronics.

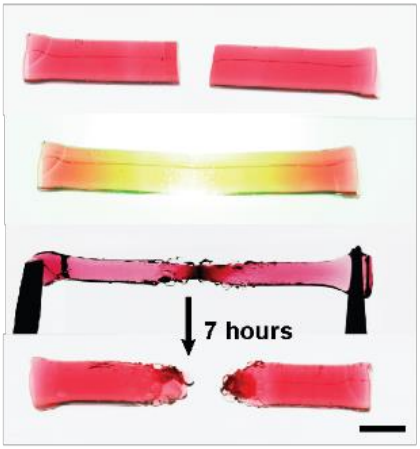

Figure 1: The phenomenon shown in four steps. First two parts, second irradiation of the interface, third the adhesion and pulling, fourth splitting of the sample after 7 hours.

[*]Corresponding author: henri.2.savolainen@aalto.fi
[†]Corresponding author: hang.zhang@aalto.fi

Measurement of the Quantum Geometry Tensor in a Plasmonic Lattice

Javier Cuerda, Jani M. Taskinen*, Nicki Källman, Jan L. Herrmann, Päivi Törmä†
Department of Applied Physics, Aalto University School of Science, Aalto FI-00076, Finland

Topologically protected modes in the field of Photonics enable fundamentally new types of optical applications which circumvent fabrication defects and may feature unidirectional propagation, in diverse platforms such as arrays of helical waveguides [1] and photonic crystals [2]. An important tool in the description of these topological systems is the quantum geometric tensor (QGT) which contains the quantum metric as the real part and the Berry curvature as the imaginary part. The QGT characterizes the Hamiltonian eigenstate structure, and it is crucially connected to an increasing number of topology-related phenomena, including superfluidity in flat bands [3].

Measurements of the QGT have been performed in several systems such as microcavities [4] or nitrogen-vacancy centers in diamond [5]. Plasmonic lattices also represent an attractive platform for topological studies as they support protected bound states in continuum [6] and polarization textures [7]. They sustain electromagnetic modes called surface lattice resonances (SLRs) that emerge from the long-range radiative interactions provided by the diffraction orders of the lattice, which mediate between the localized resonances of individual nanoparticles. The description of SLRs goes well beyond tight binding approximations, opening an intriguing new regime for studies on topological photonics.

Here we present measurements of the QGT in a plasmonic lattice, showing novel non-trivial topological features that result from time-reversal symmetry breaking. We confirm these results with extensive numerical simulations and a simplified lattice model, concluding that the observed effects emerge from the interplay of polarization-dependent properties of SLR bands and the unique mode structure ruled by long-range radiative interactions [8]. Owing to the ease of nanofabrication and flexible design of plasmonic lattices, we expect these phenomena to extend to multiple lattice geometries, exotic particle shapes and arrangements, and magnetic materials.

References

[1] M. C. Rechtsman, J. M. Zeuner, Y. Plotnik, Y. Lumer, D. Podolsky, F. Dreisow, S. Nolte, M. Segev, A. Szameit, Nature **496**, 196–200 (2013).
[2] Z. Wang, Y. Chong, J. D. Joannopoulos, M. Soljačić, Nature **461**, 772–775 (2009).
[3] S. Peotta, P. Törmä, Nat. Commun. **6**, 8944 (2015).
[4] A. Gianfrate, O. Bleu, L. Dominici, V. Ardizzone, M. De Giorgi, D. Ballarini, G. Lerario, K. W. West, L. N. Pfeiffer, D. D. Solnyshkov, D. Sanvitto, G. Malpuech, Nature **578**, 381–385 (2020).
[5] M. Yu, P. Yang, M. Gong, Q. Cao, Q. Lu, H. Liu, S. Zhang, M. B. Plenio, F. Jelezko, T. Ozawa, N. Goldman, J. Cai, Nat. Sci. Rev. **7**, 254–260 (2020).
[6] R. Heilmann, G. Salerno, J. Cuerda, T. K. Hakala, P. Törmä. ACS Photonics, **9**, 1, 224–232 (2022).
[7] J. M. Taskinen, P. Kliuiev, A. J. Moilanen, and P. Törmä, Nano Letters **21**, 5262–5268 (2021).
[8] J. Cuerda, J. M. Taskinen, N. Källman, J. L. Herrmann, P. Törmä, Manuscript in preparation (2023).

*Corresponding author: jani.m.taskinen@aalto.fi
†Corresponding author: paivi.torma@aalto.fi

Turbulence generated by large-scale velocity shears in the solar wind

J. E. Soljento*, S. W. Good, A. Osmane, E. K. J. Kilpua
Department of Physics, University of Helsinki, Finland

The solar wind, the continuous flow of plasma from the Sun into the heliosphere, contains velocity and magnetic field fluctuations on a wide range of scales. The properties of these fluctuations are consistent with the presence of a turbulence cascade. Turbulence is a fundamental process that transfers energy from large energy-injection scales to successively smaller scales through a cascade of eddies, until a scale is reached where energy is lost to particle heating.

Turbulence in the solar wind results from the nonlinear interaction between Alfvénic fluctuations propagating toward and away from the Sun. Most of the fluctuations propagate away from the Sun, with the minority sunward component being generated locally. One candidate source for the sunward fluctuations is velocity shear, which refers to the interaction that occurs between two layers of plasma that flow parallel to each other but at different speeds.

Coronal mass ejections (CMEs) are large-scale eruptions of plasma entrained in a magnetic field. They are launched from the solar corona, and from there they propagate into interplanetary space along with the solar wind. If a CME travels faster than the surrounding solar wind plasma, it drives a shock wave ahead of it. The turbulent region between the shock and the CME itself is known as the sheath region. CMEs and the solar wind disturbances they generate are the major cause of 'space weather', which encompasses the range of potentially harmful effects at Earth, such as damage to satellites and power grids.

We have conducted a statistical study of the link between velocity shear and turbulence in 74 CME-driven sheath regions observed by the *Wind* spacecraft near Earth. Sheaths were studied, because they provide an excellent natural particle laboratory to study turbulence and its evolution, and they also contain more velocity shears than the solar wind in general. We investigated how the imbalance between counterpropagating fluctuations is modified by the presence of shear regions. Our results show that strong shears are associated with increased balance between fluctuations propagating sunward and antisunward, and therefore they may play a role in the local generation of turbulence in the solar wind.

*Corresponding author: juska.soljento@helsinki.fi

3D Printed Micro-optics for Enhancing Lateral Resolution of Coherence Scanning Interferometry

Ivan Kassamakov[*,1,2], **Gordon Zyla**[3], **Anton Nolvi**[1], **Göran Maconi**[1], **Dimitra Ladika**[4], **Vasileia Melissinaki**[3], **George Barmparis**[3], **Maria Farsari**[3], **Edward Hæggström**[1]

[1] Electronics Research Laboratory, University of Helsinki, Finland
[2] Helsinki Institute of Physics, Helsinki, Finland
[3] IESL-FORTH, Heraklion, Crete, Greece
[4] University of Crete, Crete, Greece

Coherence Scanning Interferometry (CSI) is a non-contact diffraction limited technique for three-dimensional (3D) surface characterization with angstrom-scale vertical resolution. To enhance the lateral resolution of CSI based devices micro-components like microspheres and fibres can be used [1,2]. In this way an apparatus for 3D imaging with nanometre vertical resolution and lateral resolution better than 100 nm could be designed.

In this work, we used two-photon polymerization (2PP) 3D-printed microspheres as a photonics nanojet (PNJ) generating structure. Since 2PP enables true 3D processing of photoresists at the microscale with sub-100 nm resolution, it is possible to print highly complex structures without compromises to their geometry [3]. We modelled imaging properties of different PNJ generating structures using an open-source software and manufactured three versions of them using photoresists with different refractive indices (see Fig. 1).

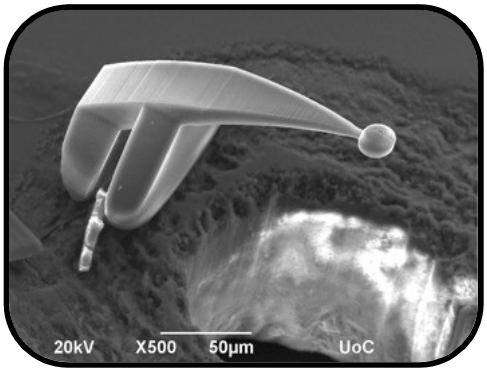

Figure 1. 3D printed photonic nanojet generating structure using two photon polymerization process. Diameter of the microsphere is 20 µm.

To test the components, we used a custom-made coherence scanning interferometer and imaged a sample with sinusoidal structure having a period of 280 nm. These first results are showing capability of new PNJ generating structures in combination with CSI device to image structures with a lateral resolution better than 100 nm (see Fig. 2).

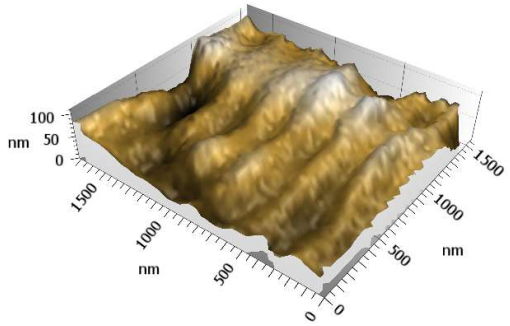

Figure 2. 3D image of a sinusoidal structure with a period of 280 nm.

3D printing by 2PP provides a high potential for mass-production of PNJ generating structures with complex shape due to its simple sample processing that does not require any vacuum or harsh chemicals and cleanroom environment. It also allows the PNJ generating structures to be manufactured with an integrated mounting solution. This will allow increasing of working distance and field of view of the next generation 3D super-resolution imaging systems.

References

[1] I. Kassamakov, S. Lecler, A. Nolvi, A. Leong-Hoi, P. Montgomery, E. Hæggström, Sci. Rep. **7**, 3683 (2017).
[2] A. Nolvi, I. Laidmäe, G. Maconi, J. Heinämäki, E. Hæggström, I. Kassamakov, Proc. SPIE **10539**, 1053912-1 (2018).
[3] M. Farsari, B. Chichkov, Nature Photon. **3**, 450 (2009).

[*]Corresponding author: ivan.kassamakov@helsinki.fi

Balanced Alfvénic fluctuations inside interplanetary coronal mass ejections

Simon Good*, **Lauri Hatakka, Matti Ala-Lahti, Juska Soljento, Adnane Osmane, Emilia Kilpua**
Department of Physics, University of Helsinki, Finland

Interplanetary coronal mass ejections (ICMEs) are vast eruptions of plasma from the Sun that propagate into the solar system. Like the solar wind, ICMEs contain fluctuating magnetic and velocity fields, with most fluctuation power at fluid scales residing in the Alfvén mode. The non-linear interaction of these Alfvénic fluctuations counter-propagating along the magnetic field drives a turbulent cascade in the plasma. The exact nature of the turbulence is partly determined by the degree to which the counter-propagating Alfvénic fluxes are balanced or imbalanced. From analysis of 226 ICMEs observed by the *Wind* spacecraft near Earth during 1995 – 2015 [1], we find that Alfvénic fluxes in ICME plasma are systematically more balanced than in the solar wind, which typically shows a strong anti-sunward imbalance. Superposed epoch profiles reveal that fluxes tend to be more balanced at the ICME front, with balance decreasing towards the ICME rear. Potential origins of the balanced state within ICMEs include the closed-loop magnetic field structure often found in ICMEs (contrasting with the open field of the solar wind) and strong ICME-solar wind interactions in interplanetary space.

References

[1] S.W. Good, L.M. Hatakka, M. Ala-Lahti, J.E. Soljento, A. Osmane, E.K.J. Kilpua, MNRAS **514**, 2425-2433 (2022).

*Corresponding author: simon.good@helsinki.fi

Proof-of-Concept project to develop a novel instrument based on cantilever-enhanced photoacoustics for global black carbon monitoring

Hilkka Timonen[*,1], **Juho Karhu**[2,3], **Joel Kuula**[1,2], **Erkki Ikonen**[3,4], **Aki Virkkula**[1], **Tuomas Hieta**[2,5], **Markku Vainio**[2,6]

1. Atmospheric Composition Research, Finnish Meteorological Institute, P.O. Box 503, FI-00101, Helsinki, Finland
2. Department of Chemistry, University of Helsinki, P.O. Box 55, Helsinki, 00014, Finland
3. Metrology Research Institute, Aalto University, Maarintie 8, Espoo, FI-02150, Finland
4. VTT MIKES, VTT Technical Research Centre Finland, P.O. Box 1000, FI-02044 VTT, Finland
5. Gasera Ltd., Lemminkäisenkatu 59, Turku, 20520, Finland
6. Photonics Laboratory, Physics Unit, Tampere University, FI-33014, Tampere, Finland

Black carbon (BC), also known as elemental carbon (EC) and soot, forms in incomplete combustion (including e.g. engines, burning devices in households and power plants). Atmospheric black carbon has adverse impacts to air quality, health and climate change [1] Due to urgent need to combat against climate change, all means to prevent and reduce the temperature increase and adverse impacts of climate change are currently sought after. Furthermore, WHO recently recommended cities to start systematical measurements of BC in urban areas to gain more information about spatial and temporal variation of BC and to reduce the uncertainties related to impacts of BC.

Current devices used in black carbon measurements are not optimal in many respects – they are based on different indirect measurement techniques (optical, thermal, photoacoustic etc) mostly developed in the 1970's, and their sensitivity and accuracy are often compromised [1]. Furthermore, calibration techniques for these instruments are missing and results are not traceable. In addition, the measurement methods used in ambient monitoring are based on collecting the BC on filter substrate, thus needing frequent manual filter change and being vulnerable to artifacts related to filter collections.

Recentlly, we have developed a more sensitive instrument for BC measurements that is based on cantilever enhanced photodetector (CEPAS) and has a noise equivalent absorption of 0.013 Mm-1 [2]. The benefits of the developed novel CEPAS BC measurement technique include:

1) Photoacoustic spectroscopy is a direct method for measuring optical absorption and thus its validity in particle measurements is not hindered by the typical uncertainty factors present in filter-based instrument.
2) improved sensitivity enables measurement of BC in clean areas
3) possibility to add different wavelenghts enables detection of other absorbing compounds such as BrC
4) possibility to miniaturize enables development of sensor type instrument.

Currently, laboratory tests are ongoing and outdoor tests for novel CEPAS instrument are planned. The aim is to compare the results of CEPAS to established methods such as Aethalometer and MAAP results as well as to sensor grade BC instruments in order to gain information about the possible issues related to field measurements.

We gratefully acknowledge proof-of-concept funding from Jane and Aatos Erkko Foundation for this instrument development.

References

[1] Bond, T. C., et al. J. Geophys. Res. Atmos., 118, 5380–5552, https://doi.org/10.1002/jgrd.50171, (2013).
[2] Karhu, J., Kuula, J., Virkkula, A., Timonen, H., Vainio, M., and Hieta, T.:, Aerosol Sci. Technol., 56, 92–100, https://doi.org/10.1080/02786826.2021.1998338, (2022).

*Corresponding author: Hilkka.timonen@fmi.fi

Urban Physics - Using Physics to Design Sustainable Cities

Anna-Kaisa Viitanen[*,1], **Jonathon Taylor**[1]
[1] Department of Civil Engineering, Faculty of Built Environment, Tampere University, Korkeakoulunkatu 5, FI-33720 Tampere, Finland

Urbanization is one of the global megatrends of our time. Around 55% of world's population lives in cities, with this projected to rise to 68% by 2050 [1]. The trend is similar in Finland too, where approximately 70% of the population now lives in urban areas [2].

Cities form complex environments with human-made materials, large structures, busy traffic, and industrial activities which generate or modify exposure to anthropogenic hazards such as air pollution, noise, and heat. These hazards can have negative health effects. For example, air pollution is estimated to contribute to around 7 million excess deaths globally each year [3], while traffic-related noise in Western Europe alone leads to loss of a million healthy years of life annually [4]. Global warming, heat waves and overheated housing pose sever health problems and loss of productivity; for example, the heatwave in 2018 has been estimated to cause 380 premature deaths in Finland alone [5]. Thus, there is a growing need to tackle these issues and ensure healthy and comfortable living environment for the residents in the cities.

A physics-based understanding of these phenomena can enable us to monitor, model, and design urban spaces to the urban environment. Urban physics seeks to deliver the knowledge and understanding on how to design healthy, comfortable, and energy efficient urban environments. While many of the disciplines related to these phenomena are well established (for example physics, environmental chemistry, aerodynamics, meteorology, and statistics), the first scientific publications referring to urban physics appear relatively recently, around the turn of the 2010s. An early paper by Blocken defined urban physics as "the science and engineering of physical processes in urban areas" [6], and aims to study phenomena such as air quality, thermal conditions, wind and energy from the perspective of urbanization and urban development. It spans a range of spatial different scales [6]. The human-scale concentrates on models of individuals and their interaction with the surrounding environments, both indoor and outdoor, for example the individual exposure to harmful air pollution and heat. At the Building-scale, building physics can evaluate issues such as indoor environmental quality and energy efficiency. The microscale approach studies the environmental conditions at the neighborhood-level (~1 km), where measurements and microclimate models provide insights how buildings, urbans structures, and human activities interact. At the larger mesoscale (10-1000 km), the climate conditions in urban areas and their surroundings can be modeled.

Physics therefore has a valuable role in understanding how to design our cities to be healthy, comfortable, and energy efficient for everyone now and in future climate, urban planning, and energetic scenarios. In Finland the first Urban physics research group [7] was established in 2022 at Tampere University under the faculty of Built Environment and in close connection to PROFI 6 Sustainable Transformations of Urban Environments (STUE) Research Platform [8]. This new research group will link existing research expertise on Building Physics, urban planning, and sustainable housing to help grow our knowledge on healthy and climate-resilient future cities in Finland and worldwide.

References

[1] United Nations, Department of Economic and Social Affairs, Population Division. World Urbanization Prospects 2018: Highlights (ST/ESA/SER.A/421) (2019).
[2] Suomen virallinen tilasto (SVT): Väestörakenne [verkkojulkaisu]. ISSN=1797-5379. Vuosikatsaus 2019. Helsinki: Tilastokeskus [refered: 27.1.2023]. Source: http://www.stat.fi/til/vaerak/2019/02/vaerak_2019_02_2020-05-29_tie_001_fi.html
[3] Compendium of WHO and other UN guidance on health and environment, 2022 update. Geneva: World Health Organization; 2022 (WHO/HEP/ECH/EHD/22.01).
[4] World Health Organization. Regional Office for Europe. (2011). Burden of disease from environmental noise: quantification of healthy life years lost in Europe. World Health Organization. Regional Office for Europe. https://apps.who.int/iris/handle/10665/326424
[5] THL, Last summer's heat wave increased the mortality of older people – prepare for hot weather in time, Finnish Inst. Heal. Welf. Off. Website. (2019). https://thl.fi/en/web/thlfi-en/-/last-summer-s-heat-wave-increased-the-mortality-of-older-people-prepare-for-hot-weather-in-time
[6] B. Blocken, Build Environ, 91, 219-245 (2015).
[7] https://research.tuni.fi/urbanphysics/
[8] https://projects.tuni.fi/stue/

*Corresponding author: anna-kaisa.viitanen@tuni.fi

Many-Body Green's Function Theory Beyond the Born-Oppenheimer Approximation

Ville J. Härkönen[*] [1]
1. Computational Physics Laboratory, Tampere University, P.O. Box 692, FI-33014 Tampere, Finland

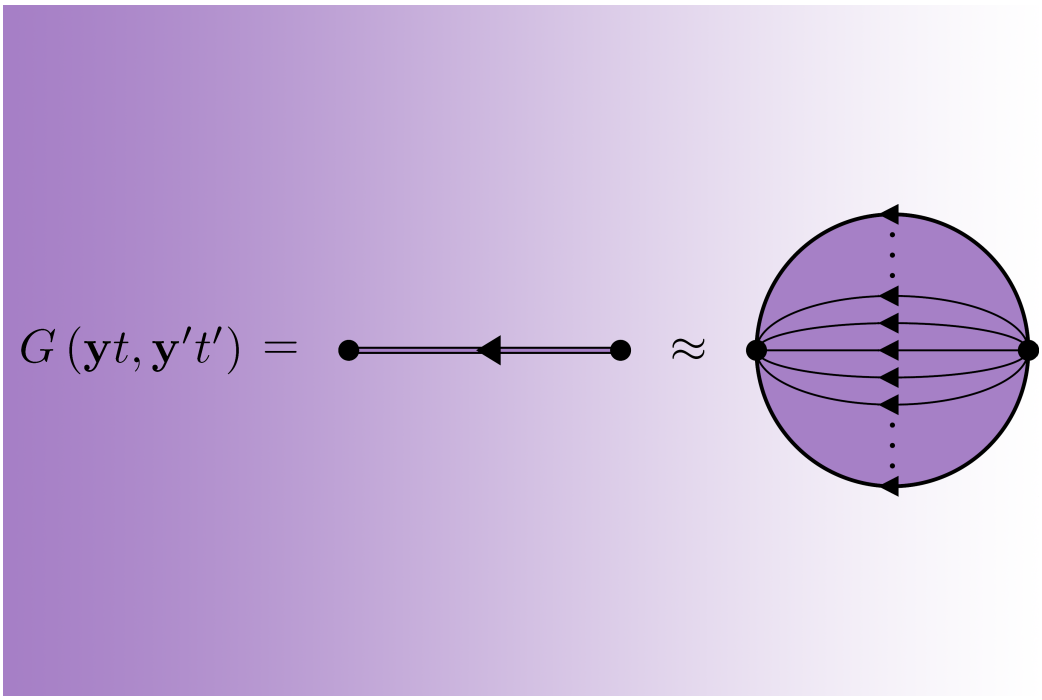

Fig. 1: Lowest order approximation for the electronic Green's function beyond the Born-Oppenheimer approximation.

The Born-Oppenheimer (BO) approximation is central to our understanding about the many-body quantum mechanical systems composed of electrons and nuclei. Its validity can be justified by the rather large mass difference between the electrons and nuclei. There are, however, systems in which the BO approximation is compromised and beyond-BO methods are needed. Examples of such systems are various molecules with conical intersections [1] and possibly the recently discovered superconductive hydrides [2].

To describe such materials, we have developed an exact many-body Green's function theory of electrons and nuclei beyond the BO approximation [3]. With this theory, we can compute the exact observables of any system that can be described by the many-body Hamiltonian comprising kinetic energies and Coulomb potential. However, the implementation of this theory is challenging as the Green's functions involved are defined with respect to the states that belong to the full electron-nuclei Hilbert space. In our recent work [4], to overcome these difficulties, we combine the exact factorization of the wave function [5] and our exact many-body Green's function theory. We obtain the exact expansions of the electron and nuclear Green's functions written in terms of exact factorized states and the BO Green's function theory follows as the lowest order special case of our approach. The lowest order terms of the exact factorized Green's function theory provide a computationally accessible tool for obtaining the properties of materials without imposing the BO approximation.

In this talk, we give an overview of our theory [3] and discuss the recent developments [4], where the beyond-BO many-body Green's function approach is combined with the exact factorization.

References

[1] D. R. Yarkony, Diabolical conical intersections, Rev. Mod. Phys. **68**, 985 (1996)
[2] M. Somayazulu, M. Ahart, A. K. Mishra, et al., Phys. Rev. Lett. **122**, 027001 (2019)
[3] V. J. Härkönen, R. van Leeuwen and E. K. U. Gross, Phys. Rev. B **101**, 235153 (2020)
[4] V. J. Härkönen, Phys. Rev. B **106**, 205137 (2022)
[5] N. I. Gidopoulos and E. K. U. Gross, Philos. Trans. R. Soc. A **372**, 20130059 (2014)

[*]Corresponding author: ville.j.harkonen@tuni.fi

Introducing fluctuations to simulations of early universe bubble collisions in O(N) scalar field theory

Oliver Gould[1], **Paul Saffin**[1], **Satumaaria Sukuvaara**[*2], **David Weir**[2]
1. School of Physics and Astronomy, University of Nottingham, Nottingham, NG7 2RD, United Kingdom
2. Department of Physics and Helsinki Institute of Physics, University of Helsinki, P.O. Box 64, FI-00014 University of Helsinki, Finland

Many beyond the Standard Model theories involve a first order electroweak phase transition. The phase transition from the metastable minimum to the true stable minimum nucleates a bubble in the stable minimum. The phase transition spreads as these bubbles expand, causing the field to oscillate when the bubbles collide. These phase transitions and the fluctuating field are presumed to contribute to the gravitational wave background, which could be measured with future gravitational wave detectors.

We look into the effects the background quantum or thermal fluctuations have on the field evolution during the phase transition in O(N) scalar field theory. We assume that the bubbles are in a vacuum, meaning that the field does not couple to thermal plasma. Specifically, we numerically simulate two colliding bubbles nucleated on top of the background fluctuation, with the field being a N-dimensional vector in the O(N) group. As the two bubble collision has O(2,1) symmetry, this system can be examined in cylindrical coordinates, lowering the number of simulated spatial dimensions. At this stage the research focuses on the behaviour of the O(N) bubble collisions with the fluctuations, later continuing to the examination of the gravitational wave spectrum originating from the field dynamics.

[*]Corresponding author: satumaaria.sukuvaara@helsinki

Multiply-resonant Waveguide Gratings for Enhanced Second-harmonic Generation

Madona Mekhael, Subhajit Bej, Ali Panah-Pour, Robert Fickler, Mikko J. Huttunen
Photonics Laboratory, Physics Unit, Tampere University, FI-33014 Tampere, Finland

Recent progress in fabrication of low-loss waveguiding structures on complementary metal–oxide–semiconductor (CMOS) compatible material platforms is enabling new applications for integrated photonic circuits. Silicon nitride (SiN) has emerged as a prominent material for nonlinear integrated photonics due to its broad transparency window, high refractive index, lower material losses, and strong third-order optical nonlinearities [1]. The recently found strong effective quadratic nonlinearities of SiN are furthermore extending its potential. For example, three-wave mixing processes could transfer generated frequency combs to new wavelength regimes, e.g. enabling self-referencing of combs [2,3]. Here, we numerically investigate how a resonant waveguide grating (RWG) with multiple resonances can be used to achieve better conversion efficiency in second-harmonic generation (SHG) via a better spatial overlap of the guided modes at the fundamental and the second-harmonic wavelengths.

The studied RWG comprises of a SiO_2 substrate, guiding layer (SiN), and a SiN grating layer (Fig. 1a). The grating layer consists of a rectangular lattice of L-shaped protrusions with dimensions shown in Fig. 1a, that enable coupling of incident radiation into multiple high quality factor (Q-factor) resonant (leaky) modes [4]. We optimized the dimensions of the L-shape simultaneously with the grating periods p_x and p_y along x- and y-directions, respectively, to match the spectral peak positions associated with the guided-mode resonances with the fundamental and the second-harmonic wavelengths. Moreover, the mirror-asymmetric (in-plane) unit cell favors SHG.

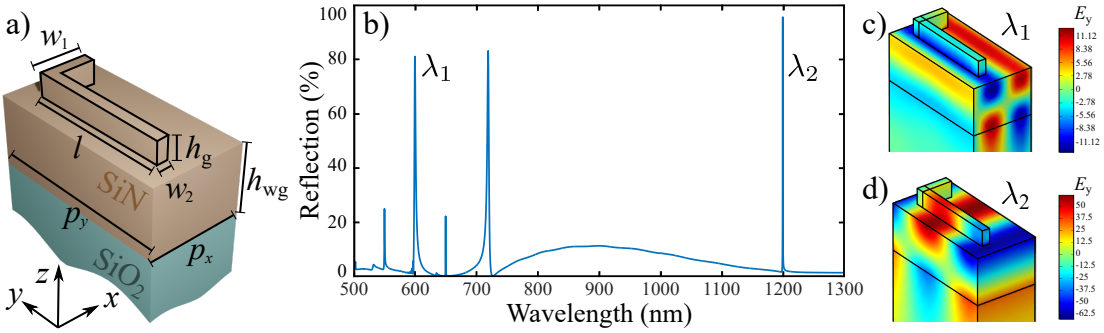

Fig. 1 (a) Schematic of the unit cell where $p_x = 404$ nm, $p_y = 780$ nm, $h_{wg} = 300$ nm, $h_g = 100$ nm, $w_1 = 200$ nm, $w_2 = 50$ nm, and $l = 600$ nm. (b) Reflectance spectrum highlighting two resonances at $\lambda_1 = 600$ nm and $\lambda_2 = 1200$ nm. (c) y-component of the electric field near the second-harmonic wavelength λ_1 and (d) the pump wavelength λ_2. Fields are scaled with respect to amplitude of incident field.

Simulated reflectance spectrum (COMSOL Multiphysics) for normally incident y-polarized light demonstrates existence of several high Q-factor resonances (Fig. 1b), such as a resonance near the wavelength $\lambda_1 = 600$ nm (SHG) and near the $\lambda_2 = 1200$ nm (pump). The estimated Q-factors of these peaks are $Q_1 = 230$ and $Q_2 = 4000$, respectively. The lower Q-factor value of Q_1 was chosen to provide some tolerance in experiments mostly arising from fabrication imperfections. The local-field distributions of the resonant modes are shown in Fig. 1c and 1d, which demonstrate the capability to couple two freely propagating plane wave modes at different wavelengths into the (leaky) slab waveguide modes (and vice versa). In addition, the estimated local-field enhancement factors near λ_1 and λ_2 are 13 and 60, respectively, suggesting potential for a dramatic SHG enhancement factor of 6×10^4. In future, we plan to fabricate the designed structure and verify its capability for enhancing SHG via multiply-resonant operation. A further investigation of how the temporal mode overlap at the pump and the SHG wavelengths impacts the conversion efficiency of the phase-matched second-order nonlinear optical process will be conducted.

References

[1] D. T. H. Tan *et al.*, "Nonlinear optics on silicon-rich nitride—a high nonlinear figure of merit CMOS platform [Invited]" Photonics Res. **6**, 50–66 (2018).
[2] A. Billat *et al.*, "Large second harmonic generation enhancement in Si3N4 waveguides by all-optically induced quasi-phase-matching" Nat. Commun. **8**, 1016 (2017).
[3] T. Ning *et al.* "Efficient second-harmonic generation in silicon nitride resonant waveguide gratings" Opt. Lett. **37**, 4269–4271 (2012).
[4] G. Quaranta, G. Basset, O. J. F. Martin, and B. Gallinet, "Recent Advances in Resonant Waveguide Gratings" Laser Photonics Rev. **12**, 1800017 (2018).
[5] T. Stolt *et al.* "Multiply-resonant second-harmonic generation using surface lattice resonances in aluminum metasurfaces" Opt. Express **30**, 3620–3631 (2022).

Generation of a cluster state cell in a Josephson parametric system

I. Lilja[*,1], E. Mukhanova[†,1], K. V. Petrovnin[1], M. R. Perelshtein[1], V. Vesterinen[2], G. S. Paraoanu[1], and P. J. Hakonen[1]
[1]*QTF Centre of Excellence, Department of Applied Physics, Aalto University, P.O. Box 15100, FI-00076 AALTO, Finland*
[2]*VTT Technical Research Centre of Finland Ltd, QTF Centre of Excellence, Espoo, Finland*

Quantum information theory studies how quantum mechanics can be used to solve information processing tasks. The exploitation of quantum mechanical properties can lead to quantum information protocols being more efficient than their classical counterparts. Continuous-Variable (CV) states offer an attractive platform for implementing various quantum information CV protocols [1].
Cluster states are multipartite entangled CV states that have a specific square lattice structure that are ideal logical units for quantum CV information processes [2]. In this work we demonstrate how by exploiting coherence effects between multiple incident pumps tones, it is possible to construct a simple cluster state by precisely controlling the phases of the pump tones. This cluster state consists of four mutually entangled modes inside a single resonance of a Josephson Parametric Oscillator (JPO). The entanglement properties of the generated state are entirely contained in its 8-by-8 covariance matrix. Various entanglement measures are applied to the covariance matrix to demonstrate that the generated state exhibits genuine multipartite entanglement.
The experimental results are verified with numerical simulations based on the nonlinear quantum Langevin equation, which we find are in good agreement with each other. The methods outlined in this work can be easily expanded to a larger cluster state network. This network can in principle be used as a universal quantum computing platform.

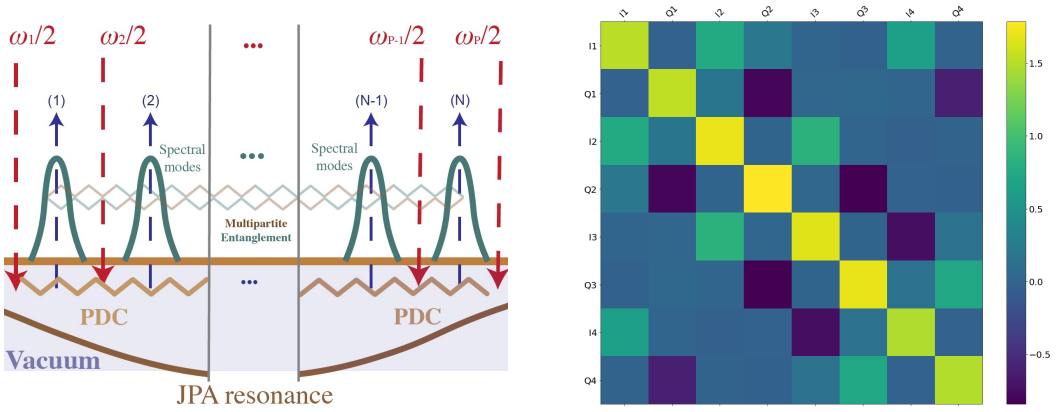

Figure 1: Illustrations on how modes are generated inside the parametric cavity (left) and a covariance matrix of a cluster state (right).

[1] M. R. Perelshtein et al. Phys. Rev. Applied 18, 024063 (2022).
[2] K. V. Petrovnin et al. Advanced Quantum Technologies 6, 2200031 (2023).

[*]Corresponding author: ilari.lilja@aalto.fi
[†]Corresponding author: ekaterina.mukhanova@aalto.fi

Isovector and isoscalar spin-multipole giant resonances in the parent and daughter nuclei of double-β-decay triplets

Elina Kauppinen[*1], **Jouni Suhonen**[†1]
1. Department of Physics, University of Jyväskylä, P.O. Box 35, FI-40014, Jyväskylä, Finland

Double beta decays, both two-neutrino ($2\nu\beta\beta$) and neutrinoless ($0\nu\beta\beta$), have been and continue to be a hot topic in nuclear and particle physics. Primarily the neutrinoless double beta decay draws much attention because it might define the nature of a neutrino, whether it is a Majorana particle. This would indicate physics beyond the standard model.

In this poster, I will present the recent study [1] we made and some of the results. The strength distributions for isoscalar and isovector transitions for double beta decay nuclei were studied. The studied nuclei compose of the double beta decay parent-daughter pairs (^{76}Ge, ^{76}Se), (^{82}Se, ^{82}Kr), (^{96}Zr, ^{96}Mo), (^{100}Mo, ^{100}Ru), (^{116}Cd, ^{116}Sn), (^{128}Te, ^{128}Xe), (^{130}Te, ^{130}Xe), and (^{136}Xe, ^{136}Ba). The transitions proceed from the ground state to the J = $0^-, 1^-, 2^-$, spin-dipole transitions, and J = $1^+, 2^+, 3^+$, spin-quadrupole transitions. The calculations were made using the quasiparticle random-phase approximation (QRPA), and the strength distributions and average energies for the excitations were obtained.

This work's results were compared to the previous studies [2] and [3]. The results seem reasonable, compared to there, although some differences were observed. Also, the calculated results could be compared with possible future experimental data. These comparisons could give insight into the reliability of the used theory.

References

[1] E. Kauppinen and J. Suhonen, Phys. Rev. C **106** 064315 (2022)
[2] L. Jokiniemi and J. Suhonen, Phys. Rev. C **96** 034308 (2017)
[3] N. Auerbach and A. Klein, Phys. Rev. C **30** 1032 (1984)

[*]Corresponding author: elina.k.kauppinen@jyu.fi
[†]Corresponding author: jouni.t.suhonen@jyu.fi

High transparency superconductor-insulator-semiconductor tunnel junctions for thermionic cooling of quantum devices

Lassi Lehtisyrjä[*1], **Joel Hätinen**[1], **Alberto Ronzani**[1], **Emma Mykkänen**[1], **Janne S. Lehtinen**[1], **Mika Prunnila**[1]
1. VTT Technical Research Centre of Finland Ltd., Espoo, Finland

Reaching millikelvin temperatures required for operation of quantum components requires the use of bulky and expensive dilution refrigerators and unsustainable ^{3}He. Cooling down such a system with total cold mass of tens of kilograms takes several days.

What if we could cool quantum circuits on chip scale instead? Our superconducting tunnel junction based thermionic coolers provide a means for sub-1 K refrigeration[1][2].

For superconducting tunnel junction based thermionic coolers, control of electric and thermal transport through material interfaces is crucial for efficient operation[1][2]. We have fabricated high transparency superconductor-insulator-semiconductor (S-Sm) tunnel junctions (Fig. 1(a)), that enable very high cooling power per unit area and are of high quality, i.e., have low sub-gap leakage. These aspects are important for operation of practical phonon-blocked thermionic coolers[2].

We have fabricated junctions with two superconducting materials, aluminium and vanadium (Fig. 1(b)). The process can potentially be expanded to use a number of superconducting materials, such as niobium and titanium. The use of materials with different superconducting gaps can enable effective cooling even from higher bath temperatures, with the ultimate goal of fabricating a platform applicable for cooling of practical quantum devices. In this communication, we will report on electronic and thermal properties of these S-Sm tunnel junctions.

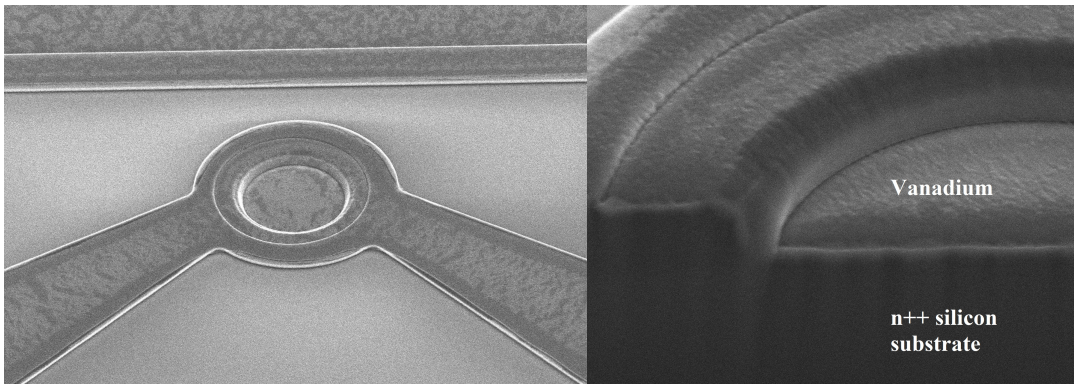

Fig. 1: Scanning electron micrographs: (a) An S-Sm tunnel junction. (b) A cross-section view of the tunnel junction prepared by focused ion beam.

References

[1] A. Kemppinen et al., Appl. Phys. Lett. **119** 052603 (2021) [2] E. Mykkänen et al., Science Advances **6(15)** eaax9191 (2020)

*Corresponding author: lassi.lehtisyrja@vtt.fi

More trustworthy Bayesian optimization of perovskite materials by adding humans into the loop

Armi Tiihonen[*1], **Louis Filstroff** [2], **Petrus Mikkola** [1], **Emma Lehto** [1], **Samuel Kaski** [1,3], **Milica Todorović** [4], **Patrick Rinke** [1]

1. Aalto University, Espoo, Finland
2. ENSAI, CREST, Rennes, France
3. The University of Manchester, Manchester, United Kingdom
4. University of Turku, Turku, Finland

Bayesian optimization (BO) is a machine learning method for the sample-efficient optimization of black-box functions [1]. BO has found application in materials science in guiding the exploration of materials domains, including optimizing perovskite properties [**??**]. However, sample quality remains a challenge in the experimental exploration of novel materials, because it may vary unexpectedly. In the worst case, samples of insufficient quality can invalidate the optimization procedure, if they remain undetected. This limits the use of highly-automated optimization loops, especially in high-dimensional materials spaces that require more samples.

We propose a human-in-the-loop strategy to ensure sufficient sample quality during BO. Human scientists are usually good at assessing sample quality, at least on a cursory yet often sufficient level, whereas sample quality may be hard to define unequivocally for a machine. In this work, we demonstrate that humans can be integrated into the BO loop as experts to comment on the quality of perovskite film samples (Fig. 1). We implement human-in-the-loop BO via two approaches, data fusion and multi-task BO. The approaches are designed to save the bandwidth of human scientists, thus the algorithm requests humans to evaluate the quality of only certain samples during the optimization process. In this work, we simulate BO of perovskite stability (experimental data from the literature [3]) and show that our human-in-the-loop approach reduces the occurrence of invalid optimization results. This benefit is gained already by requesting human evaluation of only 6% of the samples. Our human-in-the-loop approach leads to more trustworthy BO and facilitates highly-automated materials design and characterization loops.

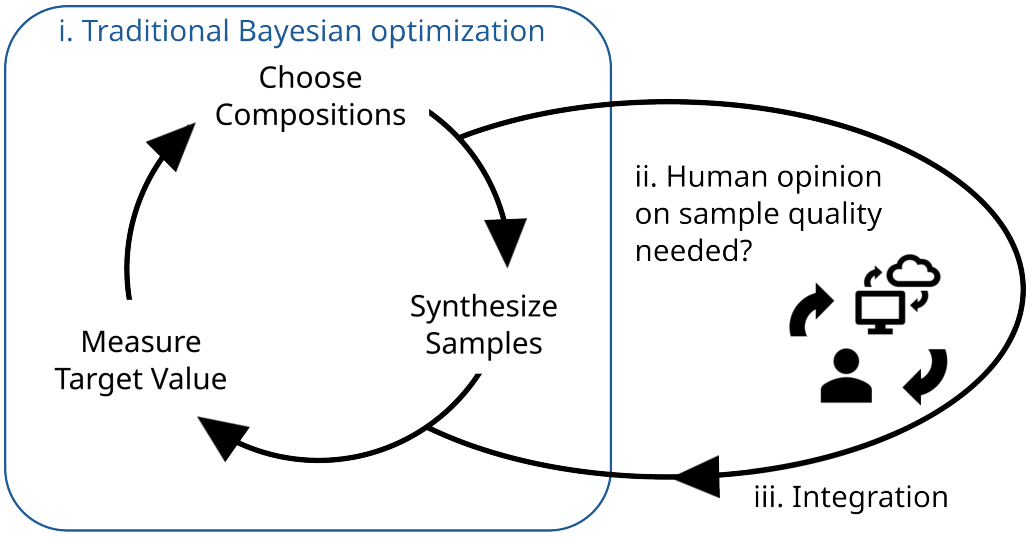

Fig. 1: Experimental Bayesian optimization of materials (i) with humans added into the loop for evaluating the quality of synthesized samples (ii-iii). Adding humans requires a query policy (ii) and the integration (iii) of the human response into the loop.

References

[1] Jones, Donald R., Matthias Schonlau, and William J. Welch. "Efficient global optimization of expensive black-box functions." Journal of Global optimization 13.4 (1998): 455.
[2] Himanen, Lauri, et al. "Data-driven materials science: status, challenges, and perspectives." Advanced Science 6.21 (2019): 1900808.
[3] Sun, Shijing, et al. "A data fusion approach to optimize compositional stability of halide perovskites." Matter 4.4 (2021): 305-1322.

[*]Corresponding author: armi.tiihonen@aalto.fi

A data-driven approach toward designing efficient catalysts for CO_2 to methanol conversion

Prajwal Dattatray Pisal[*1], **Ondrej Krejci** [1], **Lotta Järvi** [2], **Markus Laitinen** [2], **Pawel Winiarski** [2], **Toldy Arpad** [2], **Annukka Santasalo-Aarnio** [2], **Patrick Rinke** [1]

1. Department of Applied Physics, School of Science, Aalto University, Espoo, Finland
2. Department of Mechanical Engineering, School of Engineering, Aalto University, Espoo, Finland

To facilitate the efficient conversion of CO_2 to methanol, new catalysts are required. Despite advances in high-throughput experimental and computational materials screening, catalyst discovery is challenging because the available materials space is vast and catalyst testing is slow and expensive. In this work, we have begun to compile a dataset of experimentally reported catalysts and their conversion efficiencies starting from the data set by Bahri *et al.* [1]. Additionally, we combine the experimental data with Magpie descriptors for the catalysts that form a set of attributes obtained from the information available from the periodic table and are designed to approximate the chemical effects of a broad range of materials [2]. We build a random forest model that uses the Magpie descriptor and the experimental parameters as input for each material to predict the yield of methanol. After training the model on 100 catalytic materials, methanol yield predictions on a test set of 24 catalysts reveal an accuracy of 0.7 percentage points. The principal component analysis gives insight into how the attributes are correlated. Future work will embed our random forest predictor into an active learning materials discovery workflow as described in Figure 1. Available data from literature, our experimental setup and Density Functional Theory calculations will be used to create an initial dataset. The potential catalysts predicted from the machine learning model would be tested and the experimental conditions optimized using active learning techniques like Gaussian Processes and Bayesian Optimization. The active learning loop can add to the original data set to further improve the catalyst design.

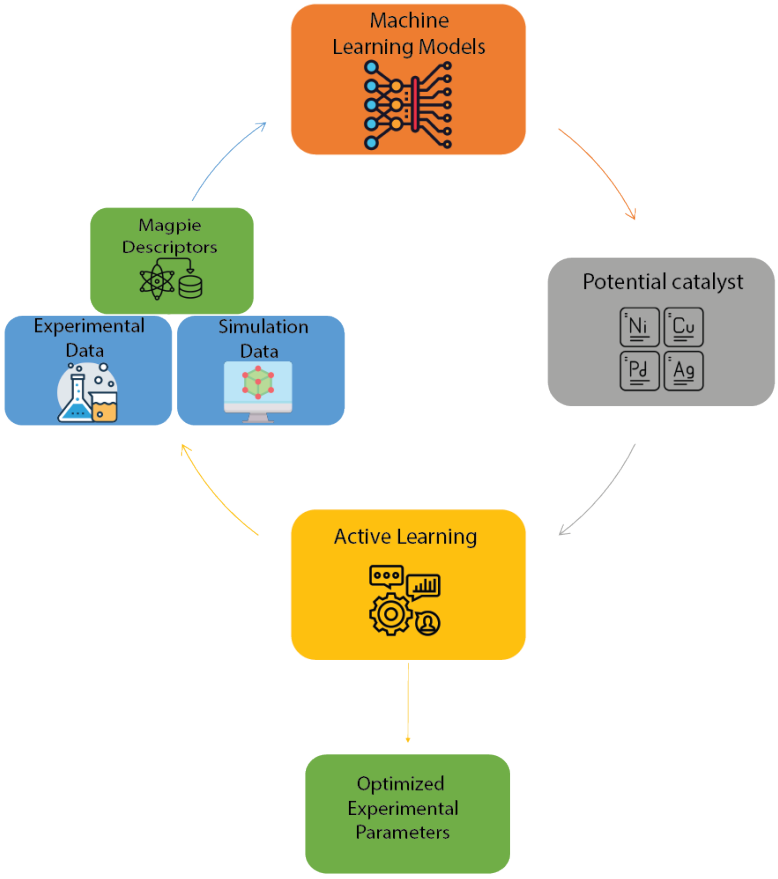

Fig. 1: Workflow for ML-guided discovery of catalysts for efficient CO_2 conversion to methanol

References

[1] S. Bahri, S. Pathak, A. Singhahluwalia, P. Malav, S. Upadhyayula, J. Clean. Prod. **339** 130653 (2022)
[2] L. Ward, A. Agrawal, A. Choudhary, C. Wolverton, Npj Comput. Mater. **2** 1–7 (2016)

*Corresponding author: prajwal.pisal@aalto.fi

Feynman Path Integral Approach to Quantum Dynamics and Eigenstates

Ilkka Ruokosenmäki and Tapio T. Rantala*
Computational Physics, P.O. Box 692, FI-33014 Tampere University, Finland

Feynman path integral (PI) [1] provides a fundamental approach to quantum theory. PI is the kernel of the integral equation for the wave function, and thus, the premise for derivation of the corresponding differential equation, the Schrödinger equation. Furthermore, with the PI and Quantum Monte Carlo (QMC) simulations the time evolution of the wave function and stationary eigenstates of a quantum system can be found with exact account of many-body effects.

In addition, PI approaches in imaginary time allow finite temperature in numerical Monte Carlo (PIMC) simulations of the stationary free energy minimum quantum states [2], see demonstration for a few small atoms and molecules [3] and for their response to external fields [4].

In this study we present a new real time PI formalism (RTPI) and its numerical realizations, which can be used to simulate time evolution of a quantum system to find the time-dependent wave function, the ground state and excited eigenstates [5]. This new method has passed some test cases like one-dimensional Hooke's atom with two electrons, where the electronic correlations are relatively strong [6]. Comparing and combining the conventional Diffusion Monte Carlo (DMC) with RTPI turns out to be a possible relief for other QMC methods suffering from the notorious fermion sign problem (FSP).

Finally, we demonstrate one more novel and robust method based on the RTPI formalism. This approach can be called as "Real Time Diffusion Monte Carlo", as the Monte Carlo walkers run in real time similarly as those of the good old DMC do in imaginary time [7].

ACKNOWLEDGEMENTS
Ilkka Kylänpää and Juha Tiihonen

References

[1] R.P. Feynman, Rev.Mod.Phys. **20**, 367 (1948). ; R. P. Feynman and Hibbs, Quantum Mechanics and Path Integrals (McGraw-Hill, 1965).
[2] D .M. Ceperley, Rev.Mod.Phys **67**, 279 (1995).
[3] I . Kylänpää *et al.*, J.Chem.Phys. **133**, 044312 (2010); Phys.Rev.A **86**, 052506 (2012); J.Chem.Phys. **135**, 104310 (2011).
[4] J . Tiihonen *et al.*, Phys.Rev.A **94**, 032515 (2016); J.Chem.Phys. **147**, 204101 (2017); J.Chem.Theor.Comput. **14**, 5750 (2018).
[5] I . Ruokosenmäki *et al.*, Comm.Comput.Phys. **18**, 91 (2015).
[6] I . Ruokosenmäki *et al.*, Comp.Phys.Comm. **210**, 45 (2017); Gholizadehkalkhoran *et al.*, J.Math.Phys. **59**, 052104 (2018).
[7] I . Ruokosenmäki *et al.*, Comm.Comput.Phys. **25**, 347 (2018).

*Corresponding author: Tapio.T.Rantala@iki.fi

Exploring the optimality of approximate state preparation quantum circuits with a genetic algorithm

Tom Rindell [1,2], **Berat Yenilen** [3], **Niklas Halonen** [1], **Arttu Pönni** [1], **Ilkka Tittonen** [1], **Matti Raasakka**[*1]

1. MQS group, Department of Electronics and Nanoengineering, Aalto University
2. Department of Physics, University of Helsinki
3. Department of Physics, RWTH Aachen University

In quantum computing, the state preparation circuits tend to generally increase the number of CNOT gates as the number of qubits grows larger. As two-qubit gates are significantly more susceptible to noise than the single-qubit ones, running these circuits in physical quantum computers, where noise is present, can result in a low fidelity final state.

We studied whether approximate state-preparation circuits with fewer CNOT gates were able to provide a better fidelity in the final state. These circuits were generated by the low-rank state preparation (LRSP) algorithm introduced by Araujo et al.[1] and further optimized by a genetic algorithm. The genetic algorithm can account for the specific characteristics of the physical machine in the evaluation of circuits, such as the native gate set and qubit connectivity. The goal is to find a circuit which offers an optimal trade-off between the circuit depth (or the CNOT count) and the noise-free error in the target state in such a way that the total error in the presence of noise is minimized. This is where a genetic algorithm may become particularly useful, as it can perform simultaneous multi-objective optimization.

Already for a 5-qubit quantum processor with limited qubit connectivity and significant noise levels (IBM Falcon 5T), we observe the maximal fidelity for the Haar random states is achieved by a short approximate state preparation circuit instead of the exact preparation circuit. The genetic algorithm was able to improve on the circuits found by the LRSP algorithm in that it found preparation circuits with the same number of CNOT gates but a higher fidelity for the output state. As a result, also the maximum fidelity with realistic noise (implemented from the IBM Qiskit 'FakeVigo' backend) was significantly improved in most cases with an average improvement of 0.0618.

Our results support the overall conclusions that (1) there is still room to improve the current state-of-the-art algorithms for approximate state preparation, (2) the maximum fidelity for generic state preparation on a NISQ computer may be achieved by using a shorter approximate circuit rather than the exact state preparation circuit, and (3) genetic algorithms continue to provide a useful tool for the quantum circuit discovery and optimization, especially as the classical computing power at the disposal of researchers increases all the time.

References

[1] I.F. Araujo, C. Blank, and A.J. da Silva. Approximated quantum-state preparation with entanglement dependent complexity, 2021, arXiv:2111.03132.

[*]Corresponding author: matti.raasakka@aalto.fi

Intermittency in interplanetary coronal mass ejections at 1 au and in the inner heliosphere

Julia Ruohotie[*1], **Simon Good** [1], **Emilia Kilpua** [1]
1. Department of Physics, University of Helsinki, Finland

Interplanetary coronal mass ejections (ICMEs) are large plasma clouds that originate from the Sun [1]. They are composed of a large-scale flux rope and are characterized by large magnetic field magnitudes and smooth rotation of the magnetic field vector. In addition, ICMEs have smaller fluctuation amplitudes compared to the solar wind and the preceding sheath region.

Intermittency is a common property of fluctuations in the solar wind, and it is seen as the non-Gaussian behaviour in probability density functions (PDFs) of fluctuations [2]. Intermittency is believed to arise due to either magnetohydrodynamic turbulence [3] or small coherent structures, like the boundaries between small flux tubes [4], that originate from the Sun. While intermittency in the solar wind has been studied for a long time, the exact cause is still unclear with both theories being supported by observations.

Intermittency has not been studied much specifically in ICMEs. This work aims at studying intermittency and its causes as well as its radial evolution in ICMEs and at comparing its properties to the ones observed in the solar wind. Methods that are used to study intermittency include analysing PFDs and structure functions. The present work will introduce preliminary results of a study on intermittency in ICMEs in two example events: one ICME observed at 1 au and the other one in the inner heliosphere.

References

[1] E. Kilpua, H. E. J. Koskinen, T. I. Pulkkinen, Liv. Rev. Sol. Phys. **14**, 5 (2017)
[2] R. Bruno, Earth Space Sci. **6**, 656 (2019)
[3] T. S. Horbury, A. Balogh, Nonlinear Process Geophys **4**, 185 (1997)
[4] J. E. Borovsky, J. Geophys. Res. Space Phys. **113**, A08110 (2008)

[*]Corresponding author: julia.ruohotie@helsinki.fi

Development of $CuFe_2O_4$ Ink for the First Time as a Promising Electrode Ink for Inkjet Printing of Low-Temperature Ceramic Fuel Cells

Sanaz Zarabi Golkhatmi[†,*,1], Muhammad Imran Asghar[1], Peter Lund[1]

[1] Department of Applied Physics, Aalto University, Finland

Developing clean energy conversion devices is crucial for emission reduction resulting from the use of fossil fuels. Ceramic-carbonate nanocomposite fuel cell (CNFC), a hybrid of solid oxide fuel cell (SOFC) and molten carbonate fuel cell technologies, is an appealing energy supply innovation due to its prominent energy conversion efficiency, reduced working temperature (400–600 °C) and enhanced electrolyte ionic conductivity. CNFC electrodes must be optimized for a thinner layer with more porosity to operate at this low temperature while maintaing a high output power owing to the decreased ion transport losses and faster charge transfer reactions. Inkjet printing, a cost-effective, mask-free, and precise fabrication technique, is a promising method for designing a porous thin film for CNFCs to provide the desired requirements [1]. In this research, $CuFe_2O_4$, a spinel ferrite ceramic with numerous applications such as energy storage, catalysis, and photocatalysis, was developed and characterized with particle size analysis based on dynamic light scattering (DLS) theory, surface tension, and density measurements for the first time for inkjet printing a CNFC cathode. A DMP-2800 Dimatix material DoD inkjet printer (Fujifilm, Santa Clara, USA) with a piezoelectric transducer and 10 pL cartridge with 16 nozzles of 21.5 µm in diameter was used for inkjet printing. The $CuFe_2O_4$ ink was prepared by making a dispersion of 3.5 wt% $CuFe_2O_4$ as solid content, 0.03 wt% Ethyl Cellulose as dispersing agent, 20 wt% 1,5 – pentandiol as humectant/surfactant, and Terpineol as the ink medium through ballmilling. The average particle size (D50 = 0.879 µm) was less than 10% of the printer nozzle, which is the recommended particle size range for inkjet printing [1]. The printability of the ink was determined by calculating its Fromm parameter (Z) defined as [1]:$Z = \frac{\sqrt{\rho.\sigma.\alpha}}{\eta}$, where ρ is the density, σ the surface tension, η the viscosity, and α is the characteristic length, which is usually related to the nozzle diameter. The $CuFe_2O_4$ ink showed outstanding jettability performance with a Z of 2.75, which is in line with the rheological requirements of a printable ink ($1<Z<10$) [1]. The ink was perfectly printed on a $(LiNaK)_2CO_3$ – $Gd:CeO_2$ porous electrolyte to make a symmetric cell. Electrochemical Impedance Spectroscopy (EIS) observations at 550°C indicated that the inkjet printing reduced the polarization resistance by 47.69% (from 9.647 Ω cm^2 to 5.046 Ω cm^2) compared to a traditional drop-cast cell (Figure 1 (b)) due to the generation of hierarchical porous microstructure, enhancing the number of reaction sites and electrode's specific surface area. It suggest that the fabrication methode can signifiantly impact the electrode's quality and electrochemical performance in a CNFC. Inkjet printing, which can create a better electrolyte/electrode interface and triple-phase boundary length, has the potential to outperform conventional fuel cell fabrication technologies.

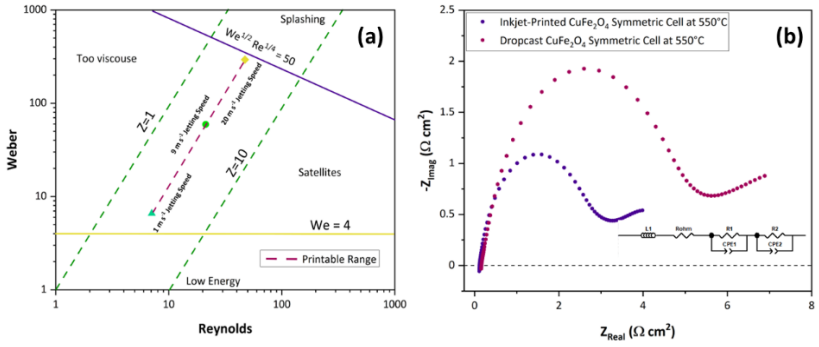

Figure 1 – (a) Derby Diagaram for $CuFe_2O_4$ ink, (b) Comparison of the electrochemical performance of inkjet printed and drop cast symmetric cells by Impedance spectra at 550°C

References

[1] Golkhatmi, S. Z., Asghar, M. I., & Lund, P. D. J. Power Sources, **552**, 232263 (2022)

[2] Asghar, M. I., Heikkilä, M., Lund, P.D, Mater. Today Energy, **5**, (2017)

[†,*]Corresponding author: sanaz.zarabigolkhatmi@aalto.fi

Bayesian optimization of discrete dislocation plasticity of two-dimensional precipitation-hardened crystals

Mika Sarvilahti[*1], **Lasse Laurson** [1]
1. Computational Physics Laboratory, Tampere University, P.O. Box 692, FI-33014 Tampere, Finland

Discovering relationships between materials' microstructures and mechanical properties is a key goal of materials science. Here, we outline a strategy exploiting Bayesian optimization to efficiently search the multidimensional space of microstructures, defined here by the size distribution of precipitates (fixed impurities or inclusions acting as obstacles for dislocation motion) within a simple two-dimensional discrete dislocation dynamics model. The aim is to design a microstructure optimizing a given mechanical property, e.g., maximizing the expected value of shear stress for a given strain. The problem of finding the optimal discretized shape for a distribution involves a norm constraint, and we find that sampling the space of possible solutions should be done in a specific way in order to avoid convergence problems. To this end, we propose a general mathematical approach that can be used to generate trial solutions uniformly at random while enforcing an Euclidean norm constraint. Both equality and inequality constraints are considered. A simple technique can then be used to convert between Euclidean and other Lebesgue p-norm (the 1-norm in particular) constrained representations. Considering different dislocation-precipitate interaction potentials, we demonstrate the convergence of the algorithm to the optimal solution and discuss its possible extensions to the more complex and realistic case of three-dimensional dislocation systems where also the optimization of precipitate shapes could be considered. [1]

References

[1] M. Sarvilahti, L. Laurson, Phys. Rev. Materials **6**, 123801 (2022)

[*]Corresponding author: mika.sarvilahti@tuni.fi

The scaling of 't Hooft-Polyakov monopoles in the early universe

Riikka Seppä[*1], **Mark Hindmarsh** [1,2], **Asier Lopez-Eiguren** [3], **David J. Weir** [1]

1. Department of Physics and Helsinki Institute of Physics, University of Helsinki
2. Department of Physics and Astronomy, University of Sussex
3. Department of Physics, UPV/EHU

't Hooft-Polyakov monopoles are a type of magnetic monopole, which can be formed in a phase transition of a Grand Unified Higgs field in the early universe. If one of these phase transitions took place, an abundance of monopoles would have been formed. With a standard Big Bang cosmology, a detectable number would survive to the present day. This has been called 'The Monopole Problem' for the unification of forces, since no observation of magnetic monopoles has ever been made. This has historically been one of the reasons to consider inflation, since a period of inflation in the early universe dilutes the monopoles enough to explain the lack of observation in the present.

We study the behaviour of these monopoles as a network in an expanding flat and otherwise empty universe, using a lattice simulation with SU(2) gauge fields and a Higgs field in the adjoint representation. While the particular fields we use very likely never filled our universe, they are the simplest way to investigate the behaviour of 't Hooft-Polyakov monopoles. We are interested in how the average separation of the monopoles behaves as a function of conformal time. There is some indication that the separation should scale linearly, and we seek to confirm this. Our preliminary results show this might be the case. Linear scaling in a non-standard cosmology would allow monopoles to annihilate with each other efficiently, and so reduce the impact of the monopole problem for grand unification. Our lattice study is the first of its kind on this particular system, and might thus provide new insights.

*Corresponding author: riikka.seppa@helsinki.fi

2D Weyl Materials in the Presence of Constant Magnetic Fields

Yaraslau Tamashevich[*1], **Leone Di Mauro Villari** [2], **Marco Ornigotti** [1]
1. Faculty of Engineering and Natural Sciences, Tampere University, Tampere, Finland
2. Department of Physics and Astronomy, University of Manchester, Manchester M13 9PL, UK

In this work we investigate the effect of a constant, external or artificial, magnetic field $\mathbf{B} = B\hat{\mathbf{z}}$, on the nonlinear response of 2D Weyl materials [1]. We calculate the Landau Levels (LL) for tilted cones in 2D Weyl materials by treating the tilting in a perturbative manner, and employ perturbation theory to calculate the tilting-induced correction to the magnetic field induced Landau spectrum. We then calculate the induced current as a function of the tilting coefficients and extract the correspondent nonlinear signal. Then, we analyze how changing tilting parameter affects nonlinear signal.

The Hamiltonian for a general 2D Weyl material in the presence of an external electromagnetic field (described by the vector potential $\mathbf{A}(t)$) and a gauge field (described by the U(1) gauge potential $\mathbf{A}^{(g)}(\mathbf{x}) = By\hat{\mathbf{x}}$) is given by

$$\hat{H} = \sum_{i=1}^{2} v_i p_i \hat{\sigma}_i + \Delta\hat{\sigma}_3 + \mathbf{a}\cdot\mathbf{p}\,\hat{\sigma}_0, \tag{1}$$

where $\hat{\sigma}_k$ are Pauli matrices (with $\hat{\sigma}_0 = I$ being the two-dimensional identity matrix), $\mathbf{a} = (a_x, a_y)$ is the tilting vector, $v_{x,y}$ is the (anisotropic) Fermi velocity along the x- and y-direction, respectively, Δ is a staggered potential, which accounts for the gap between the valence and conduction bands, and $\mathbf{p} = \mathbf{k} + (e/c)(\mathbf{A}(t) + \mathbf{A}^{(g)}(\mathbf{x}))$ is the minimally coupled kinetic momentum, which takes into account both the impinging electromagnetic field and the external (or artificial) magnetic field. The Hamiltonian above can be split into two contributions, one of which only contains the magnetic field through the magnetic momentum π_μ, and the other containing only information about the tilt, though the parameters $a_{x,y}$. At first order in perturbation theory, the tilting only affects the eigenstates $|\psi_n\rangle$ but not the redenergetics of the LL. With the light-matter Hamiltonian, we then cast the time-dependent Dirac equation in the following form

$$i\frac{\partial}{\partial t}|\Psi(t)\rangle = \left(\hat{H}_0 + \hat{H}_{tilt} + \hat{H}_{light}(t)\right)|\Psi(t)\rangle. \tag{2}$$

To solve it, we expand the real solution in the instantaneous eigenstates calculated above to get the set of coupled mode equations for the time-dependent coefficients for population of LL.

To solve these coupled mode equations, one first needs to write down the matrix elements $\langle\psi_m^{\pm}|\hat{H}_{light}(t)|\psi_n^{\pm}\rangle$, then solve the above system of differential equations.

In the untilted case, selection rules only allow transitions that obey $\Delta|n| = 1$ [2], which corresponds to choosing matrix elements of the form $\langle\psi^{(0)}_{m,\pm}|\hat{H}_{light}|\psi^{(0)}_{n,\pm}\rangle \simeq \delta_{|m|,|n|+1} + \delta_{|m|,|n|-1}$.

The tilt in Dirac cones introduces an extra set of selection rules for light-matter interaction, which essentially originates from the eigenstate mixing imposed by the tilt itself. The effect of the tilting of the cones on the nonlinear signal can be seen in panel (a) of Fig.1. Increasing the tilt of Dirac cones corresponds to a blue shift of the harmonic spectrum. This, in turn, results in the generation of higher harmonics, than the untilted case [see Fig. 1(c)]. It can be seen how the blue shift of the maximum of the harmonic spectrum is approximately linear with τ. This phenomenon is a consequence of the fact, that the kinetic momentum of an electron in the vicinity of a tilted cone is given by $\mathbf{p} = \mathbf{k} + (e/c)\mathbf{A}^{(g)} + (e/c)\mathbf{A}$. In this scenario, the vector potential $\mathbf{A}^{(g)}$ linearly displaces the electron momentum. The action of this linear displacement, combined with the action of the tilting on the interaction Hamiltonian, makes sure, that the blue shift experienced by the nonlinear spectrum is linear in τ.

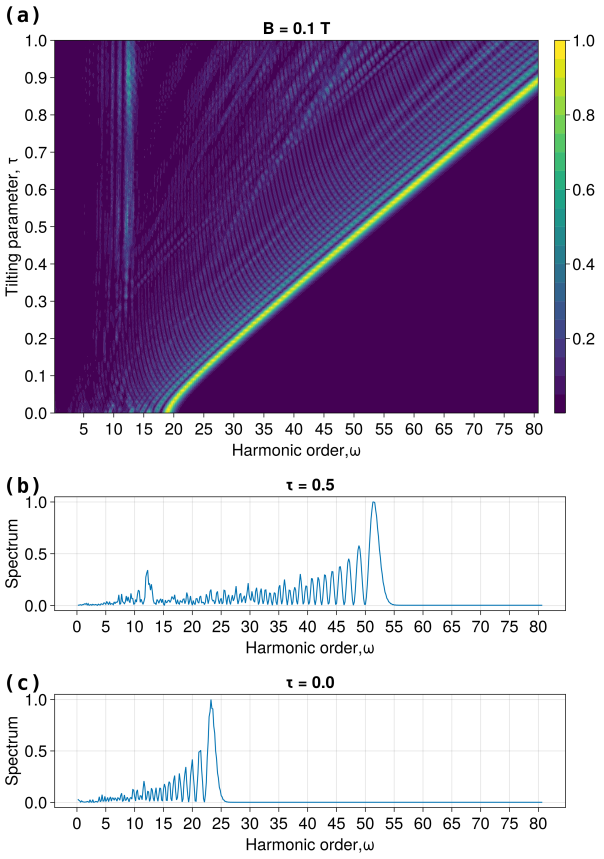

Figure 1: (a) Spectrum of the nonlinear signal for different values of tilting parameters, corresponding to a magnitude of the magnetic field of $B = 0.1$T. Panels (b) and (c) depict the individual spectrum for different values of τ, namely $\tau = 0.0$ (no tilting) and $\tau = 0.5$ respectively. We see that tilting of a cone shifts higher harmonic of the spectrum in higher orders.

References

[1] Q. Lin, M. Xiao, L. Yuan, and S. Fan, Photonic weyl point in a two-dimensional resonator lattice with a synthetic frequency dimension, Nature Communications 7,**13731** (2016)

[2] D. S. L. Abergel and V. I. Fal'ko, Optical and magneto-optical far-infrared properties of bilayer graphene, Phys. Rev. B 75, **155430** (2007).

*Corresponding author: yaraslau.tamashevich@tuni.fi

Numerical Analysis of Measurement Induced Phase Transition in a Transmon Array

Taneli Tolppanen[*1], **Gonzalo Martín-Vázquez**[1], **Matti Silveri**[1]
1. Nano and Molecular Systems Research Unit, University of Oulu

A phase transition in the entanglement properties of a quantum system has been studied theoretically [1], [2] and experimentally [3] when the unitary dynamics of the system are interleaved with quantum measurements. These measurements tend to reduce the entanglement generated by the unitary evolution, following a volume-law for $p < p_c$ and an area-law for $p > p_c$, where p is the probability of doing a projective quantum measurement and p_c is the critical probability where the phase transition occurs. The measurements here can be loosely interpreted as interaction with noisy environment. Realizing the measurement induced phase transition experimentally is a challenge, since the phase transition is seen in the average values of entanglement, calculated over several trajectories. In experiments one would need to produce the same trajectory several times to measure a quantity.

In our work we have realized the quantum system as a transmon array, described by the Bose-Hubbard model [4]. We have studied the phase transition for measurements which locally measure the boson number of a site, but also for predetermined measurements, which we define as measurements of the local boson number followed by a unitary transformation to a predetermined state. The predetermined measurements were shown to be able to circumvent the post-selection. The algorithm for numerically simulating the measurement induced phase transition is formed by the unitary evolution, which simulates the dynamics of the transmon array, followed by measurements, which are realized numerically by using random number generation to make a measurement happen according to the Born's rule. These are then repeated to generate a single trajectory of a randomly measured transmon array. Several trajectories need to be calculated for each measurement probability p, to finally be able to see the phase transition as a function of the measurement probability. We have studied the phase transition in detail for qubits, and also observed it for higher dimensional systems. In our work we used the Krylov method to simulate up to 12 qubits. With our resources simulating a longer array became unmanageable. Here the computational bottleneck is simulating the unitary evolution of the quantum system.

In this work we are interested in studying even longer transmon arrays, with higher local dimensions. Numerically this can be achieved by using matrix product states with the time-evolving block decimation method [5].

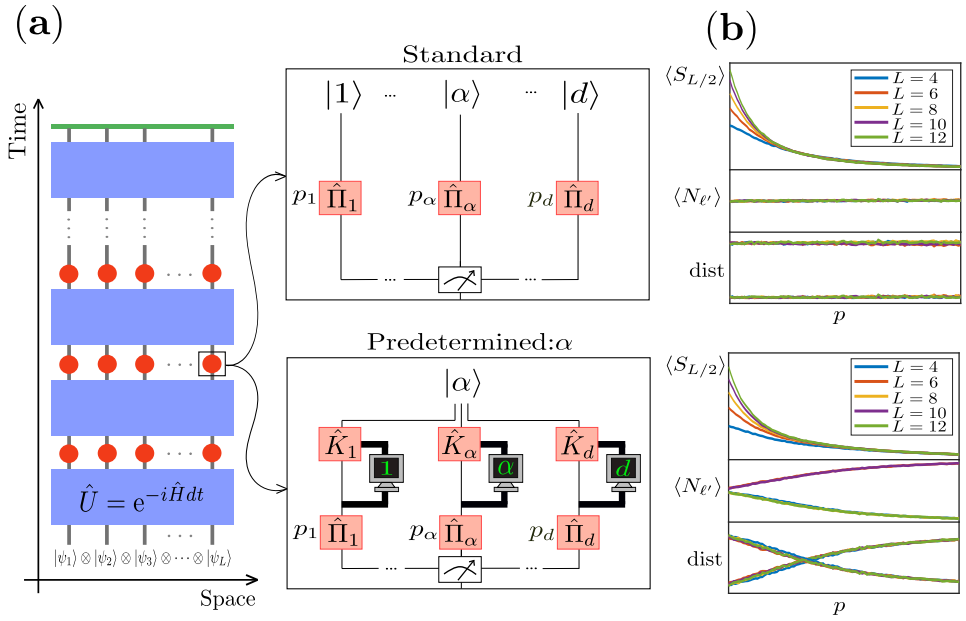

Fig. 1: (a) Schematic of the measurement induced phase transition. The transmon array is initially in a product state and it then undergoes unitary evolution (blue rectangles), followed by a layer of measurements (red circles). A measurement is placed to measure a transmon locally with the probability of p. This is repeated until a steady state is achieved, represented as the green line. For standard measurements, the measurement is split into measurement operators, which are used to calculate the probabilities of different measurement outcomes. These are used to produce a measurement outcome according to the Born's rule. After this, according to the measurement outcome the quantum state is projected and normalized. With predetermined measurements, following the projection the outcome of the measurement is classically accessed and a specific local unitary operation is applied, so that after the measurement the quantum state of the transmon measured is always the same. **(b)** Numerical results on the observation of the measurement induced phase transition as a function of the measurement probability p. The collapse can be seen in the entanglement for both types of measurements. For predetermined measurements, the distribution of the number of bosons in the middle site shows information about the location of the phase transition.

References

[1] Y. Li, X Chen, M. P. A. Fisher, Phys. Rev. B **98** 205136 (2018) [2] A. C. Potter, R. Vasseur, arXiv:2111.08018 (2021) [3] S. Czischek, G. Torlai, S. Ray, R. Islam, R. G. Melko, Phys. Rev. A. **104** 062405 (2021) [4] G. Martín-Vázquez, T. Tolppanen, M. Silveri, Manuscript in Preparation (2023) [5] U Schollwöck, Ann. Phys. (N. Y.) 326, 96 (2011)

[*]Corresponding author: Heikki.Tolppanen@oulu.fi

Formation of Hydrated Magnesium Carbonate Cement from the Carbonation of Magnesium Hydroxide/Brucite

Md Thasfiquzzaman[1], Minna Patanen[2], Paivo Kinnunen[3], Hoang Nguyen[4] , Ekta Rani[5]

[1,2,5]Nano and Molecular Research Unit, University of Oulu, Oulu, Finland
[3,4]Fibre and Particle Engineering Research Unit, University of Oulu, Oulu, Finland

Formation of hydrated magnesium carbonate (HMC) from magnesium hydroxides is one of the promising ways for capturing CO_2. During this HMC formation reaction, a surface passivating hydrated and carbonated product layer of $MgCO_3.3H_2O$ precipitates onto the surface of $Mg(OH)_2$, prohibits further contact between brucite and aqueous sources which limits the carbonation to proceed. One way to make the reaction more efficient is to add ligand [1], such as magnesium acetate to the suspension that promote the dissolution of brucite and thus increase the precipitation of HMC's. The ligand interacts with the carbonate sources, making them more soluble and thus prevent the formation of passivating layer. As a result, higher amount of brucite reacts with carbonate which is favorable for an increased carbonation. Here, we present the outcome of a synchrotron radiation (SR)-based scanning transmission X-ray microscopic (STXM) study, both at Mg 1s (1295-1340 eV) and O 1s (525-560) K-edge, in order to capture the magnesium carbonate layer formed onto the surface of magnesium hydroxide particles. Our STXM-based NEXAS study, as presented in Fig. 1b and 1c, clearly shows the formation of one HMC phase called Nesquehonite upon addition of magnesium acetate ligand. Nesquehonite is the main crystalline phase of this sample, has proven binding properties which helps to increase the strength of magnesium carbonate cement. We also identified another phase, Brucite, as shown with different color compositions, which is the raw materials of our study. The microscopic image in Fig. 1a and the spectrum analysis of STXM helps us to identify the HMC phase very clearly, makes STXM [2] a preferred tool, for studying cement or nano sized materials.

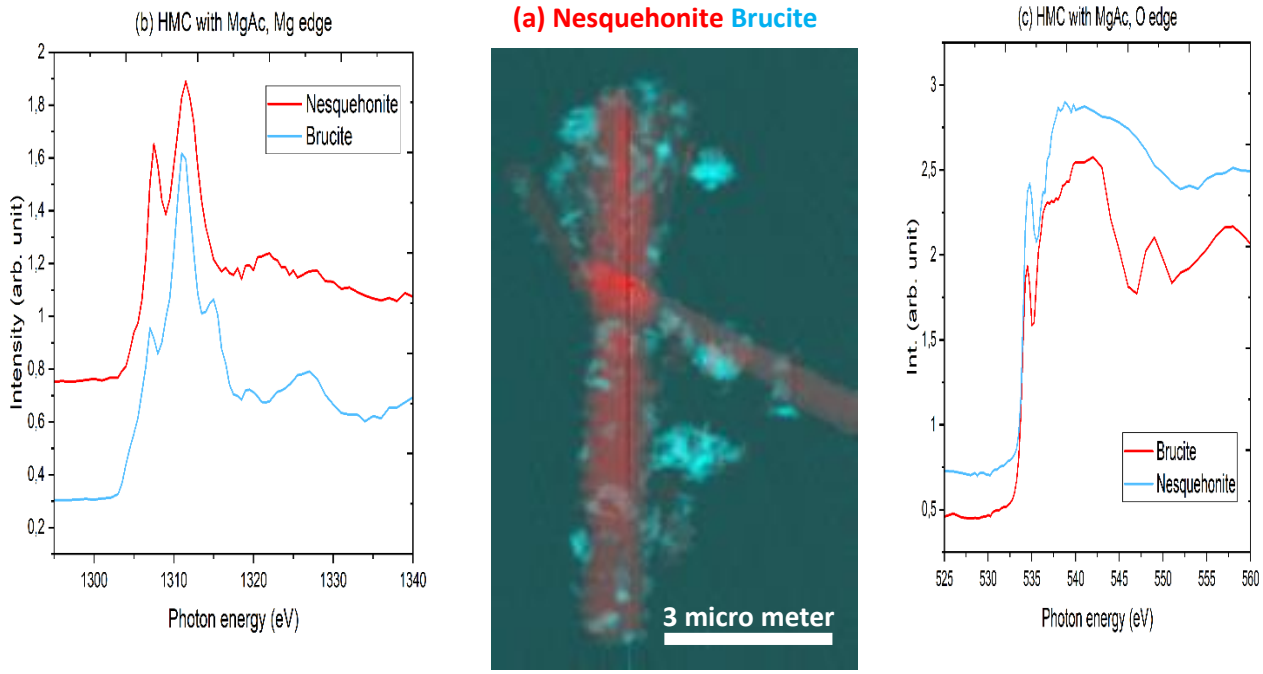

Figure 1. (a) shows the particle with needle shape morphology, whereas (b) and (c) shows the spectrum of Brucite and carbonate phase Nesquehonite for Mg and O K-edge respectively.

References

[1] Dung, N.; Unluer, C. Carbonated MgO concrete with improved performance: The influence of temperature and hydration agent on hydration, carbonation and strength gain. Cement and Concrete Composites 2017, **82,** 152–164.

[2] Hitchcock, A. P. Soft X-ray spectromicroscopy and ptychography. Journal of Electron Spectroscopy and Related Phenomena 2015, **200**, 49–63.

Corresponding author: md.thasfiquzzaman@oulu.fi

Path Integral Monte Carlo approach to properties of Photonic Materials

David Trejo-Garcia[*1] **Ilkka Kylänpää**[†1], **Tapio Rantala**[‡1], **Marco Ornigotti**[§2]
1. Computational Physics, P.O. Box 692, FI-33014 Tampere University, Finland
2. Photonics Laboratory, Tampere University, Finland

Deepmost understanding of material properties, beyond experimental data, can only be increased with the study of electronic structure. At the core of the research on molecules and atoms that compose materials, lies the many-body problem of electrons. As it is well known, it becomes increasingly complex, or outright impossible, to exactly find the wavefunction or density matrix that completely describes a system larger than a single hydrogen atom. For example, the conventional method of density functional theory (DFT) operates under the Born–Oppenheimer (BO) approximation, which means that even for the simplest of molecules, one can only gain knowledge of the system at zero Kelvin. This, of course, is far from true for most applications, which leads to an incomplete description of many materials.

Methods based on Feynman's path integrals provide an exact solution to the many-body problem. Specifically, the method known as Path Integrals Monte Carlo (PIMC) [1] utilizes the imaginary time formalism, and achieves *ab initio* solutions to the many-body problem at finite temperature, in the form of the stationary state density matrix [2]. This comes at a cost of higher computational power but provides unparalleled insight into materials.

One of the fields where PIMC could provide new insight is photonics. Path integrals have been used to compute polarizabilities of small atoms and molecules at a finite temperature [3, 4]. More recently, path integral methods have been proposed as a viable approach to design and investigate complex photonic nanostructures [5]. This has led to a more precise description of the optical response of a material, usually given at zero Kelvin in the literature. A more accurate description of light-matter interaction at the quantum level, especially in new materials like 2D or epsilon-near-zero (ENZ), will lead to a whole new generation of nanophotonic devices.

In this poster, we aim at giving an overview of the PIMC method and its applications to photonics, the challenges it faces, its achievements, and future prospects.

References

[1] D. M. Ceperley, *Path Integral Monte Carlo Methods for Fermions*. 1996.

[2] I. Kylänpää, F. Berardi, E. Räsänen, P. García-González, C. A. Rozzi, and A. Rubio, "Stability of the Dirac cone in artificial graphene formed in quantum wells: a computational many-electron study," *New Journal of Physics*, vol. 18, p. 083014, Aug. 2016.

[3] J. Tiihonen, I. Kylänpää, and T. T. Rantala, "Computation of Dynamic Polarizabilities and van der Waals Coefficients from Path-Integral Monte Carlo," *Journal of Chemical Theory and Computation*, vol. 14, pp. 5750–5763, Nov. 2018.

[4] M. Difallah, A. Szameit, and M. Ornigotti, "Path-integral description of quantum nonlinear optics in arbitrary media," *Physical Review A*, vol. 100, p. 053845, Nov. 2019. Publisher: American Physical Society.

[5] C. W. Robson, Y. Tamashevich, T. T. Rantala, and M. Ornigotti, "Path integrals: From quantum mechanics to photonics," *APL Photonics*, vol. 6, p. 071103, July 2021.

[*]Corresponding author: david.trejogarcia@tuni.fi
[†]Corresponding author: ilkka.kylanpaa@tuni.fi
[‡]Corresponding author: Tapio.T.Rantala@iki.fi
[§]Corresponding author: marco.ornigotti@tuni.fi

Composite silica fiber with $YbPO_4$ nanocrystals

Natalia Vakula[1,*], Zhuorui Lu[2,3], Michèle Ude[2], Martiane Cabié[4], Thomas Neisius[4], François Orange[5], Franck Pigeonneau[3], Wilfried Blanc[2], Laeticia Petit[1]

1. Photonics Laboratory, Tampere University, Korkeakoulunkatu 3, 33720 Tampere, Finland
2. Université Côte d'Azur, Institut de Physique de Nice, CNRS UMR7010, Nice, France
3. MINES Paris, PSL Research University, CEMEF - Centre for material forming, CNRS UMR 7635, CS 10207, rue Claude Daunesse 06904 Sophia Antipolis Cedex, France
4. Aix Marseille Univ, CNRS, Centrale Marseille, FSCM, CP2M, 13397 Marseille, France
5. Université Côte d'Azur, CCMA, Nice, France

*Corresponding author: natalia.vakula@tuni.fi

Fiber optics have been of great interest since the ground-breaking discovery in the 1960s by Charles K. Kao. Silica-glass fibers with losses of about 0.2 dB/km have led to the fiber-optic communications, connecting millions of people all over the world. Silica fibers can be prepared with rare-earth ions (RE) and such active fibers can find uses for application like lasers, amplifiers, sensors [1]. These silica fibers are produced using different methods, one of them being the combination of modified chemical vapor deposition (MCVD) and solution doping technique.

In recent years, effort has been focused on the development of a new generation of optical fibers based on silica glass matrix which contains crystals doped with rare-earth ions (RE). By adding RE doped crystals to the glass matrix, the site of the RE can be controlled independently of the glass composition leading to glasses with unique spectroscopy properties. In 2009, silica fibers, prepared with Al_2O_3/Er nanoparticles (NPs) using an MCVD-compatible process, showed improved performances in terms of erbium homogeneity along the fiber length for standard doping levels [2].

Yb^{3+} ion is a RE of interest since it has a favorable energy level structure for high power laser amplifiers due to the direct excitation of the $^2F_{5/2}$ level which can be efficiently achieved with high power and efficiency InGaAs commercial [3].

In this presentation, we will explain how to prepare $YbPO_4$ crystals and how to incorporate them in a germanosilica glass matrix using MCVD. The crystals were embedded in the silica soot prior to the collapsing step. Using scanning/transmission electron microscope and confocal Raman microscope, it was demonstrated that the $YbPO_4$ crystals survive during MCVD process and the drawing process with temperature more than 2000 °C. We will show that the crystals in the fiber have the same composition and structure as the as-prepared crystals. No elongation of the crystals induced by the drawing process was observed clearly demonstrating the perspectives to fabricate glass-based composite fibers.

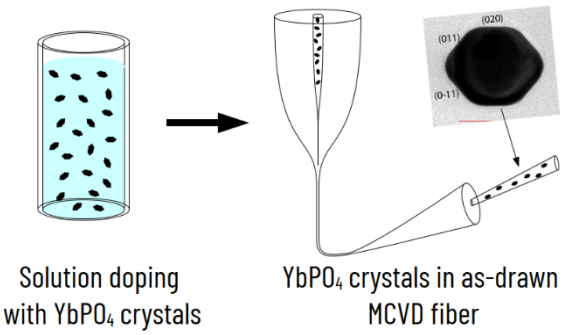

Figure 1. Solution doping with $YbPO_4$ crystals

Acknowledgements

CCMA electron microscopy equipment was funded by Région Sud - Provence-Alpes-Côte d'Azur, the Conseil Départemental des Alpes-Maritimes, and the GIS-IBiSA. The Faculty of Engineering and Natural Sciences, Tampere University, is greatly acknowledged for the Doctoral Grant for NV. This work was supported by Academy of Finland [Flagship Programme, Photonics Research and Innovation PREIN-320165].

References

[1] W. Blanc, Z. Lu, T. Robine, F. Pigeonneau, C. Molardi, D. Tosi, Nanoparticles in optical fiber, issue and opportunity of light scattering, Opt. Mat. Express 12 (2022) 2635-2652

[2] J. Koponen, L. Petit, T. Kokki, V. Aallos, J. Paul, H. Ihalainen, Progress in direct nanoparticle deposition for the development of the next generation fiber lasers, Opt. Eng. 50 (2011) 111605

[3] S. Xu, Z. Yang, W. Zhang, X. Wei, Q. Qian, D. Chen, Q. Zhang, S. Shen, M. Peng, J. Qiu, 400 mW ultrashort cavity low-noise single-frequency Yb^{3+}-doped phosphate fiber laser, Opt. Lett. 36 (2011) 3708

My Abstract for Physics Days 2023

Xueyin Bai[*,1], Zhenyu Xu[†,2], Esko I. Kauppinen,[2] and Zhipei Sun [1,3]
[1] Department of Electronics and Nanoengineering, Aalto University, Finland
[2] Department of Applied Physics, Aalto University, Finland
[3] QTF Centre of Excellence, Department of Applied Physics, Aalto University, Finland.

Mixed-dimensional heterostructures which combine materials with different dimensions have emerged to expand the scope and functionality of van der Waals heterostructures. Here, a direct synthesis method of molybdenum disulfide/double-wall carbon nanotube (MoS_2/DWCNT) mixed-dimensional heterostructures by sulfurating a molten salt, Na_2MoO_4, on a substrate covered with a DWCNT film is reported. The synthesized heterostructures are comprehensively characterized, and their stacking order is confirmed to be MoS_2 under the DWCNTs, although the DWCNT film is transferred to the substrate first. Moreover, field-effect transistors based on the heterostructure are fabricated for photodetection, and an abnormal negative photo response is discovered due to the strong carrier transfer in the mixed-dimensional heterostructures under light incidence. The MoS_2/DWCNT heterostructure results provide a new approach for the synthesis and applications of mixed-dimensional heterostructures.

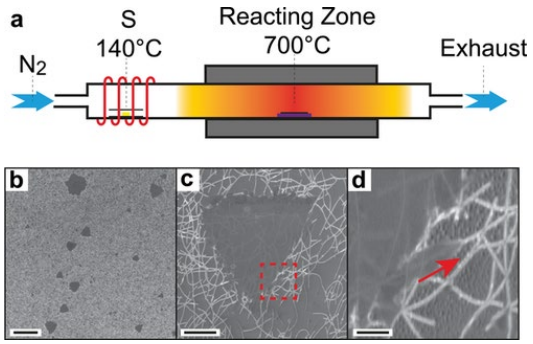

Figure 1 Schematic illustration of the growth setup and images of the MoS_2/DWCNT heterostructures. a) Schematic illustration of the CVD system. b) Scanning electron microscopy (SEM) image of MoS_2/DWCNT heterostructures (scale bar, 20 μm). c) High magnification SEM image of a MoS_2 flake (scale bar, 2 μm). d) Enlarged image of the marked area in (c) (scale bar, 400 nm).

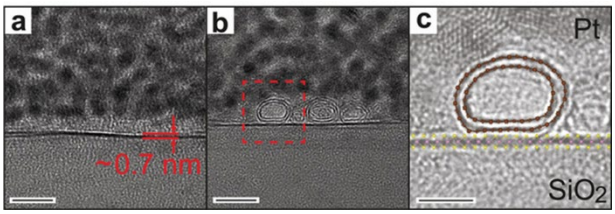

Figure 2 Cross-sectional HR-TEM images. a) Cross-sectional TEM image of a MoS_2 flake (scale bar, 5 nm). b) Cross-sectional TEM image of a MoS_2/DWCNT heterostructure (scale bar, 5 nm). c) Schematic illustration of the selected area in (b) (scale bar, 2 nm).2

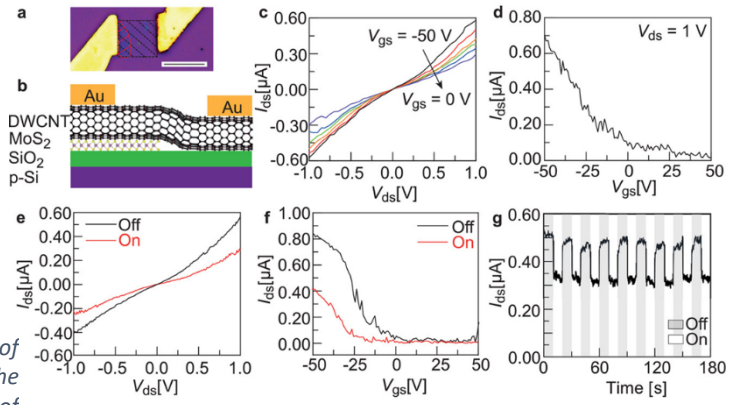

Figure 3 MoS_2/DWCNT heterostructures transistors. a) Optical image of a typical asymmetric transistor with the black part of DWCNT film and the red part of MoS_2 (scale bar, 10 μm). b) Schematic illustration of the asymmetric transistor. c) Output characteristics of the device in (a) at Vgs of 0 V (purple curve), −10 V (blue curve), −20 V (green curve), −30 V (orange curv00e), −40 V (red curve), and −50 V (black curve), respectively. d) transfer characteristics of the device in (a) at Vds of 1 V. e,f) Output and transfer characteristics of the device in a without light (off, black curve) and with 0.1 mW light incidence power (on, red curve), respectively. g) Transient photoresponse of the device in (a) with a light duration of 10 s.

References

[1] X. Bai, Z. Xu, E. I. Kauppinen, Z. Sun, Adv. Mater. Interfaces, **9**, 2200193. (2022)

[*]Corresponding author: xueyin.bai@aalto.fi
[†]Corresponding author: zhenyu.xu@aalto.fi

Study of Helium Bubble Immigration in Additively Manufactured Refractory High Entropy Alloy

Zhehao Chen*[,1], Eryang Lu[1], Xudong An[1], Xuan Meng[2], Filip Tuomisto[1]
[1] Department of physics, University of Helsinki, Helsinki, Finland
[2] Department of physics, Lanzhou University, Lanzhou, China

Material degradations caused by helium irradiation is a serious challenge in fission or fusion reactor[1]. Due to better mechanical properties and apparent irradiation resistance, High entropy alloys (HEAs) have drawn lots of attention in the nuclear material application [2]. Additive Manufacturing (AM) or 3D printing technic is a rapid fabrication method that allows for unique component design, it has also been used to produce HEAs [3]. However, the helium immigration behaviour in 3D printed HEAs is not yet clear. Thus, we conducted irradiation experiments and in-situ annealing to understand the helium bubble thermal evolution mechanism in 3D printed HEA. Cantor alloy is a well-studied HEA[4], which contains CrMnFeCoNi in equal atomic. We use arc-melted Cantor alloy, 3D printed Cantor alloy and 304 steel to conduct the experiments. 304 steel and arc-melted Cantor alloy was used as reference material. Before irradiation, all samples were pre-exanimated by Scanning electron microscopy (SEM) and Positron lifetime annihilation (PAS)[5]. We found the average positron lifetime in 3D printed Cantor is ~8 ps larger than the arc-melted Cantor sample, which means there are more vacancy-type defects in 3D printed Cantor. All samples were firstly irradiated by 3 MeV Ni with fluence of 10^{16} ion/cm^2, and then implanted by 500 KeV Helium ions with fluence of 5×10^{17} ion/cm^2. All irradiation was done at room temperature. The Ni irradiation was supposed to simulate neutron irradiation. After irradiation, the main characterization method is in-situ transmission electronic microscopy (TEM) annealing up to 873K.

No clear changes were found after Ni irradiation. After helium irradiation, the helium bubbles and density are similar between each sample. Differences appear after annealing at 873K. The arc-melted Cantor alloys have the smallest size of bubbles. In 3D printed Cantor, a clear helium bubble belt was observed at the irradiation damage peak area. Bubbles in 3D printed cantor alloy were much larger than arc-melted Cantor, even larger than 304 steel. The pre-existing vacancy-type defects in 3D printed Cantor act as sink sites and trap helium atoms, which can explain the helium bubbles growth. Our results suggest that 3D printed HEA may not be as good as arc-melted HEA when considering helium irradiation caused degradations.

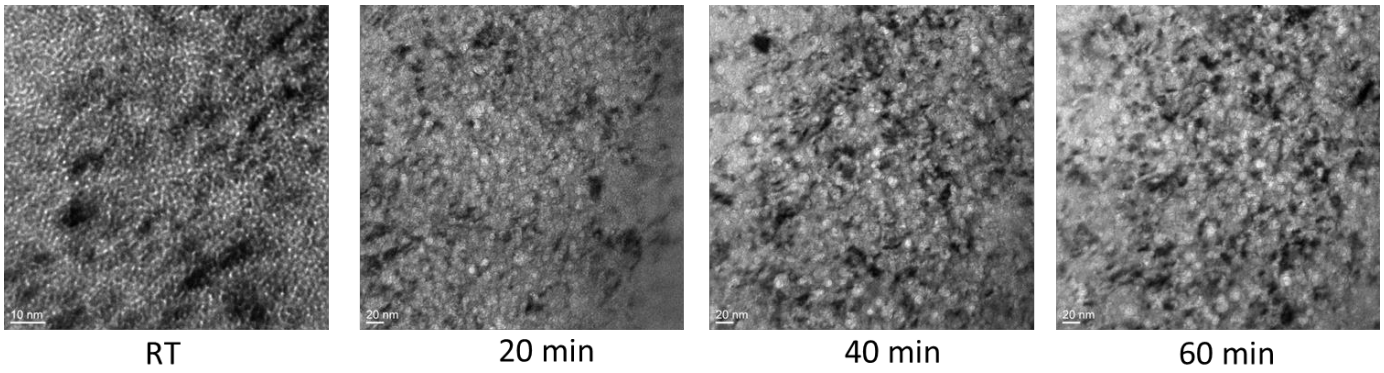

Fig,1 **Arc-melted Cantor alloy:** Helium bubbles evolution during 873K 1h annealing after irradiation, TEM in-situ Bright field observation.

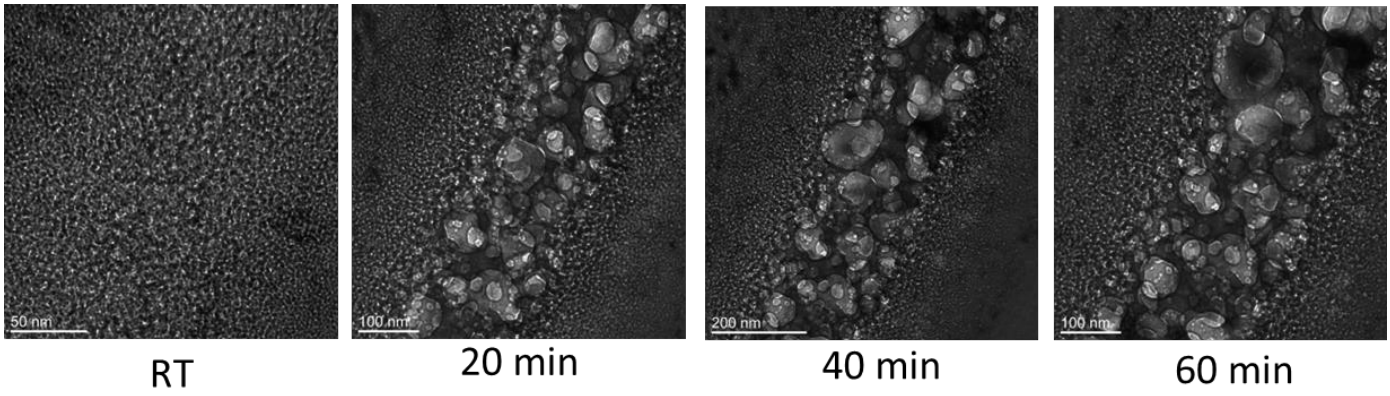

Fig,2 **3D printed Cantor alloy:** Helium bubbles evolution during 873K 1h annealing after irradiation, TEM in-situ Bright field observation.

References

[1]Trinkaus H, Singh B N. Helium accumulation in metals during irradiation–where do we stand?[J]. Journal of Nuclear Materials, 2003, 323(2-3): 229-242.
[2]Xia, Song-qin, et al. "Irradiation behavior in high entropy alloys." *Journal of Iron and Steel Research, International* 22.10 (2015): 879-884.
[3] Han, Changjun, et al. "Recent advances on high-entropy alloys for 3D printing." Advanced Materials 32.26 (2020): 1903855.
[4] Zhang, Zhouran, David EJ Armstrong, and Patrick S. Grant. "The effects of irradiation on CrMnFeCoNi high-entropy alloy and its derivatives." Progress in Materials Science 123 (2022): 100807.
[5] Tuomisto F, Makkonen I. Defect identification in semiconductors with positron annihilation: Experiment and theory[J]. Reviews of Modern Physics, 2013, 85(4): 1583.

*Corresponding author: zhehao.chen@helsinki.fi

Point defects in beta-Ga2O3

I. Zhelezova[1], F. Tuomisto[1]

[1]*Department of Physics, University of Helsinki, Helsinki, Finland*

email: iuliia.zhelezova@helsinki.fi

β-Ga2O3 is an emerging direct wide bandgap (4.9 eV) semiconductor with higher figures of merit for power electronics than widely used GaN and SiC. Material is intended for high power electronic devices able to work at elevated temperatures and at high operation voltages [1]. β-Ga2O3 has high empirical estimated critical electric field of 8 MV/cm, and the availability of large-area, inexpensive bulk substrates grown from the melt. It demonstrated a relatively high electron mobility as well as excellent thermal and chemical stability. However, beta-Ga2O3 semiconductor has a new crystal structure in dislocation theory and its defects behavior are almost unknown.

We were able to build an initial picture explaining what type of defects we are dealing with in monoclinic β-Ga2O3 samples with different doping (Fe, Mg and Sn dopants). These data were obtained at the hand of Doppler-broadening spectroscopy (DBS) in combination with Positron annihilation lifetime spectroscopy (PALS), which allow simultaneous temperature- and orientation-dependent measurements. Both methods are non-destructive and particularly well adapted to studying compensating acceptor-type vacancy defects [2]. The recently discovered unusually strong Doppler broadening signal anisotropy in beta-Ga2O3 [3, 4] not only sets additional restrictions and requirements for positron experiments but also creates a new approach for defect identification with positron annihilation without the need of defect-free reference samples. Thus, comparison of the obtained experimental data with the computational one published earlier [4] allows us to make detailed interpretations on the point defect distribution and exact nature of the split Ga vacancy complexes in the samples.

In contrast to earlier experiments in n-type and undoped Ga2O3 [4], the proton irradiation was found to dramatically change the positron lifetime in Fe-doped Ga2O3. In addition, 3D Doppler experiments show that the overall anisotropy has reduced. Together, these are a clear sign that unrelaxed vacancy-type defects are created in the irradiation, and that the overall defect density before irradiation is significantly lower than in the other Ga2O3 crystals. Interestingly, initial data in Mg-doped Ga2O3 suggest similar behavior to n-type and undoped Ga2O3. These results are extremely exciting, since they make it possible for the first time to determine the nature and density of vacancy-type defects in Ga2O3 crystals.

[1] M. Higashiwaki and S. Fujita (eds.), Gallium Oxide, *Springer Series in Materials Science,* 293 (2020).

[2] F. Tuomisto and I. Makkonen, *Rev. Mod. Phys*. **85**, 1583 (2013).

[3] A. Karjalainen, V. Prozheeva, K. Simula, I. Makkonen, V. Callewaert, J. B. Varley,

and F. Tuomisto, *Phys. Rev. B* **102**, 195207 (2020).

[4] A. Karjalainen, I. Makkonen, J. Etula, K. Goto, H. Murakami, Y. Kumagai, and F. Tuomisto, *Appl. Phys. Lett*. **118**, 072104 (2021).

Ultra-low frequency (ULF) waves in the Pc5 range, with periods between 150 – 600 s, play a key role in the dynamics of Earth’s magnetosphere, in particular through their interaction with radiation belt electrons. One important source of magnetospheric Pc5 waves are fluctuations of the upstream solar wind parameters in the same frequency range. Pressure variations in the solar wind are thought to result in a forced breathing of the magnetosphere, as the magnetosphere would expand and compress in response to the changing upstream conditions, which drives ULF waves inside the magnetosphere. The details of the interaction of these solar wind variations with the Earth’s bow shock and magnetosheath, their impact on the magnetosheath plasma properties and how the fluctuations would change before reaching the magnetopause, remain however unclear. In this study, we investigate the influence of externally-driven density variations in the near-Earth space using global 2D simulations performed with the hybrid-Vlasov model Vlasiator. The new time-varying boundary setup in Vlasiator allows us to set Pc5 periodic density pulses coming from the upstream. The density pulses cause the breathing motion of the bow shock, create clear stripes of variations inside the magnetosheath, and modulate the electromagnetic ion cyclotron (EMIC) and mirror modes. We characterize the spatial-temporal variations of waves on the simulation plane within the magnetosheath and discuss the potential impact on the near-Earth environment.